

NO-A179 783

INVESTIGATION OF NON-SYMMETRIC JETS IN CROSS FLOW  
(DISCRETE WING TIP JET.. (U) TENNESSEE UNIV SPACE INST  
TULLAHOMA J H WU ET AL. DEC 86 UTSI-86-13

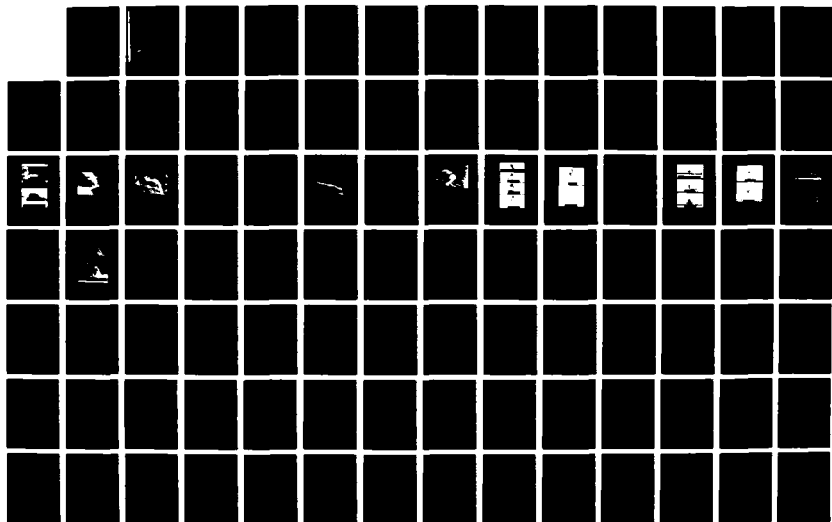
1/2

UNCLASSIFIED

AFOSR-TR-87-0543 AFOSR-84-0114

F/G 20/4

NL





MI

AD-A179 783

DTIC FILE COPY

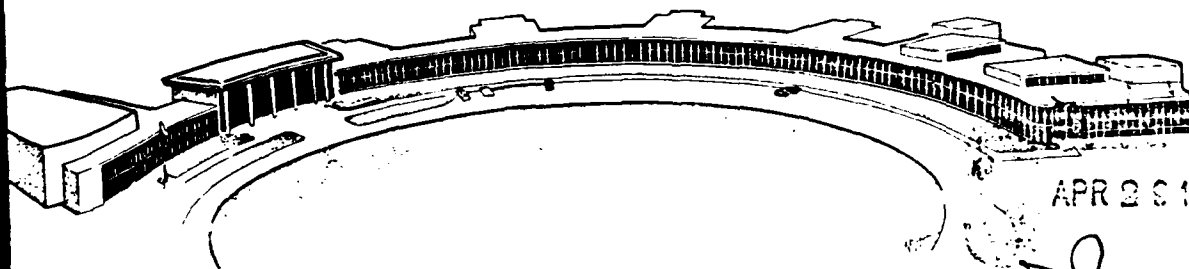
AFOSR-TR- 87 - 0543

GRADING SCHEDULE		APPROVED FOR DISTRIBUTION
ON REPORT NUMBER(S)		5. MONITORING ORGANIZATION <b>AFOSR - T</b>
ORGANIZATION SPACE INST	6b OFFICE SYMBOL T// applicable	7a NAME OF MONITORING AFOSR/NA
Code: 37388		7b ADDRESS (City, State and BUILDING 4 BOLLING AFB
8a OFFICE SYMBOL	8b OFFICE SYMBOL	9 PROCUREMENT INSTR



Approved for public release,  
distribution unlimited.

AIR FORCE OFFICE OF SCIENTIFIC RESEARCH (AFSC)  
NOTICE OF TRANSMITTAL TO DTIC  
This technical report has been reviewed and is  
approved for public release IAW AFR 190-12.  
Distribution is unlimited.  
MATTHEW J. KERPER  
Chief, Technical Information Division



APR 28 1987

# THE UNIVERSITY of TENNESSEE SPACE INSTITUTE

Tullahoma, Tennessee

874 24 031

UNCLASSIFIED

SECURITY CLASSIFICATION OF THIS PAGE

## REPORT DOCUMENTATION PAGE

1a. REPORT SECURITY CLASSIFICATION UNCLASSIFIED			1b. RESTRICTIVE MARKINGS		
2a. SECURITY CLASSIFICATION AUTHORITY			3. DISTRIBUTION/AVAILABILITY OF REPORT  APPROVED FOR PUBLIC RELEASE DISTRIBUTION IS UNLIMITED		
2b. DECLASSIFICATION/DOWNGRADING SCHEDULE					
4. PERFORMING ORGANIZATION REPORT NUMBER(S)			5. MONITORING ORGANIZATION REPORT NUMBER(S)  <b>AFOSR-TR- 87-0543</b>		
6a. NAME OF PERFORMING ORGANIZATION UNIV TENNESSEE SPACE INST		6b. OFFICE SYMBOL (if applicable)	7a. NAME OF MONITORING ORGANIZATION AFOSR/NA		
6c. ADDRESS (City, State and ZIP Code) TULLAHOMA, TN 37388 ! !			7b. ADDRESS (City, State and ZIP Code) BUILDING 410 BOLLING AFB, DC 20332-6448		
8a. NAME OF FUNDING/SPONSORING ORGANIZATION AFOSR/NA		8b. OFFICE SYMBOL (if applicable) NA	9. PROCUREMENT INSTRUMENT IDENTIFICATION NUMBER AFOSR-84-0114		
8c. ADDRESS (City, State and ZIP Code) BUILDING 410 BOLLING AFB, DC 20332-6448			10. SOURCE OF FUNDING NOS.		
			PROGRAM ELEMENT NO. 61102F	PROJECT NO. 2307	TASK NO. A1
11. TITLE (Include Security Classification) (U) INVESTIGATION OF NON-SYMMETRIC			JETS IN CROSS FLOW (Discrete Wing Tip Jet Effects)		
12. PERSONAL AUTHOR(S) J M WU, A D VAKILI, F M YU					
13a. TYPE OF REPORT FINAL	13b. TIME COVERED FROM _____ TO _____	14. DATE OF REPORT (Yr., Mo., Day) DEC 1986		15. PAGE COUNT 97	
16. SUPPLEMENTARY NOTATION					
17. COSATI CODES			18. SUBJECT TERMS (Continue on reverse if necessary and identify by block number)  ASYMMETRIC JETS, CROSS-FLOW, DISCRETE JETS		
FIELD	GROUP	SUB GR			
19. ABSTRACT (Continue on reverse if necessary and identify by block number)  Asymmetric jets in cross flow provide complex interacting flow fields which contain many vortices. Four different cross section geometries were studied and compared with a circular cross section jet with the same exit area. Various flow visualization techniques were used and four major vortices were identified.					
20. DISTRIBUTION/AVAILABILITY OF ABSTRACT UNCLASSIFIED/UNLIMITED <input checked="" type="checkbox"/> SAME AS RPT <input type="checkbox"/> DTIC USERS <input type="checkbox"/>			21. ABSTRACT SECURITY CLASSIFICATION UNCLASSIFIED		
22a. NAME OF RESPONSIBLE INDIVIDUAL HENRY E HELIN, CAPTAIN, USAF		22b. TELEPHONE NUMBER (Include Area Code) 202-767-4935		22c. OFFICE SYMBOL AFOSR/NA	

2

**Investigation of  
Non-Symmetric Jets in Cross Flow  
(Discrete Wing Tip Jet Effects)**

*by*

J. M. Wu, A. D. Vakili and F. M. Yu  
The University of Tennessee Space Institute  
Tullahoma, Tennessee 37388

December 1986

Prepared Under Financial Support of  
US Air Force Office of Scientific Research  
Contract # AFOSR-84-0114

8

UTSI Report 86-13

## Table of Contents

Summary . . . . .	1
I. Introduction . . . . .	2
II. Experimental Procedure . . . . .	4
III. Principle Observation . . . . .	9
1. Jet Vortices . . . . .	9
2. Pulsating Jet . . . . .	14
3. Swirling Jet . . . . .	14
IV. Hot-Film Measurements Results . . . . .	16
V. Concluding Remarks . . . . .	17
References . . . . .	19
Appendix A . . . . .	42
Appendix B . . . . .	70



A-1

## Summary

Asymmetric jets in cross-flow provide complex interacting flow fields which contain many vortices. These vortices vary significantly with variations of the jet and the cross-flow and under certain specific conditions where shedding vortices appear and disappear periodically. Four different cross section geometry jets were studied and compared with a circular cross section jet with the same jet exit area. Various flow visualization techniques were used to aid in understanding of the highly three dimensional and complex flow field. Among many forms of secondary vortices produced, in general four major vortices were identified. The most notable and interesting kind was the "spin-off" vortices observed previously in our study of discrete jets blowing from a wing tip. These shedding vortices were formed under certain flow conditions and jet orientations. The shedding vortices were nearly parallel to the jet exit axis with periodicity depending on the jet to the free stream velocity ratio. A schematic reconstruction of the asymmetric flow field based on observations of the flow evolution is made and relationships with established symmetric jet in cross-flow are made. Unsteady jets created by pulsation of the jet flow at low pulsation frequencies behaved significantly differently than the steady jets, and penetrated more into the cross-flow. Limited quantitative flow measurement made with three-component hot-film anemometer are discussed.

A major part of this report (based on AIAA-86-0280) has been accepted for publication to appear in the Journal of American Institute of Aeronautics and Astronautics in 1987.

## I. Introduction

Jets in a cross-flow are of practical interest to many engineering fields. From the VSTOL aircraft in a transition flight to the waste disposal into water bodies or to the atmosphere, the characteristics of jets in cross-flow play a dominating role. Consequently, a large volume of literature have been devoted to this topic as a result of many basic studies which have been carried out in the past (see for instance, a survey by Rajaratnam<sup>(1)</sup> in 1976 and subsequently many papers scattered in various journals). In spite of such extensive investigations on the subject of jets in cross-flow, we have encountered the asymmetric jet problem which has not received proper attention anywhere, to our knowledge.

The motivation for this study, reported herein, stems from our previous investigation<sup>(2-4)</sup> where discrete jets, blowing from the wing tip, were used in order to improve the wing aerodynamic performance. When discrete jets were applied at a wing tip on a rectangular wing, it resulted in significant lift improvements with small jet blowing momentum coefficients. It was observed that the entire wing circulation has been altered<sup>(3-4)</sup>. This was evidently the result of interaction of flow around the wing with the wing tip jets. The wing tip jets were blown from rectangular exit cross sections (Figure 1), and therefore asymmetric jet flows were believed to be essential for understanding the whole flow field of the wing tip jets. The major axis of rectangular jet ports were placed parallel to the wing chord line, so that the individual jet ports were inclined to the local oncoming free stream flow as shown in Figure 1. Various peculiarly behaving auxiliary vortices were observed (Figure 2). It was suspected that the non-symmetric jet in cross-flow created by yawing a symmetric elongated jet, caused these vortices. Consequently, the study was undertaken to investigate the flow field of asymmetric jets in uniform cross-flow.

Undoubtedly such asymmetric flow fields may be encountered in many actual occurrences in the nature or in the engineering applications. As a simplest example one may think of a situation for a vertical jet take-off aircraft with

the jet blown from non-circular jet ports (say rectangular) encountering a cross wind which is not aligned to either of their major axes. With the courtesy of Prof. G. Carrier of Harvard University, we obtained a photograph showing an oil rig which is caught fire in a strong wind over the ocean. An example that occurred in nature, can be seen in Figure 3. Judging by the size of a nearby ship, the Reynolds number involved in this case (photo) must be very large. The jet (smoke) plume with cross wind induced many vortices which are *very similar* to what we have observed in the water tunnel experiments on asymmetric jets (see typical flow field shown in Figure 4). Therefore, the phenomenon observed in this study is not only limited to moderately small Reynolds numbers as apparent.

There have been many investigations performed on circular jets in cross-flow and limited studies on rectangular jets oriented symmetrically aligned with oncoming flow <sup>(5-9)</sup>. Vortices shedding from such flow phenomena have been studied in detail in the past. Some of the observations are relevant to the present asymmetric jet study. Moreover, the Karman vortices and wake instability of flow over a cylinder or bluff-bodies are also relevant to the problem.

The present study concentrates on the detail features associated with the non-symmetric jets in cross-flow and which could be enhanced by proper geometrical modification or introduction of periodic excitations, to aid the wing tip jet flow interaction effects. Recent papers by Wu <sup>(10-11)</sup> indicates the wing tip vorticity distribution has a significant impact on the wing performance.

## II. Experimental Procedure

At the onset, the basic goal of this study was to understand fundamental flow phenomenon which may lead to design jet shapes whose flow field would resemble some of the key flow features observed in the wing tip jet flow study as described in the introduction. In order to avoid added complexities of the near wing tip flow field, the problem has been simplified to non-symmetric jets blown perpendicularly from a *flat plate* into uniform cross-flow.

Five jet ports with different cross sections geometry but with equivalent cross sectional area were designed and manufactured. Figure 5 shows the dimensions and coordinates for these jet ports. These five shapes are numbered and named for ease of reference. Number one jet which is the circular jet, is the basic reference geometry. A large number of studies and measurements are available for the circular jet in cross-flow hence it is naturally a good geometry to be used for comparison with observations on the other four jets.

Each jet was installed on the water tunnel floor to a modular common base extending into the tunnel 1.9 cm (0.75 in) where the jet exit was flush mounted onto a boundary layer splitter plate. The splitter plate was 150 cm (60 in) long and was extended 19 cm (7.5 in.) upstream of the jet port center to allow for the development of the flat plate laminar boundary layer. The modular components mechanism allowed adjustments to be made in the orientation of various jets only in the plane of jet exit with respect to the uniform cross-flow. Therefore, the jets were always perpendicular to their exit plane or the tunnel floor, but could be easily rotated to create yaw angles of  $\beta = 0^\circ$  to  $180^\circ$ . Figure 5b.

The UTSI water tunnel is a closed circuit, continuous flow facility especially designed for low turbulence and high quality flow visualization. The tunnel lies in a horizontal plane and is powered by a twin bladed propeller in the return leg of the tunnel circuit. The tunnel free stream speed is varied from 1.5 cm/sec. to 60 cm/sec by changing the propeller rotational speed. The Reynolds number based on the jet diameter was in the range of 200 to 500.

Test section dimensions are 35.6 cm high, 45.7 cm wide and 150 cm long (14 in x 18 in x 60 in). The test section walls are made of Plexiglas for versatility in observing and photographing the flow field. The experimental setup is schematically shown in Figure 6.

Two types of flow visualization techniques have been used to extract maximum information from the flow field. The first was by using regular milk and dye technique. Dye was a mixture of alcohol, milk, and commercial food coloring in such a way to ensure specific gravity equivalent to water. The second type was the laser induced fluorescence technique. Three chemicals were used: Rhodamine 6G, Rhodamine B and Fluorescein Sodium Salt. Once dissolved in water and under the excitation of Argon-ion laser light: yellow, red and green fluorescent colors were made visible. Dye was injected to the specific areas of the model at controlled rates desired for each dye exit port. Many distributed small dye exit ports were built into the plate and jets exit neighborhood so the dye could be introduced at the desired points on the surface. Small dye probes, capable of being positioned inside the flow were also used to introduce dye at regions of flow which the surface dye was not carried to.

An Argon-ion laser light source (1 to 2 watts power) was used for the laser fluorescence flow visualization. A 4mm cylindrical lens in front of the laser beam produced a plane laser light sheet. Rotation of the cylindrical lens results in rotation of the light sheet plane. Combined translation and rotation of the light sheet plane provide visibility into the complete flow field at any desired orientation. Frequently the dye for laser flow visualization was introduced into the jet fluid itself. In this way it became possible to observe the jet fluid deformation directly, which was not visible otherwise. On the whole the two flow visualization techniques complemented each other for a complete observation of the details. The general arrangement of experimental set up is shown on Figure 6 and the coordinates system is shown on Figure 5b.

In order to study different jet entrainment and interaction effects, the tunnel velocity and the area-averaged jet exit velocity was chosen such that the velocity ratio was  $1 \leq V_j/V_\infty \leq 7$ . For each jet the major axis of jet

exit model was adjusted and the relative yaw angle  $\beta$  was varied to study the vortical flow interaction effects. The pulsation of jet at frequencies between 1 Hz to 16 Hz were applied. An oscillating small rectangle in the wake of a jet was used to amplify the periodic vortical flow interaction effects. Various observations made and the resulting analysis of the flow visualization study are discussed in the following sections.

The velocity measurement of vortical flow field was done by a three components hot-film anemometer. This system is combination of a customized TSI three-component hot-film probe, a TSI model IFA 100 Intelligent Flow Analyzer, a Scientific Solution's Lab Master 16 channels analog-to-digital converter and an IBM PC/XT compatible computer with 20 mega bytes hard disk.

The signals from three-component hot-film probe were fed into the three channels of IFA 100 system which is connected with Lab Master A/D converter. The signals were digitized at 0.25 K HZ per channel and temporarily stored on the hard disk. The laboratory computer data acquisition system is networked with the main computer system, VAX 11/785, through communication lines. The data were sent to this computer for storage and latter evaluation. The whole data acquisition system was designed in such a way that the probe can be calibrated *in situ* and on-line with the aid of computer, which makes the results independent of any possible attenuation or amplification in the process of transmitting signals from the anemometers to the computer or in the low-pass filters.

The three-component hot-film probe is illustrated with the coordinates systems on Figure A.7. The three films are orthogonal to each other and parallel to the axes of Cartesian coordinate system  $(x', y', z')$  which is defined as wire coordinate system. Let  $X, Y, Z$  be the instantaneous velocity components in wire coordinate system and be parallel to axes  $(x', y', z')$  respectively. The effective cooling velocity for each wire can be written in the following form by using Jorgensen's decomposition relationship (1971)<sup>(12)</sup> and coordinates system relationships for the calibration of  $k$  and  $h$ .

$$U_{eff1}^2 = k_1^2(\phi_1) \cdot X^2 + 0.5(1+h_1^2(\theta_1)) \cdot Y^2 + 0.5(1+h_1^2(\theta_1)) \cdot Z^2 + (1-h_1^2(\theta_1)) \cdot Y \cdot Z$$

$$U_{eff2}^2 = 0.5(1+h_2^2(\theta_2)) \cdot X^2 + k_2^2(\phi_2) \cdot Y^2 + 0.5(1+h_2^2(\theta_2)) \cdot Z^2 + (1-h_2^2(\theta_2)) \cdot Z \cdot X$$

$$U_{eff3}^2 = 0.5(1+h_3^2(\theta_3)) \cdot X^2 + 0.5(1+h_3^2(\theta_3)) \cdot Y^2 + k_3^2(\phi_3) \cdot Z^2 + (1-h_3^2(\theta_3)) \cdot X \cdot Y$$

where

$$\phi_1 = \tan^{-1} \frac{\sqrt{2} X}{Z+Y}, \quad \theta_1 = \tan^{-1} \frac{Z-Y}{Z+Y}$$

$$\phi_2 = \tan^{-1} \frac{\sqrt{2} Y}{X+Z}, \quad \theta_2 = \tan^{-1} \frac{X-Z}{X+Z}$$

$$\phi_3 = \tan^{-1} \frac{\sqrt{2} Z}{Y+X}, \quad \theta_3 = \tan^{-1} \frac{Y-X}{Y+X}$$

Note that  $k$  and  $h$  are coefficients for the tangential and binormal cooling components with the defined tangential velocity component on the plane formed by each hot-film component and probe axis and the defined normal velocity component perpendicular to it, which are defined as the yaw factors and pitch factors. These factors have been obtained from individual calibrations of each hot-film. The details of the calibration of three-component hot-film probe are discussed on Appendix A.

The system of equations is non-linear with respect to the three unknowns  $X^2, Y^2, Z^2$ . These instantaneous velocity components in the wire coordinates can be obtained easily by a successive approximation method. The present approach is fully digital with data acquisition system and hence no linearizers were used. This allows the yaw factors  $k$  and pitch factors  $h$  to vary with the yaw angle  $\phi$  and pitch angle  $\theta$  respectively as defined on Figure A.4. Since the yaw and pitch angles are not known *a priori*, an iterative numerical scheme has been used to solve the above equations.

After solving the instantaneous velocity components  $X, Y, Z$ , with the knowledge of the relative coordinates relationship between lab coordinate system  $(x, y, z)$  and wire coordinate system  $(x', y', z')$  as shown on the sketch of Figure A.8, the instantaneous velocity components  $U, V, W$  in the lab coordinate system can be found immediately. It is just a transformation of coordinates:

$$\begin{pmatrix} U \\ V \\ W \end{pmatrix} = \begin{pmatrix} \cos\omega & -\sin\omega & 0 \\ \sin\omega & \cos\omega & 0 \\ 0 & 0 & 1 \end{pmatrix} \begin{pmatrix} 1 & 0 & 0 \\ 0 & \cos\alpha & \sin\alpha \\ 0 & -\sin\alpha & \cos\alpha \end{pmatrix} \begin{pmatrix} \frac{\sqrt{3}}{3} & \frac{\sqrt{3}}{3} & \frac{\sqrt{3}}{3} \\ \frac{\sqrt{6}}{3} & -\frac{\sqrt{6}}{6} & -\frac{\sqrt{6}}{6} \\ 0 & \frac{\sqrt{2}}{2} & -\frac{\sqrt{2}}{2} \end{pmatrix} \cdot \begin{pmatrix} X \\ Y \\ Z \end{pmatrix}$$

In above equation the rolling angle  $\alpha$  and pitching angle  $\omega$  are the two parameters which link those two coordinate systems as shown on Figure A.7 where  $\alpha$  is taken to be zero when wire No.1 as on  $x'$  axis is in  $x - y$  plane with its longer prongs at the smallest  $x$  values.

### III. Principle Observations

#### 1. Jet Vortices

Jets in uniform cross-flow are acted on by the momentum of the cross stream from the point of exit until complete balance and alignment between the two flows are reached. Due to the jet bending and curvature a pressure gradient is generated in planes perpendicular to the centerline of the jet flow. The jet fluid and the entrained cross-flow form two distinct vortices (called Prandtl's secondary flows of the first kind <sup>(12)</sup>). For a symmetric jet in a uniform cross stream these two vortices are symmetrically generated with the jet wake also being symmetric. Such observations have also been made in many studies as noted earlier.

If the jet forms a non-symmetric configuration with the cross-flow, the resulting flow field around the jet and in the downstream is highly asymmetric, three-dimensional and usually unsteady. Various vortices are formed and their interactions with the wake flow produces a highly complex flow field. The jet vortices, under these conditions are not symmetric and their strength are different. Also, the jet fluid is acted on by the non-uniform cross-flow momentum, hence the two jet vortices follow two different trajectories. All these, introduce a significantly different flow field compared to the symmetric jets.

By introducing colored dye from appropriate locations near the jet exit, it was possible to make the vortex core regions visible. The core traces also correspond to their mean trajectories. A typical illustration of the major vortex trajectories for model 4 can be seen in Figure 7. This side view photo was taken with moderately high jet to free stream velocity ratio of 3.70 with the short tear drop shape jet port (model 4) yawing at  $\beta = 30^\circ$  relative to on-coming free stream. Three distinct major vortex systems could be identified in the above flow and the jet orientation conditions. The most penetrated wind side jet-vortex appeared to be the strongest one, and usually less visible in the down-stream, with regular dye, due to strong entrainment of the cross-flow and locally higher turbulence level. With the laser-fluorescence flow visualiza-

tion, this vortex flow became very distinct, however. Rotational sense of these various vortices are discussed in Figure 10.

For small jet to free stream velocity ratios all three vortices were lying closer to the flat plate and less distinguishable as they were closer, weaker and nearly merged together. For small yawing angles  $\beta$  the jet-vortices represented by the upper two trajectories followed similar path and appeared to coincide from the side view. This was expected as the jet-vortices appeared to be almost symmetric for decreasing yaw angle  $\beta$ . For increased jet to free stream velocity ratio the jet-vortices represented by the upper two trajectories penetrated further away into the free stream. At the mean time, it appeared that an additional pair of less distinct vortices also was formed from the jet exit to join the major (stronger) wind side jet-vortex flow. In other words, there is a possibility of forming more major vortex systems with higher velocity asymmetric jet in cross-flow.

Flow on the plate around the circular jet and the teardrop asymmetric jet is shown in Figure 8. Similar to the horse shoe vortices in front of a solid cylinder in cross-flow there also exist a separation region in the flow just upstream of the various jets. For the circular jet the flow pattern is schematically shown in Figure 8a. The horse shoe vortices and the flow around the jet exit on the plate are symmetric for a symmetric jet exit. For an asymmetric jet exit with respect to the cross-flow, the flow pattern is not symmetric even though the basic flow physics are preserved. Surface flow pattern in the downstream of the teardrop shape jet (model 3) is shown in a top view photograph in Figure 8b. Even though the jet is issued perpendicular to the surface, the surface wake is dominated by the non-uniform entrainment hence non-symmetric. The surface shear stress lines, visualized by placing dye upstream on the plate around the jet, are used to help the interpretation of flow field near the flat plate surface. The flow field near the plate resembles that of a wing at an incidence to a uniform flow.

Figure 9 shows the development of jet-vortices for a teardrop shape jet (model 3) at various downstream distances. These photos are taken in a plane

inclined  $45^\circ$  toward the oncoming flow using laser fluorescence flow visualization technique. This figure shows how the jet fluid is deforming into the jet-vortices and demonstrates the formation of a wake-vortex near the flat plate surface.

Based on evidence described above, the explanation of how the flow developed from a symmetric jet to a non-symmetric jet in cross flow is given in Figure 10. With the aid of an imaginary plane (A), a pair of jet-vortices and a pair of wake vortices can be seen. If the jet is symmetric, these two pair of vortices would be symmetric as schematically illustrated in Figure 10a. With a non-symmetric jet yawed to oncoming flow, on the same plane (A), the wind side jet-vortex moves away from the base plate and the lee side jet-vortex moves closer to the plate which would result in enhancing the lee side wake-vortex and degenerating the wind side wake-vortex as shown in Figure 10b. The pair of wake vortices are the product of induced flow by the counter rotating jet vortices near the plate (laser-fluorescence photos have clearly shown this wake vortices formation). Figure 10 explains the sense of rotation for the wake vortices. Note here that the shearing to the jet fluid by the cross-flow is quite different on the wind and the lee sides. This explains why there are three distinct vortices in the flow field of Figure 7.

For a teardrop shape cross section jet positioned in the cross-flow, with the narrow end forward ( $\beta = 180^\circ$ ), the observed flow field is shown in Figure 11. Under cross-flow shearing action on the jet in a symmetrical manner there are vortices forming around it which shed from the jet trailing end in a periodic but symmetric manner. Figure 11 shows cross sections of jet flow developing in parallel planes at  $45^\circ$  to the flat plate, after the jet exit into the downstream.

### 1.1 Unsteady Jet Vortices

The existence of periodicity in the flow behind jets in cross-flow has been reported by many investigators before, for instance, Gordier <sup>(14)</sup>. McAllister <sup>(15)</sup> related the shedding frequencies of vortices due to cross-flow and a circular jet with the Strouhal number based on the jet diameter. Reilly <sup>(16)</sup> identified

two eddy groups shed periodically from different regions of the jet.

In the present non-symmetric jet study it was found that under certain flow conditions especially at higher jet to free stream velocity ratios, periodic shedding vortices were observed in the downstream of asymmetric jets in the cross flow (Figure 12). These periodic vortices were initiated on the jet wind side through shearing generated at the interface between the jet flow and the uniform cross-flow.

These types of periodic vortices were observed primarily for the jet models 2, 3 and 4 at relative yaw orientations of  $5^\circ$  to  $30^\circ$  to the tunnel free stream and with the jet to the tunnel velocity ratios of higher than three ( $V_j/V_\infty > 3$ ). Figure 12 shows two typical photographs of the flow containing the periodic vortices. We have labeled these as "spin-off" vortices, this terminology was borrowed from our wing tip work <sup>(2-4)</sup>, and is due to the similarities between these vortices and the spin-off vortices observed there. The spin-off vortices shared a common root, with their other ends entrained into the steady jet vortices. The strength and shedding frequency of these spin-off vortices appeared to increase with the jet velocity or its velocity ratio  $V_j/V_\infty$ .

Boldman et al <sup>(17)</sup> studied two dimensional vortices shedding from a flat plate blunt trailing edge with equal and unequal velocities applied on both sides of the plate. They found that symmetric and alternating Karman vortices appeared in the wake with equal velocities applied as is expected. However, by decreasing the velocity only on one side of the plate, it resulted in degenerating the strength on that side of vortices. And in the limit it was possible to eliminate completely that side of vortices altogether.

This analysis could be used to explain the result of present observation of the 'spin-off' vortices shedding from the wind side of jet only and with the same sense of rotation. Referring to Figure 10, one would expect a higher shear on the wind side of jet surface than on the lee side. This would be more profound with moderately increasing the jet velocity and with a moderately yawing angle  $\beta$  which would provide a larger shearing surface. The shedding

frequency appeared related to the jet velocity to the free stream velocity ratio and the jet orientation. In the lee side of the jets certain periodicity was present in the separated flow which was either coupled with the vortices and the shedding frequencies or was influenced by it, since the frequency of the wake unsteadiness and shedding were the same.

Typical common root of the spin off vortices is shown in the various figures, we named this as the jet "wake-vortex" in the previous subsection. Both laser-fluorescence and the regular dye indicated the jet wake-vortex was initiated from the lee side of the jet and developed parallel to the jet vortices but close to the flat plate. The wake-vortex was visible for moderate to higher jet flow rates only for non-symmetric jet configurations.

When spin-off vortices were present, they appeared to roll around each other and the wake-vortex. It should be noted here that many investigators (18-21) have observed also similar rolling up vortices in observation of the wake flow structure behind a cylinder with its axis perpendicular to a flat plate in uniform cross-flow. In Taneda's observation (18), he explained that vortices from the end of a cylinder must rotate in alternating sense and connected to similar strength yet alternatively shedding Karman vortices behind the cylinder. In our present observation, the wake-vortex bundled with spin-off vortices were always rotating in the same sense as that of the wind side jet-vortex flow. Figure 13 shows a schematic of various vortices and features of the asymmetric jets in a uniform flow field.

To clarify the relationship between unsteadiness in the jet wake and the spin-off vortices, artificial periodic perturbations of various frequencies were produced on the plate in the lee side of the jets. Perturbations were created by oscillating in an angular manner, a cylindrical rod at the tip of which a small flat plate fin was installed. The 6mm by 4mm rectangular fin was positioned at the tip of the 3mm diameter rod and its presence in the wake, while not being rotated, did not influence the flow. As a result of the added periodicity, vortices similar to spin-off vortices were shed for asymmetric jets and for frequencies corresponding to the wake fluctuations. Figure 14 shows

two flow fields, indicating the difference due to the added perturbations.

## 2. Pulsating Jet

In order to investigate the effect of jet flow periodicity on the resulting flow field and especially on the various vortices in the down stream, pulsation was applied to the jet flow. A frequency generator and a solenoid valve were used to introduce pulsation in the jet. That is, the continuous jet was replaced by a periodically blown jet. The circular jet (model 1) and the teardrop jet shape (model 3) were subjected to variable frequency pulsations.

At low frequencies, 1 Hz to 4 Hz, the jet penetration into the cross-flow increased significantly for both models 1 and 3. Vortex rings were produced by the pulsation at 1 Hz which actually impinged on the tunnel top wall. The vortex rings were symmetric for the circular jet but they had a complicated shape for the teardrop shape model 3. The vortex rings of this model were also rotating around the axis of the jet along which they were moving into the cross-flow. The increased penetration of the jet is believed to be partially due to the increased momentum in the jet pulses, since the mean flow rate was maintained constant.

As the frequency of the pulsation increased, gradually the flow field returned to the normal pattern with not much difference from that of the steady jet including its penetration height. At low pulsation frequencies, spin-off vortices were not observed for the teardrop shape jet. But, they reappeared as the frequency of pulsation increased beyond 16 Hz. A qualitative representation of the jet plume center trajectory is shown in Figure 15.

## 3. Swirling Jet

Two different techniques were used to introduce swirl into the jets. First, the flow was rotated in the plenum chamber prior to the jet exit. The rotation of the flow was produced using a wheel with radial spokes of rectangular form. The wheel shaft was rotated by a variable speed motor. This created a rotational

flow inside the plenum. However, the fluid exiting the jet did not appear to contain a uniform rotational characteristic. Therefore, this technique was not very successful. Second, a turning vane was placed inside the jet just before the exit plane. The flow following the vane would turn by itself. In both cases the turbulence level of the jets were considerably increased. This was evidenced from the rapid mixing of the dye in the flow and made observation difficult. Introduction of swirl in the jet was found to reduce the effective jet velocity to the free stream velocity ratio.

The second technique, noted above, visibly produced more swirl and showed to be more effective for the circular jet model 1. Due to the swirl in the jet, the flow of circular jet was not symmetric any more. However, its extent of asymmetry was not as strong as altering the jet port shape and jet flow as observed earlier. Introducing swirl in the jet should increase the entrainment of the main stream fluid into the jet <sup>(22)</sup>. As a result of the increased entrainment, the jets were deflected rapidly toward the surface. This observation is in agreement with those of the above reference. It was expected that part of the jet axial momentum is transformed into angular momentum which has little influence on the jet penetration. Experiments made on swirling jets in cross-flow<sup>(23)</sup> point to opposite observations. Reduced shearing action, due to the swirl in the jet flow, across the jet which would otherwise set up pressure differential necessary to deflect the jet is discussed as the physics of higher penetration of the swirling jet into the cross-flow.

#### IV. Hot-Film Measurements Results

The process of measurements with the aide of hot-film has not been completed in time for preparation of this report and especially the analysis of the large volume of data obtained is just beginning. Selected measurement stations have been analyzed and evaluated in a preliminary level. Because of the fact that these data have not been fully evaluated, they represent typical information which will be included in the final report for the next contract.

Measurements are made using the 3-D hot-film probe, in three longitudinal plane stations in the downstream of the tear drop jet exit for yaw angle  $\beta = 20^\circ$ . In each plane, at downstream stations of  $\frac{X}{D} = 5, 10$  and  $15$ , traverses were made at four heights of  $\frac{Z}{D} = 1, 3, 5$  and  $7$ . Mean velocity, root mean square of velocity fluctuations and cross-correlations are shown on plots in Appendix B.

Because of the analysis not being finalized, only limited discussions are made in the following paragraphs.

Observations by McMahon et al.<sup>(6)</sup> have indicated that for a circular jet the energy of periodic fluctuations is larger near the boundary of the jet plume than at the center of the jet induced vortices. Measurements obtained in the present investigation, Figure 16 for a non-symmetric jet in cross-flow are in agreement with the result of the reference 6. Figure 17 illustrates the effective blockage created by the tear drop jet at  $\beta = 20^\circ$  yaw angle. The flow represents a similarity with the wake of a solid cylindrical body. The velocity defect can be used as a measure of solid blockage effect, which is decreased as the distance from the flat plate wall is increased. At higher distances from the plate the deflection of the jet due to the cross-flow reduces the blockage and eventually, the jet fluid is aligned with the uniform flow where there is no wake.

## V. Concluding Remarks

The flow field of jets in cross-flow of four different cross section geometry jets have been studied and compared with that of a circular cross section jet. The jets had equal cross section areas but different geometries. This qualitative study was conducted in a water tunnel for detail flow field visualization. The flow around asymmetric jets in cross-flow is of a very complex nature and contained many features which were significantly different than that of symmetric jets in cross flow. The flow field has been reconstructed schematically with flow physics discussed.

Periodic vortices were observed perpendicular to the cross-flow, these were called "spin-off" vortices. Spin-off vortices were only observed for asymmetric jets and appeared only at jet velocity to the free stream velocity ratios usually higher than 2.5 or 3 and were dependent on jet port shape and orientation.

Perturbations introduced in the wake of asymmetric jets produced the spin-off vortices artificially, only when the frequency of the perturbations matched the separated wake flow fluctuations. The amplitude of the natural fluctuations was not sufficiently large enough to cause the vorticity created due to shearing between the jet and the cross-flow to shed under such situation.

A wake-vortex was observed for asymmetric jets which was lying parallel and close to the floor plate. Once the spin-off vortices were present they became twisted and linked near the flat plate and wrapped around the wake-vortex.

Pulsating the jet flow at low frequencies resulted in formation of vortex rings which penetrated into the main flow more than the jet for high pulsation frequencies. Under this condition no spin-off vortices could be produced. At higher pulsation frequencies ( $f > 16\text{Hz}$ ), the flow fields were similar to that of the steady jets with increased mixing present at the jets boundary. Introduction of swirl in the jet flows was found to increase the jet turbulence and to reduce the effective jet velocity to the free stream velocity ratio.

There appears to be quite some similarities between jet flows and the flow around asymmetric cylindrical bodies in uniform cross flow<sup>(21)</sup>. The presence and the identification of these flow features is considered to be a first step toward their full understanding, utilization, enhancement or suppression of selected desired vortices in many fluid mechanics situations.

Quantitative results based on limited measurements indicate general trend agreements with other data for symmetric jets. For asymmetric flows of this investigation the downstream flow is quite more complex as discussed in the flow visualization and highly non-symmetric.

## References

1. Rajaratnam, N. "Turbulent Jets." Amsterdam; New York: Elsevier Scientific Pub. Co., Chapter 9, pp. 184-210, 1976.
2. Wu, J. M. and A. D. Vakili. "Wing Tip Jets Aerodynamic Performance," Proceedings of the 13th International Council for Aeronautical Science, Edited by B. Laschka and R. Staufenbiel, Seattle, Washington, August 1982.
3. Wu, J. M., A. D. Vakili and F. T. Gilliam; "Investigation on the Effects of Discrete Wing Tip Jets." AIAA Paper No. 83-0546. AIAA 21st Aerospace Science Meeting, Reno, Nevada, January 1983.
4. Wu, J. M. and A. D. Vakili. "Aerodynamic Improvements by Discrete Wingtip Jets." WPAFWAL TR 84-3009, 1984.
5. Weston, R. P., F. C. Thames. "Properties of Aspect-Ratio-4.0 Rectangular Jets in a Subsonic Cross Flow." AIAA Journal, Vol. 16, No. 10, pp. 701-707, October 1979.
6. McMahon, H. M., D. D. Hester, J. G. Palfery. "Vortex Shedding From a Turbulent Jet in a Cross Wind." Journal of Fluid Mechanics, Vol. 48, Part 1, pp. 73-80, 1971.
7. Wu, J. C., "Experimental and Analytical Investigation of Jets Exhausting Into a Deflecting Stream." AIAA Paper No. 69-225. AIAA/AHS VTOL Research, Design and Operation Meeting, Atlanta, Georgia, February 17-19, 1969.
8. Andreopoulos, J., "Initial Conditions, Reynolds Number Effects and the Near Field Characteristics of the Round Jets in a Cross Flow," Journal of Flight Sciences and Space Research, Vol. 8, No. 2, March/April 1984, pp. 118-124.
9. Crabb, D., D. F. G. Durão, J. H. Whitelaw, "A Round Jet Normal to a Crossflow," Journal of Fluid Engineering, Transactions of the ASME, Vol. 103, March 1981, pp. 142-153.

10. Wu, J. Z., 1986 a.b. Incompressible Theory of The Interaction Between Moving Bodies and Vorticity Field. I. "The Production of Vorticity by Body Surfaces and its Dissipation"; II. "Force Acted on Bodies by Vorticity Field". Acta Aerodyn. Sinica 4, No.2, 168; to appear.
11. Wu, J. Z. & Wu, C.J. 1986. A Viscous Compressible Theory on The Interaction Between Moving Bodies and Flow Fields in the  $(\vec{x}, \theta)$  Framework Submitted for Publication.
12. Jorgensen, F.E., 1971. "Directional Sensitivity of Wire and Fiber-film Probes," DISA Information No. 11, pp. 31-37. May.
13. Prandtl, L., "Essentials of Fluid Dynamics, pp. 145-149. Blackie & Son Ltd., London, 1963.
14. Gordier, R. L., "Studies of Fluid Jets Discharging Into Moving Liquid." St Anthony Falls Hydro Lab., Univ. of Minnesota. Tech. Paper No. 28 Series B, 1959.
15. McAllister, J. D., "A Momentum Theory for the Effects of Crossflow on Incompressible Turbulent Jets." Ph.D. dissertation. University of Tennessee, 1968.
16. Reilly, R. S., "Investigation of the Deformation and Penetration of a Turbulent Subsonic Jet Issuing Transversely into a Uniform, Subsonic Main Stream." Ph.D. dissertation. University of Maryland, 1968.
17. Boldman, D. R., P. F. Brinich and M. E. Goldstein, "Vortex Shedding from a Blunt Trailing Edge with Equal and Unequal External Mean Velocities." Vol. 75, part 4, pp. 721 - 735. J. of Fluid Mech., 1976.
18. Taneda, S., "Studies on Wake Vortices: An Experimental Study on the Structure of the Vortex Street Behind a Circular Cylinder of Finite Length." Reports of Research Institute for Applied Mechanics, Vol. I, No. 4, Dec. 1952.
19. Sakamoto, H., "Vortex Shedding from a Rectangular Prism and a Circular Cylinder Placed Vertically in a Turbulent Boundary Layer." Journal of Fluid Mechanics, Vol. 126, pp. 147-165, 1983.

20. Hussain, A.K.M.F. and V. Ramjee. "Periodic Wake Behind a Circular Cylinder at Low Reynolds Numbers." *Aero. Quarterly*, Vol. 27, pp. 121-142, May, 1976.
21. Slaouti, A. and J. H. Gerrard. "An Experimental Investigation of the End Effects on the Wake of a Circular Cylinder Towed Through Water At Low Reynolds Numbers." *Journal of Fluid Mechanics*, Vol. 112, pp. 297-314, 1981.
22. Simon, F.F. and J.L. Ciancone. "Flow Visualization Study of the Effect of Injection Hole Geometry on an Inclined Jet in Cross Flow". Heat Transfer and Fluid Flow in Rotating Machinery edited by: Wen-Jei Yang. Hpc, 1986.
23. Pratte, B.D., and J.F. Keefer. "Swirling Turbulent Jet Flows - Part 1: The Single Swirling Jet." UTME-TP-6901. University of Toronto, Toronto, Canada, 1969.

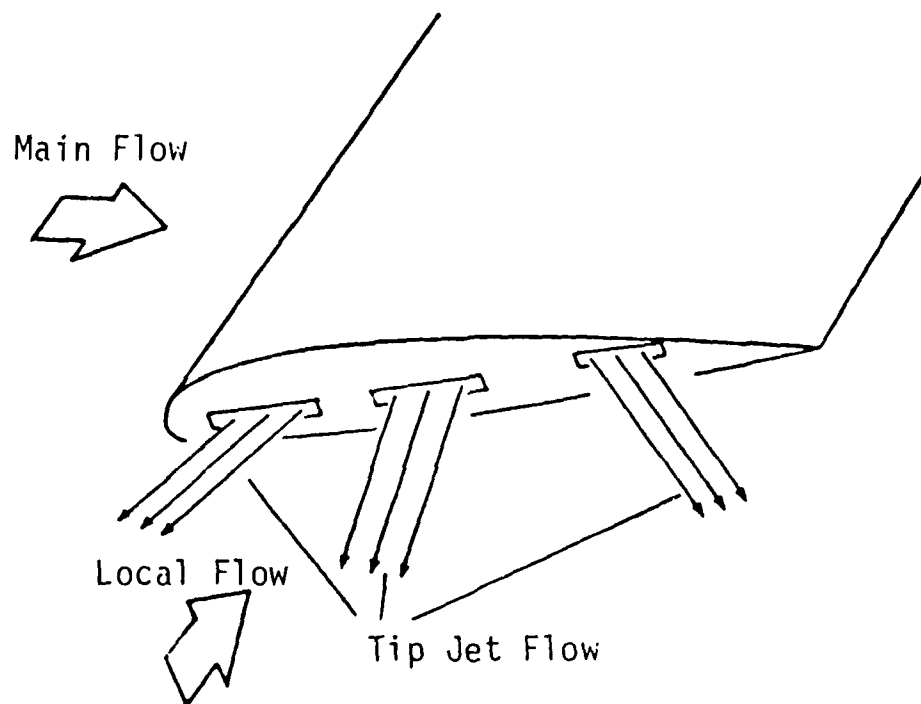
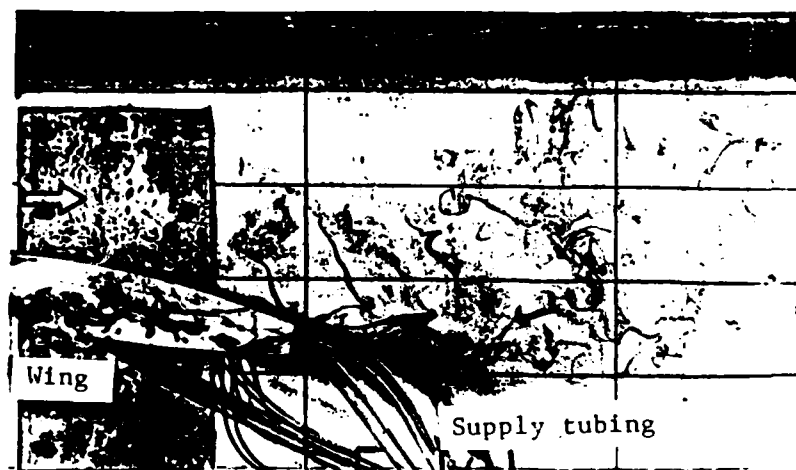
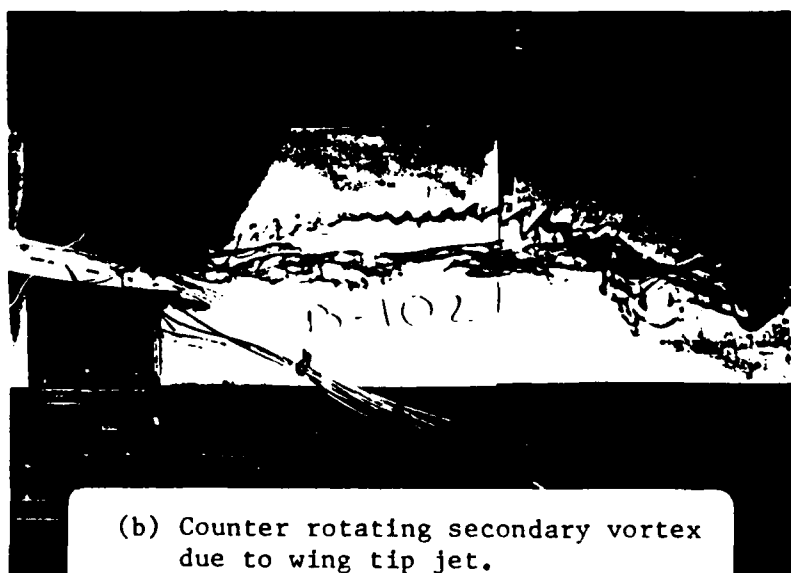


Figure 1. Individually controlled discrete wing tip jets.



(a) Periodic "spin-off" vortices with wing tip jet blowing.



(b) Counter rotating secondary vortex due to wing tip jet.

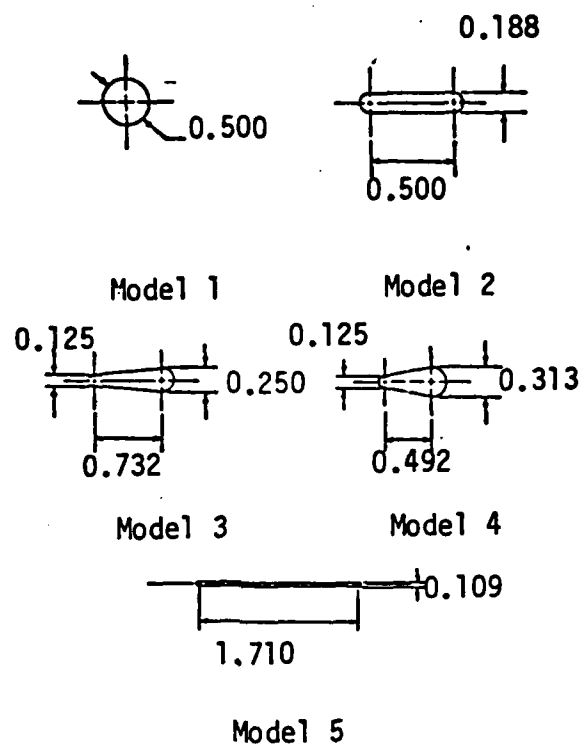
Figure 2. Wake flow field with jet blowing.



Figure 3. Off-shore oil rig caught fire.  
(private communication with G. Carrier)

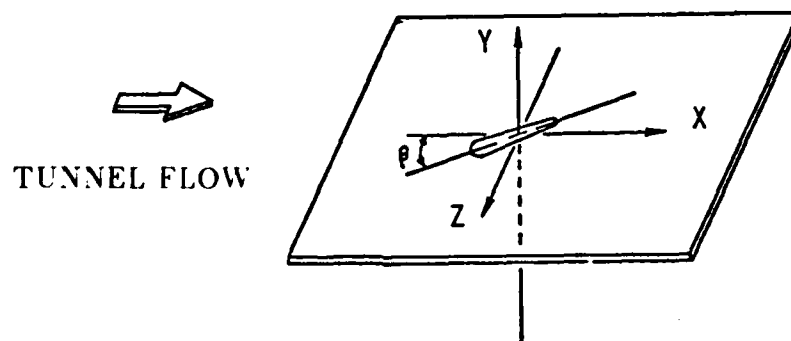


Figure 4. Non-symmetric jet in cross flow of present study.



All dimension in inches

(a) Geometry of five jet exit models.



(b) Coordinates and yawing angle  $\beta$ .

Figure 5. Schematic of experimental arrangement.

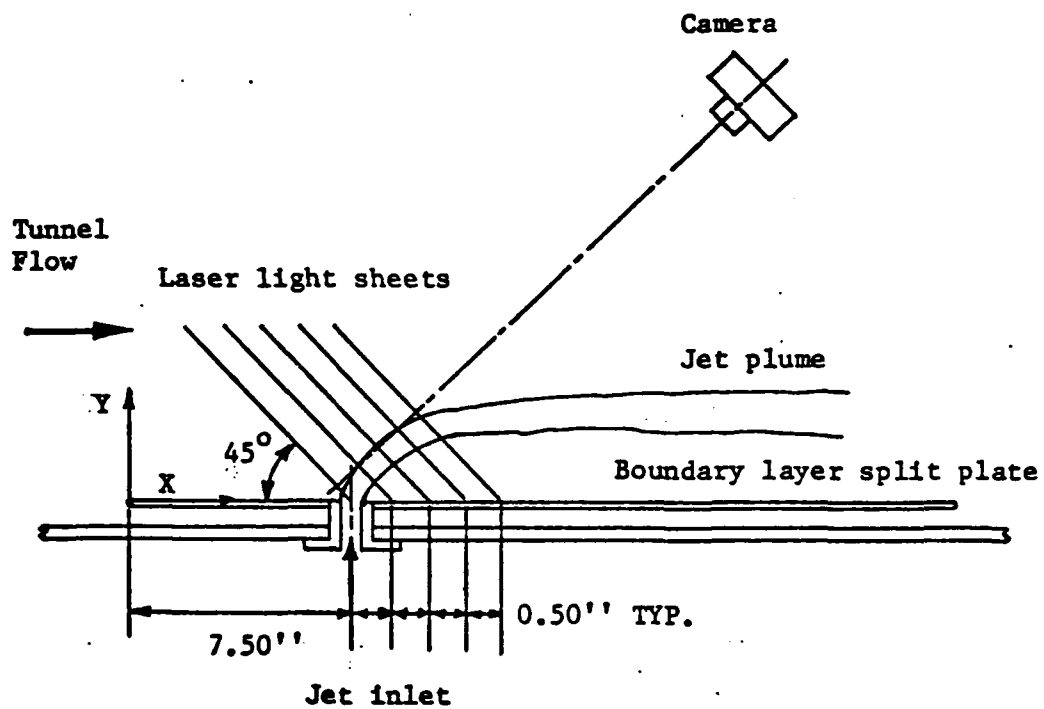
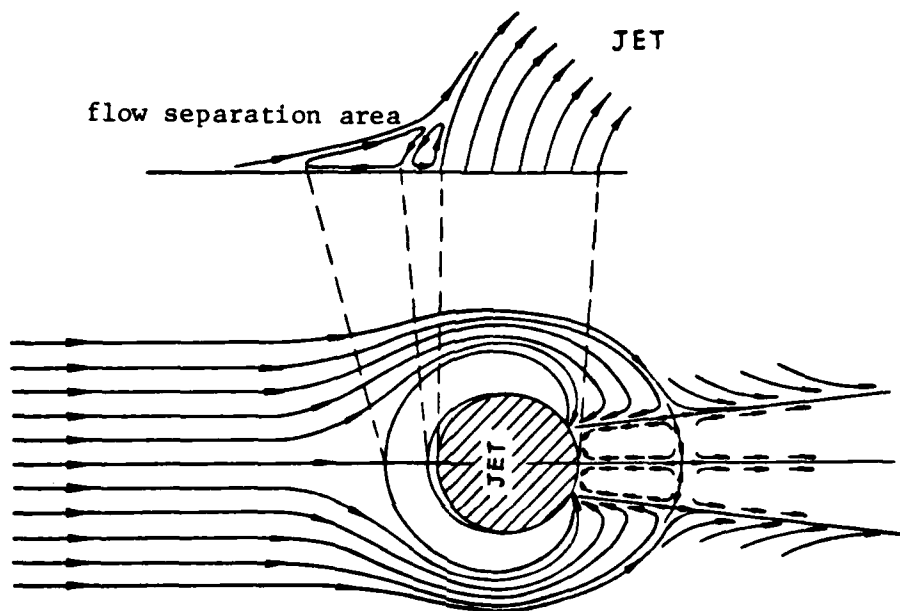


Figure 6. The arrangement of Laser induced fluorescent flow visualization of sectional view of jet plume.

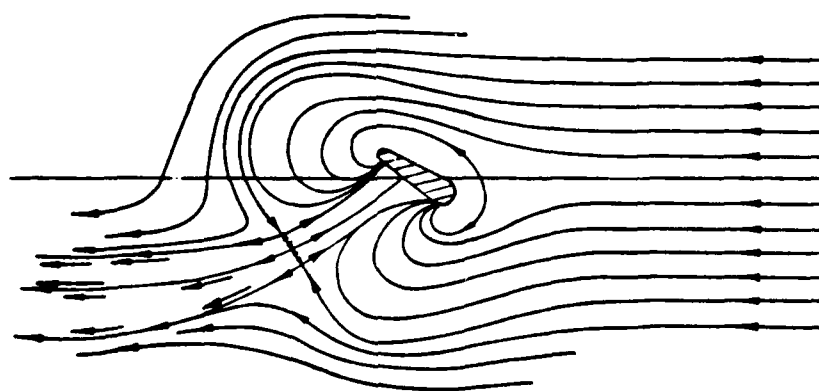
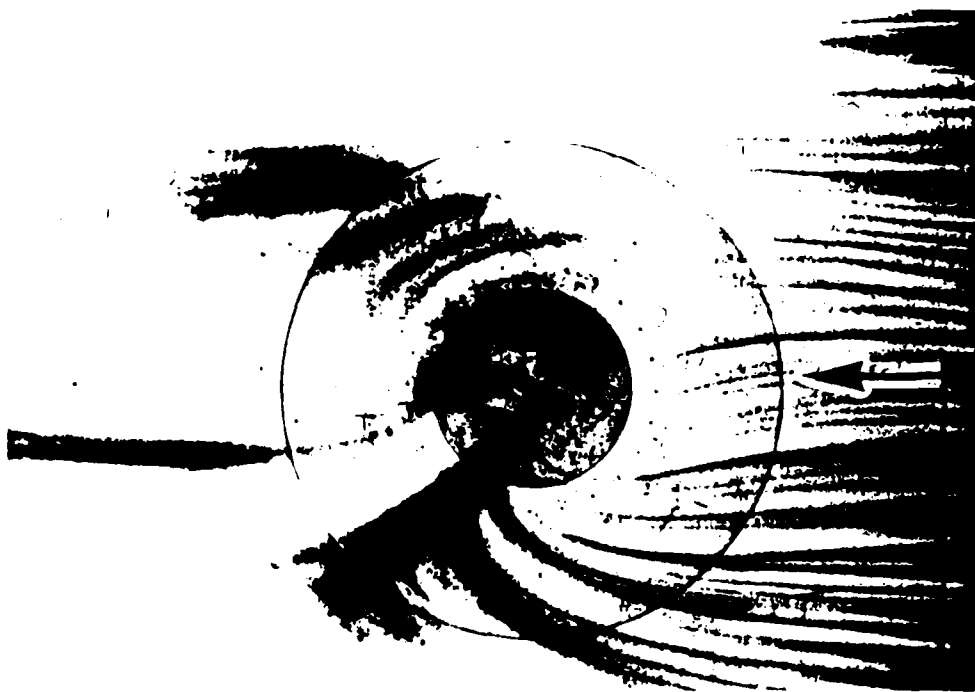


Figure 7. Flow in the downstream of the jet model 4 indicating various steady vortices:  
 $V_j/V_\infty = 3.7$ ,  $\beta = 30^\circ$ ,  $Re_t = 240$ .



(a) circular jet

Figure 8. Surface flow pattern and flow separation zone in front of jet.



(b) tear-drop shape jet

Figure 8. Surface dye flow pattern around jet model 3;  $V/V_j = 9.0$ ,  $\beta = 31$ ,  
 $Re_j = 240$ . (Continued)

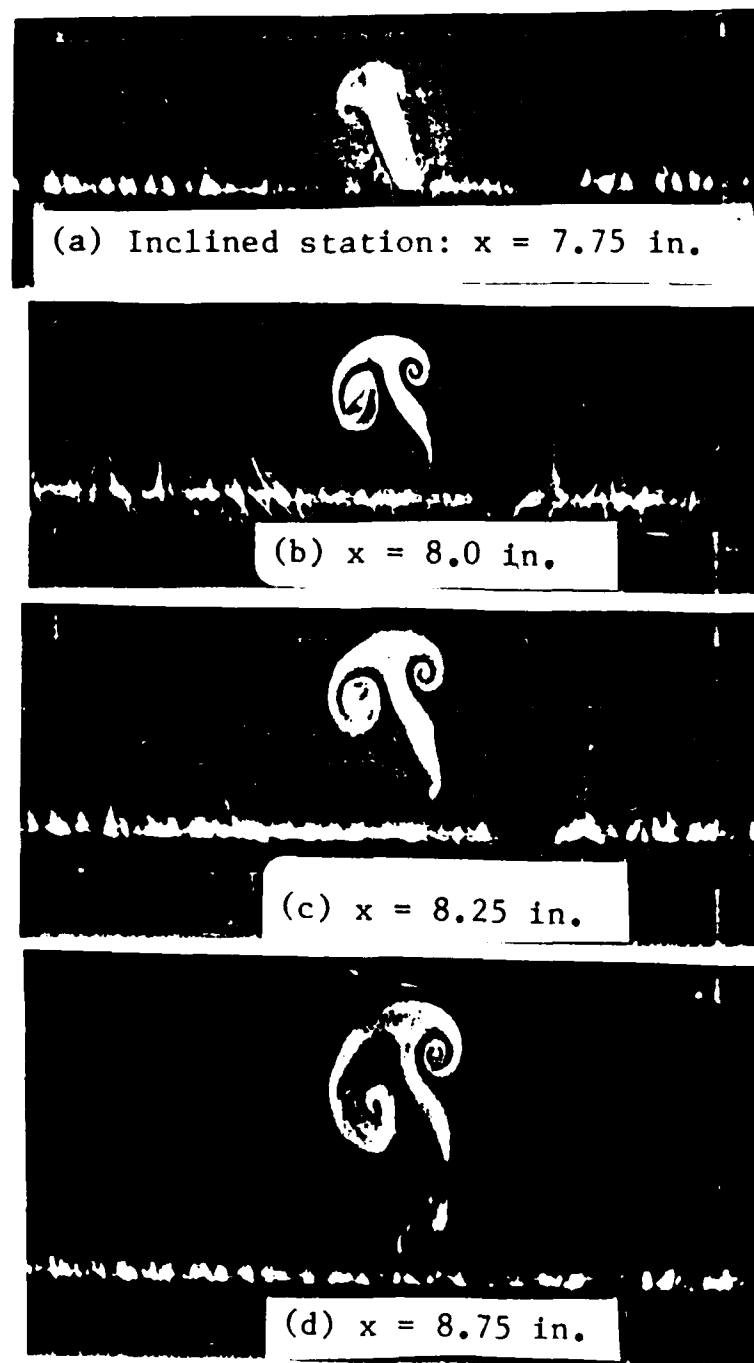


Figure 9. The sectional view of the evolution of jet stream in crossflow of  $45^\circ$  inclined planes at discrete downstream stations:  $V = V_{cr} = 2.0$ ,  $\beta = 20^\circ$ ,  $Re_L = 470$ ; model 3.

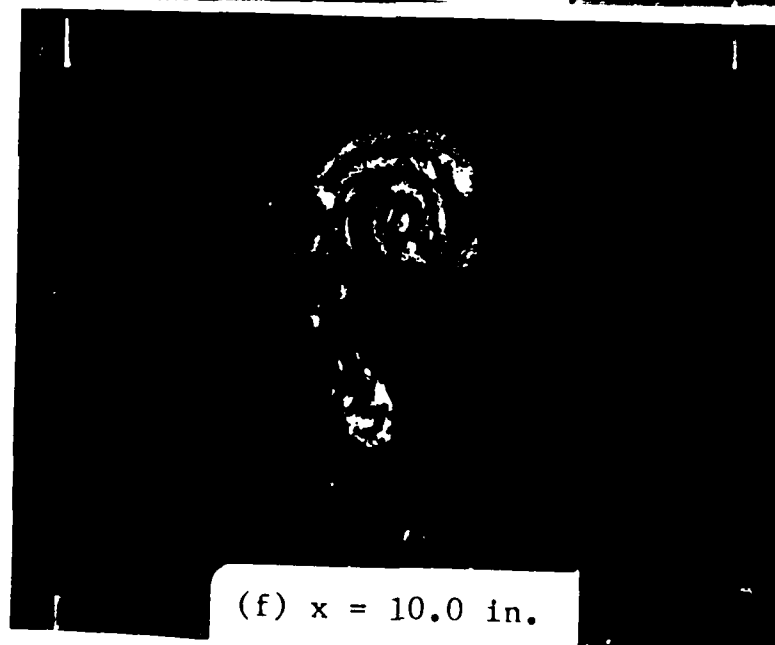
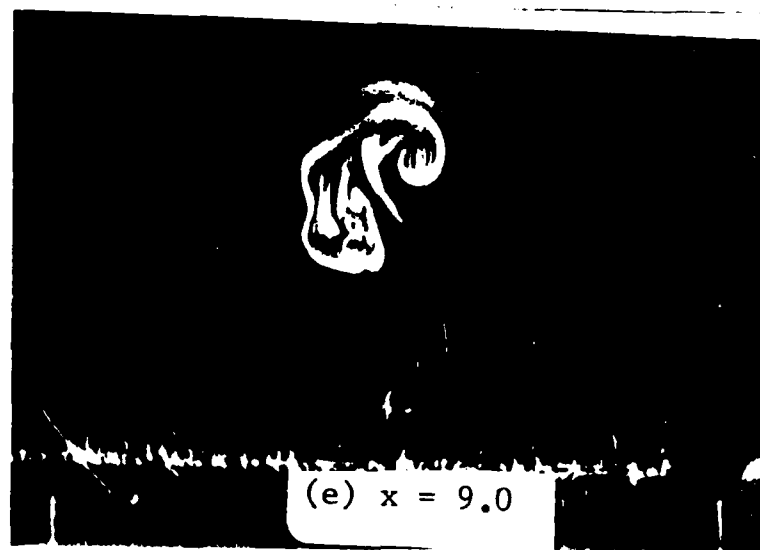
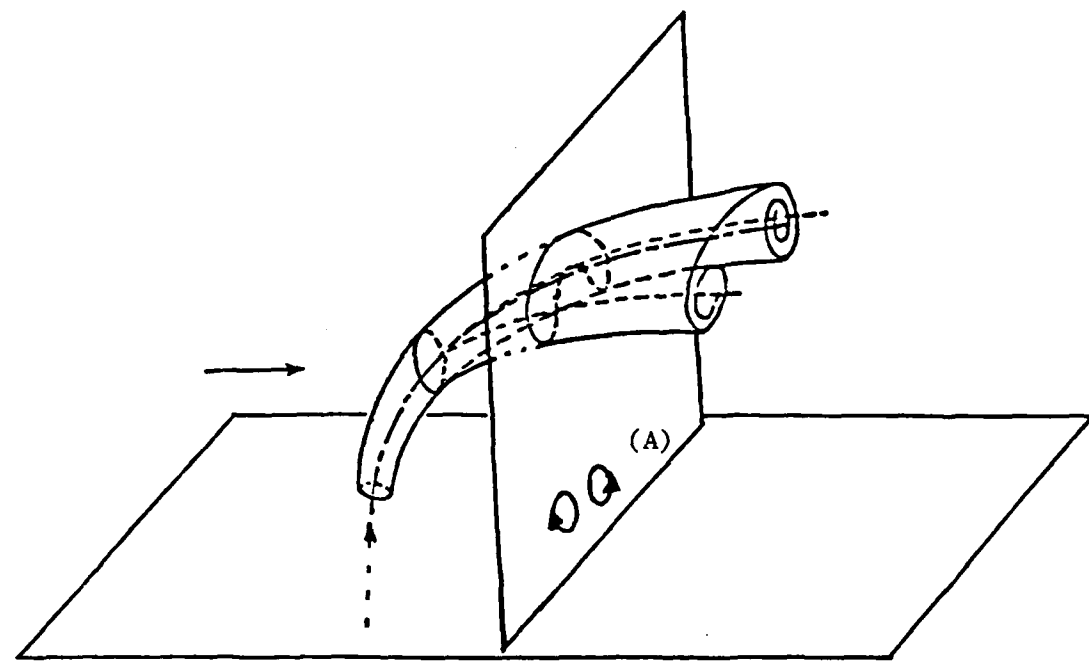
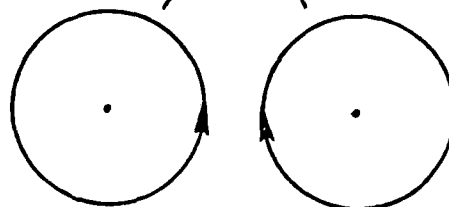


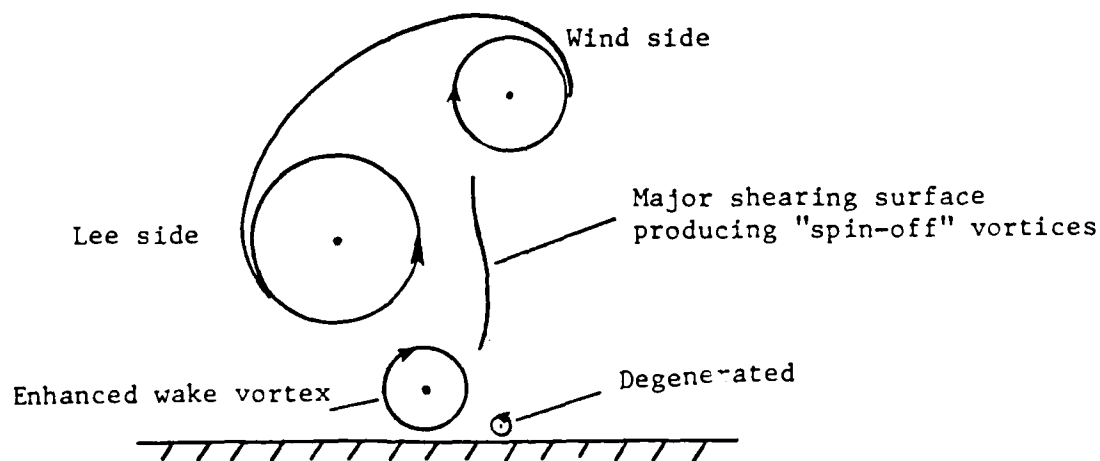
Figure 9. (Continued)



Counter rotating jet vortices



(b) Vertical sectional view of asymmetric jet in crossflow



(a) Vertical sectional view of circular jet in crossflow

Figure 10. The comparison of jet induced vortices.

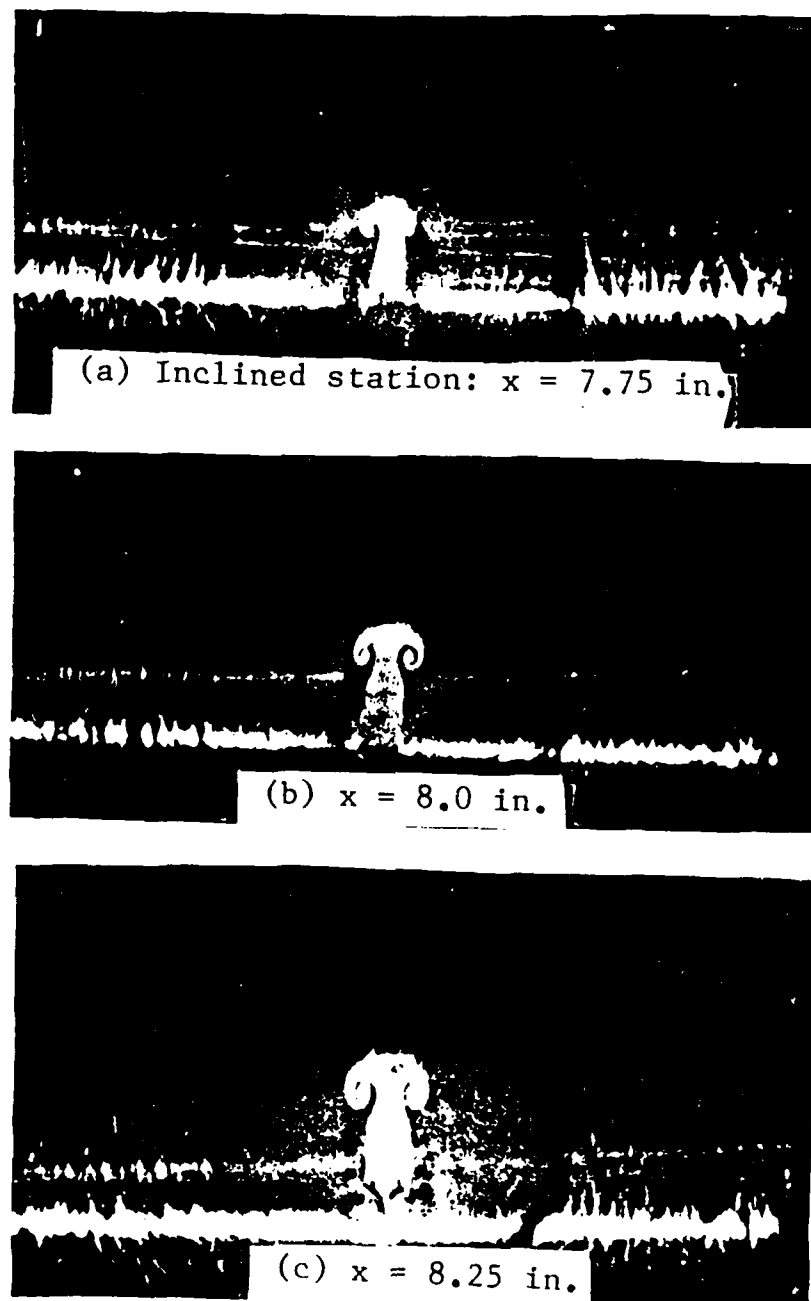


Figure 11. The sectional view of the evolution of jet vortices and shearing on the jet side surface with  $45^\circ$  inclined cutting planes:  
model 3,  $V_j/V_\infty = 2.0$ ,  $\beta = 180^\circ$ ,  $Re_j = 170$ .

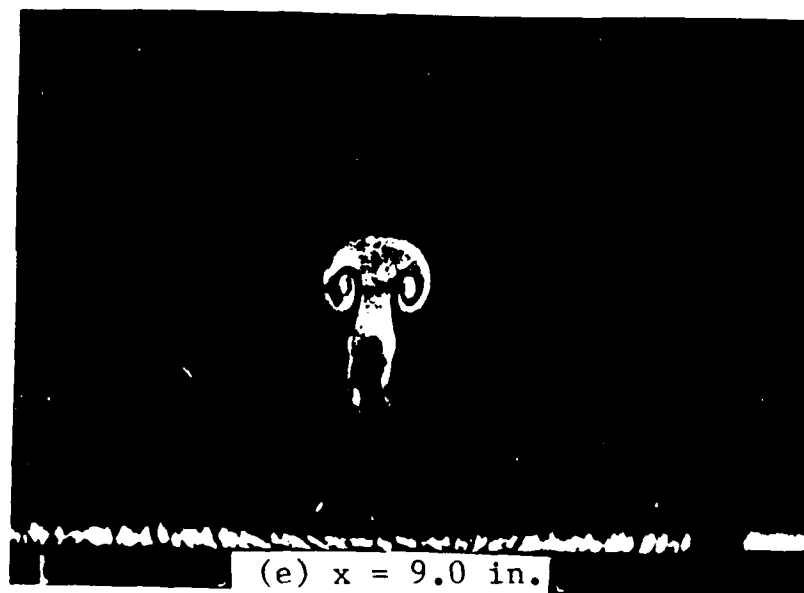
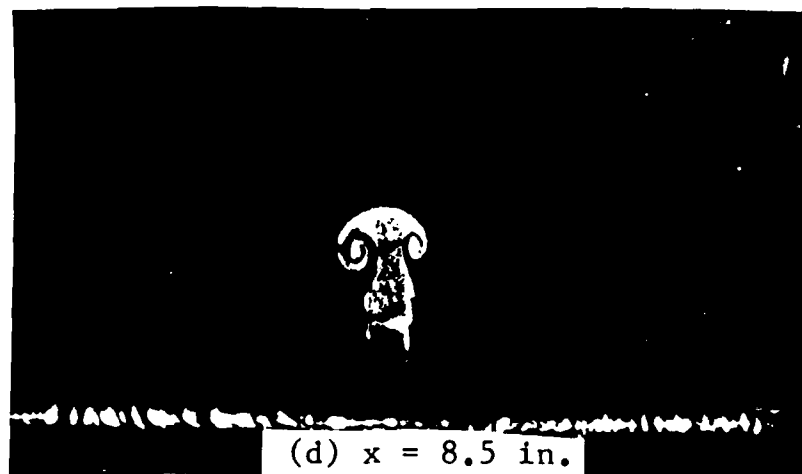
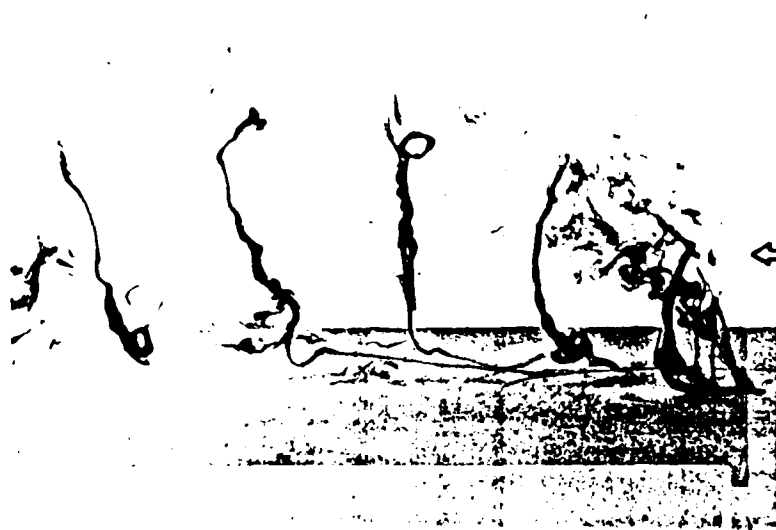


Figure 11. (Continued)



(a) Overall view



(b) Close-up view

Figure 12. Periodically shed "spin-off" vortices in the downstream of jet model 3:  
 $V_j/V_\infty = 3.3, \beta = 20^\circ, Re_L = 240$ .

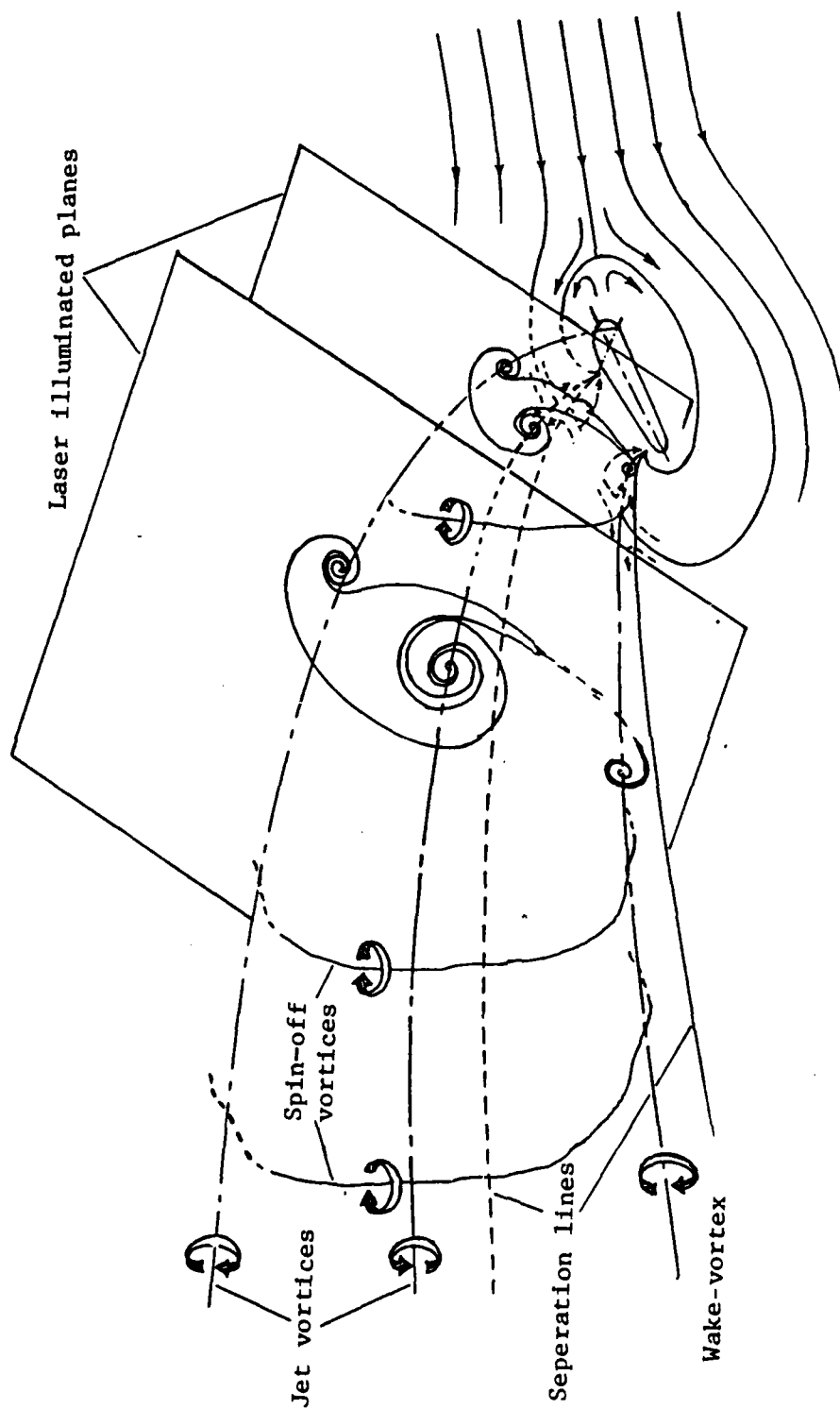


Figure 13. Schematic of the flow field of yawed jet in crossflow.



(a) Without excitation.



(b) With excitation.

Figure 14. Artificially induced spin-off vortices with oscillating fin behind jet port;  $V_j/V_\infty = 2.5$ ,  $\beta = 10^\circ$ ,  $Re_d = 540$ , model 3.

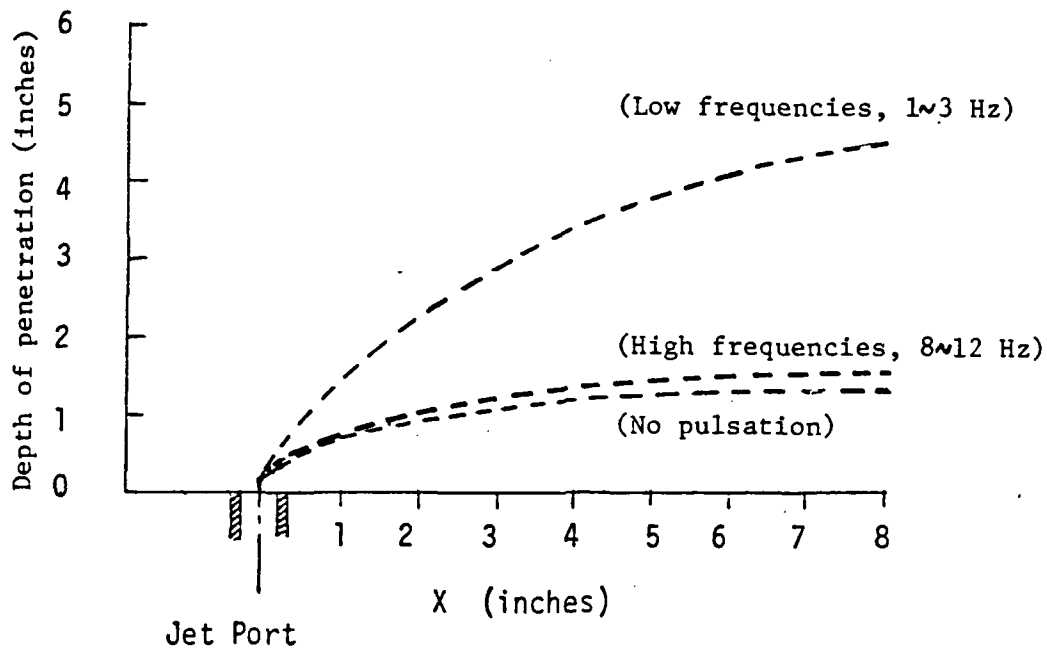


Figure 15. Jet plume centerline trajectory with pulsating jet stream; model 3,  $V_j/V_\infty = 4.7$ ,  $\beta = 45^\circ$ ,  $Re_d = 470$ .

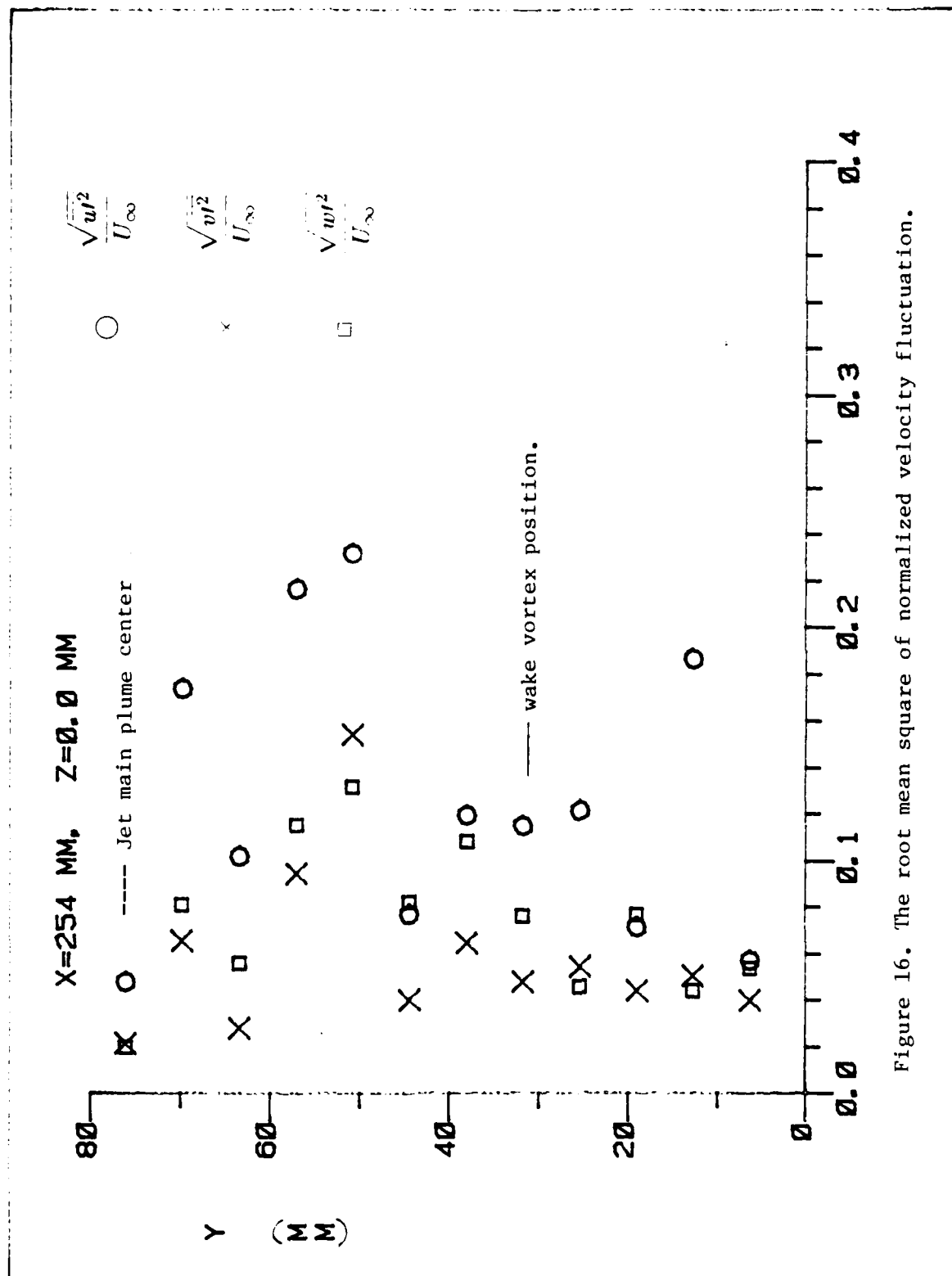


Figure 16. The root mean square of normalized velocity fluctuation.

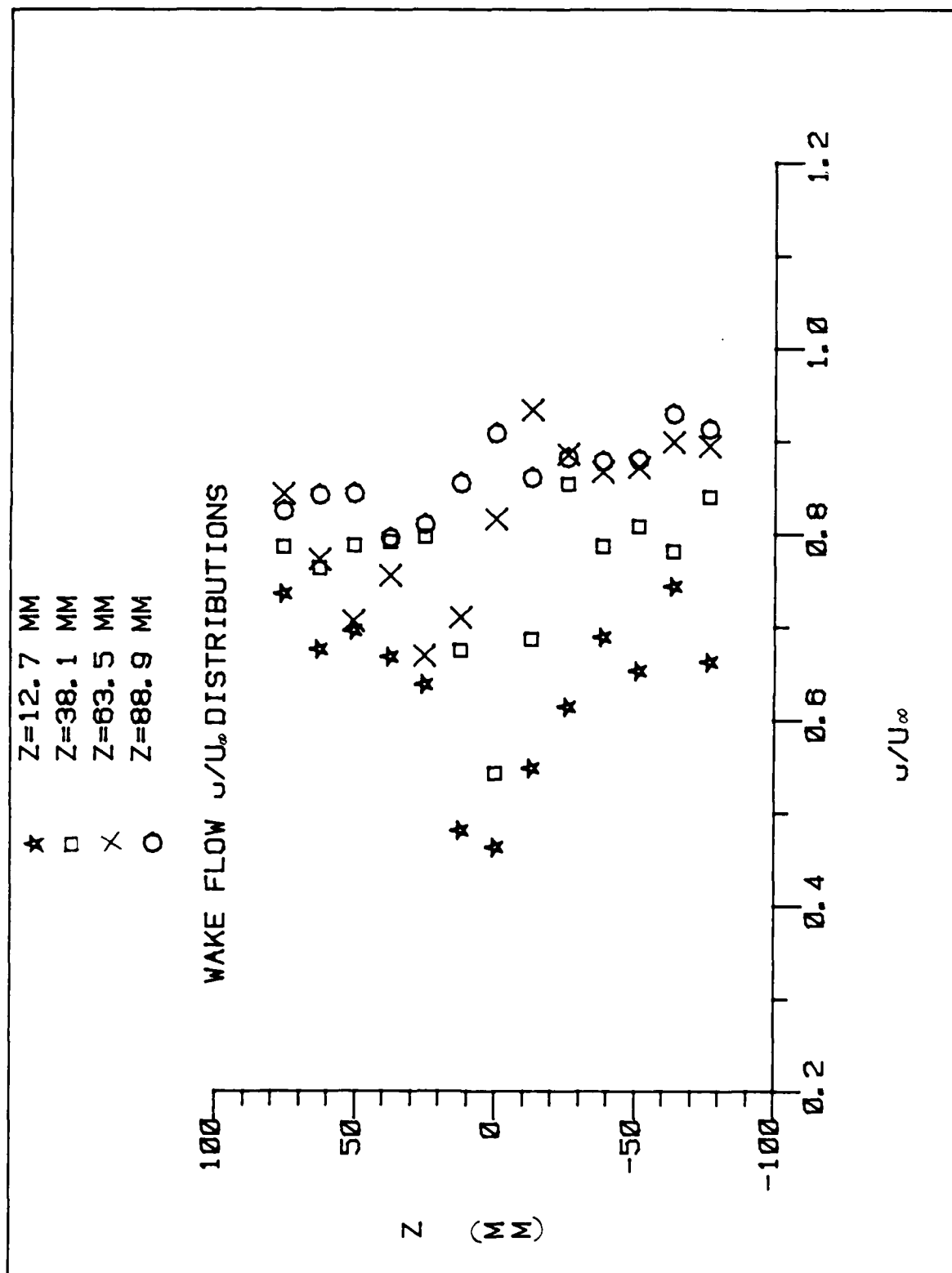


Figure 17. The velocity distribution of  $u/U_\infty$  at various distance above boundary layer split plate.

## Appendix A

### CALIBRATION OF THREE-COMPONENT HOT-FILM ANEMOMETER

The calibration of anemometer was done by towing the hot-film probe through water tunnel with opening top wall and sationary water at various constant probe speeds. The advantages for this arrangement are that the water to probe relative velocity is measured directly and the time of calibration is sufficiently short for measurement to be made above or below the ambient temperature without any form of temperature control being required.

The calibration appratus is shown on Figure A-1. The probe to be calibrated is mounted on a carriage which runs on the rails and is attached to an aluminum drive drum and an idle drum through a steel wire. This wire is wounded on both drum with two ends fixed on opposite side of the carrage. With this way any rotational movement of drive drum is immediately reflected as longitudinal movement of the carrage. The motion is provided by a D. C. Servo motor generator with a close loop controler. The drive drum is connected to motor directly. The speed of carriage is selected from a potential meter on the motor controler for a speed range of 15 mm/sec to 570 mm/sec. The frequency at which runs can be repeated is determined by the period required for the water to subside to an acceptable level, generally no more than 2 minutes.

The first requirement for the calibration of three-component hot-film anemometer is to find the characteristic constants of each hot-film component which is placed in the flow without any pitch angle or yaw angle. This is done by the combination of pitch, yaw and roll mechanisms built on the probe carriage. With the proper arrangement of these mechanisms every hot-film component can be set perpendicular to the relatively on coming flow.

The calibration of this probe is on the component basis, that means each time we can work with one hot-film component only. The velocity range for our calibration is 15 mm/sec to 500 mm/sec. With the equipments mentioned in Chaper II, the output voltage of anemometer is digitized and stored in the computer. A data reduction program was written which fit the anemometer

output voltage  $V$  to the constant probe speed  $U$  to an expression of the form as

$$V^2 = A + BU^N, \quad (A1)$$

where it is assuming that  $V$  is the only parameter in error. A linear regression analysis between  $V^2$  and  $U^N$  was done in the data reduction program by considering  $N$  as a constant and being selected to give the best correlation coefficient (i.e.,  $r > |0.999|$ ). With this analysis the characteristics constants  $A$ ,  $B$  and  $N$  for each hot-film component were determined. The calibration curves with anemometer output voltage versus probe speed are shown on Figure A-2. The continuous solid line on the figure is the best fit curve of equation (A1). The characteristics constant for all three components of probe at  $T = 25^\circ\text{C}$  are tabulated on Table A-1.

Table A-1. The Component Calibration Constants

Hot-Film Component	A	B	N
No. 1	-0.9823	3.4774	0.3000
No. 2	-0.6069	3.3148	0.3000
No. 3	-2.0679	3.8789	0.3000

It should be noted that above tabulated calibration constants are done at one specified fluid temperature. However, during the measurement the fluid temperature can not be always the same as the calibration fluid temperature. Thus the effect of temperature drift on hot-film measurement should be take into account. This effect was noted by Bearman (1971) for hot-wire measurement in incompressible flow. The similar effect for hot-film probe measurement in incompressible fluid flow is derived as following.

Let temperature of fluid be  $T_o$ , equation (A1) can be written as

$$V(T_o)^2 = A + BU^N. \quad (A2)$$

When temperature of fluid is  $T$ , it becomes

$$V_m(T)^2 = A_1 + B_1U^N. \quad (A3)$$

where  $V_m(T)$  is the measured anemometer output voltage and

$$\frac{A}{A_1} = \frac{B}{B_1} = \frac{T_F - T_0}{T_F - T}$$

Let

$$\frac{T_0 - T}{T_0} = \epsilon$$

and

$$\frac{T_F}{T_0} = \theta \quad \text{over heat ratio,}$$

then

$$\frac{A}{A_1} = \frac{B}{B_1} = \frac{\theta - 1}{\theta - 1 + \epsilon} = \frac{\sigma}{\sigma + \epsilon} \quad (\text{A4})$$

where  $\sigma = \theta - 1$ .

Substituting equation (A4) into equation (A3) gives

$$V_m(T)^2 = A \frac{(\sigma + \epsilon)}{\sigma} + B \frac{(\sigma + \epsilon)}{\sigma} U^N \quad (\text{A5})$$

Now let

$$V_m(T) = V_c(T) + \delta V \quad (\text{A6})$$

where  $V_c(T)$  is the bridge voltage in the absence of any temperature change. Substituting equation (A6) into equation (A2), it becomes

$$(V_c(T) + \delta V)^2 = A + B U^N \quad (\text{A7})$$

and combining equation (A5) and (A7)

$$V_m(T)^2 = \left(1 + \frac{\epsilon}{\sigma}\right) (V_c(T) + \delta V)^2$$

and

$$V_m(T) = \left(1 + \frac{\epsilon}{\sigma}\right)^{\frac{1}{2}} V_c(T). \quad (\text{A8})$$

If the change in fluid temperature are small compared with the difference between hot-film temperature and fluid temperature. i.e.  $\epsilon/\sigma$  is small. Equation (A8) becomes

$$V_c(T) \cong V_m(T) \left( 1 - \frac{\epsilon}{2\sigma} \right). \quad (B9)$$

This relationship gives the temperature drift correction for the measurement which is done at fluid temperature different from the calibration fluid temperature.

Above realtionships are derived with the assumption that the anemometer output voltage change has a linear relation with the variation of fluid temperature. However, it would be more practical if we can found their relationship through calibration.

It was found by Saunders & Lawrence (1972) that the change in anemometer output with fluid temperature can be expressed with the form as

$$\frac{V(T)}{V(T_o)} = \left[ 1 - \frac{T - T_o}{T_F - T_o} \right]^{\frac{1}{2}}. \quad (A10)$$

where  $T_F$  is hot-film operation temperature,  $T_o$  is the reference temperature and  $T$  is the fluid temperature during measurement. For small temperature variation with respect to reference temperature  $T_o$ , it is adquate to rewrite equation (A2) in the form as

$$\frac{V(T)}{V(T_o)} = 1 - \frac{\Delta T}{2(T_F - T_o)}. \quad (A11)$$

With above formulation, it is possible to describe the approximate temperature dependent of a anmometer with a single constant as

$$M = \frac{1}{2(T_F - T_o)}. \quad (A12)$$

It should be also noted that above relation is only suitable for small temperature deviation to  $T_o$  and do not be confused by its form as a constant.

The calibration of temperature dependence was done by trying to find out the ratio of  $V(T)/V(T_o)$  as function of  $T$  for a number of probe speeds. The calibration results of each hot-film component with five different free stream velocities with three temperature setting are shown on Figure A-3. It can be found from these figures that the temperature gradient does not depend on free stream velocity very much.

With the completion of the calibration of characteristics constants on equation (A1) for each hot-film and the calibration of temperature dependence relationship, the following work need to be done is the angular characteristics calibration of each hot-film to find out the pitch factor and yaw factor of it. With the completion of angular characteristics calibration, than this probe is ready for the measurement in three-dimensional flow field. The mechanism for the measurement of three-dimensional velocity field has been explaint in Chapter II.

The method being used here for finding pitch factor and yaw factor was suggested by Jorgensen (1971). Consider the sketch on Figure A-4. as one component hot-film in a cross-flow, the effective cooling velocity acting on it can be expresses as

$$U_{eff}^2 = U_x^2 + k^2 U_y^2 + h^2 U_z^2. \quad (A13)$$

For a hot-film with zero yaw angle (i.e.,  $\theta = 0$ ), equation (A13) becomes

$$U_{eff}^2(\phi) = U(0)^2 (\cos^2 \phi + k^2 \sin^2 \phi). \quad (A14)$$

For a hot-film with zero pitch angle (i.e.,  $\phi = 0$ ), equation (A13) becomes

$$U_{eff}^2(\theta) = U(0)^2 (\cos^2 \theta + h^2 \sin^2 \theta). \quad (A15)$$

In above equations the parameters  $h$  and  $k$  are defined as

$$h \equiv \text{pitch factor}$$

$$k \equiv \text{yaw factor.}$$

With the calibration constants of equation (A1) and the anemometer output voltage, the pitch factor and yaw factor can be calculated from the following

relations, they are derived from the combination of equations (A1), (A14) and (A15).

$$h = \frac{1}{\sin \theta} \left[ \left( \frac{V^2(\theta) - A}{V^2(0) - A} \right)^{\frac{2}{N}} - \cos^2 \theta \right]^{\frac{1}{2}}. \quad (A16)$$

$$k = \frac{1}{\sin \phi} \left[ \left( \frac{V^2(\phi) - A}{V^2(0) - A} \right)^{\frac{2}{N}} - \cos^2 \phi \right]^{\frac{1}{2}}. \quad (A17)$$

The calibration results of yaw factor and pitch factor for three hot-film components are shown on Figure A-5 and Figure A-6 respectively.

All of these results of yaw factor and pitch factor are tabulated on a look-up table and stored in the computer for the measurement data reduction program to call-up.

### References for Appendix A

Saunders L. J. and P. Lawrence (1972). "Calibration of Hot-film Anemometers," Proceedings of the DISA Conference on Fluid Dynamics Measurements in the Industrial and Medical Environments. Leicester University Press, pp. 125-130.

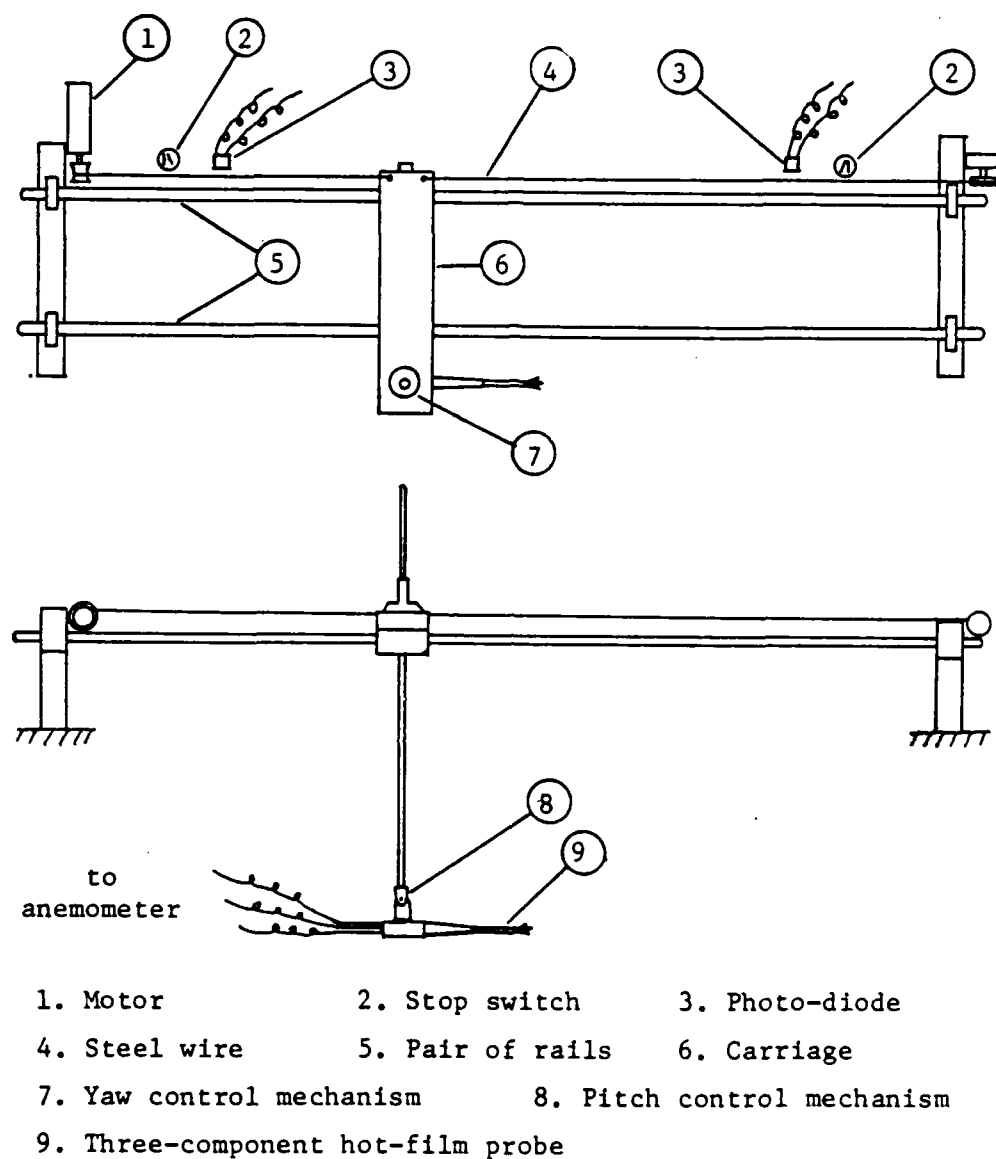


Figure A-1 The calibration apparatus for three-component hot-film probe.

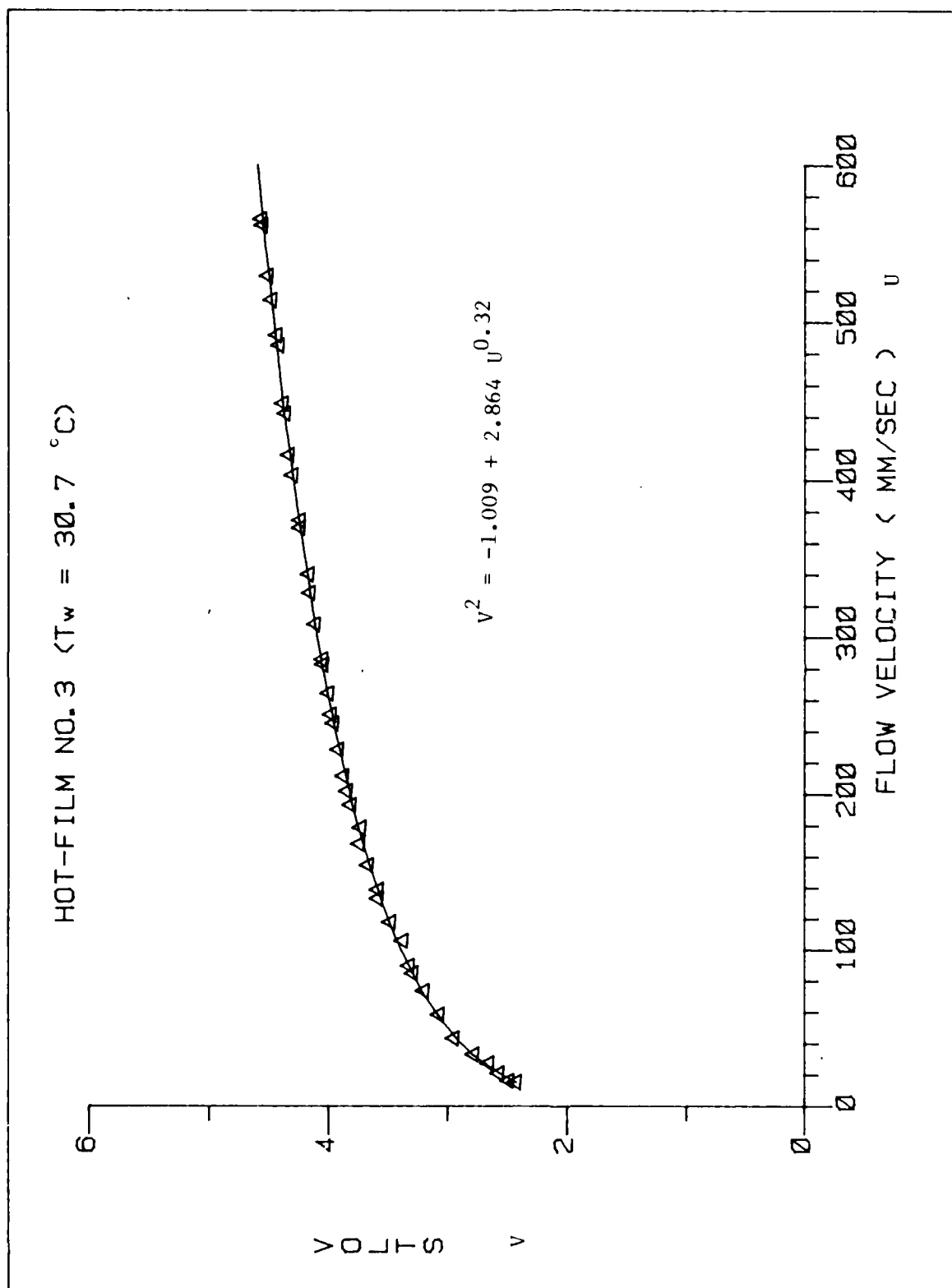


Figure A-2 (Continued)

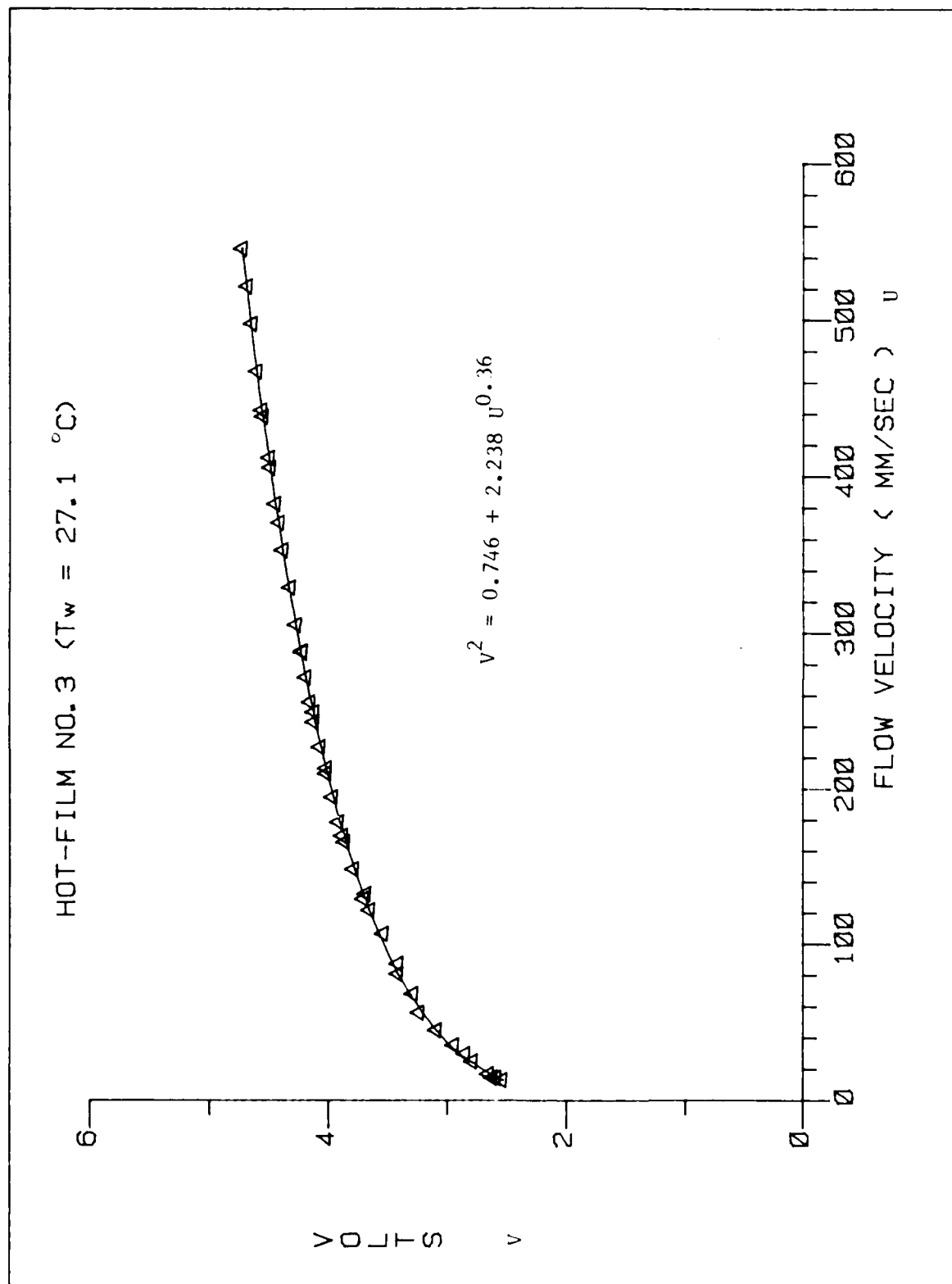


Figure A-2 (Continued)

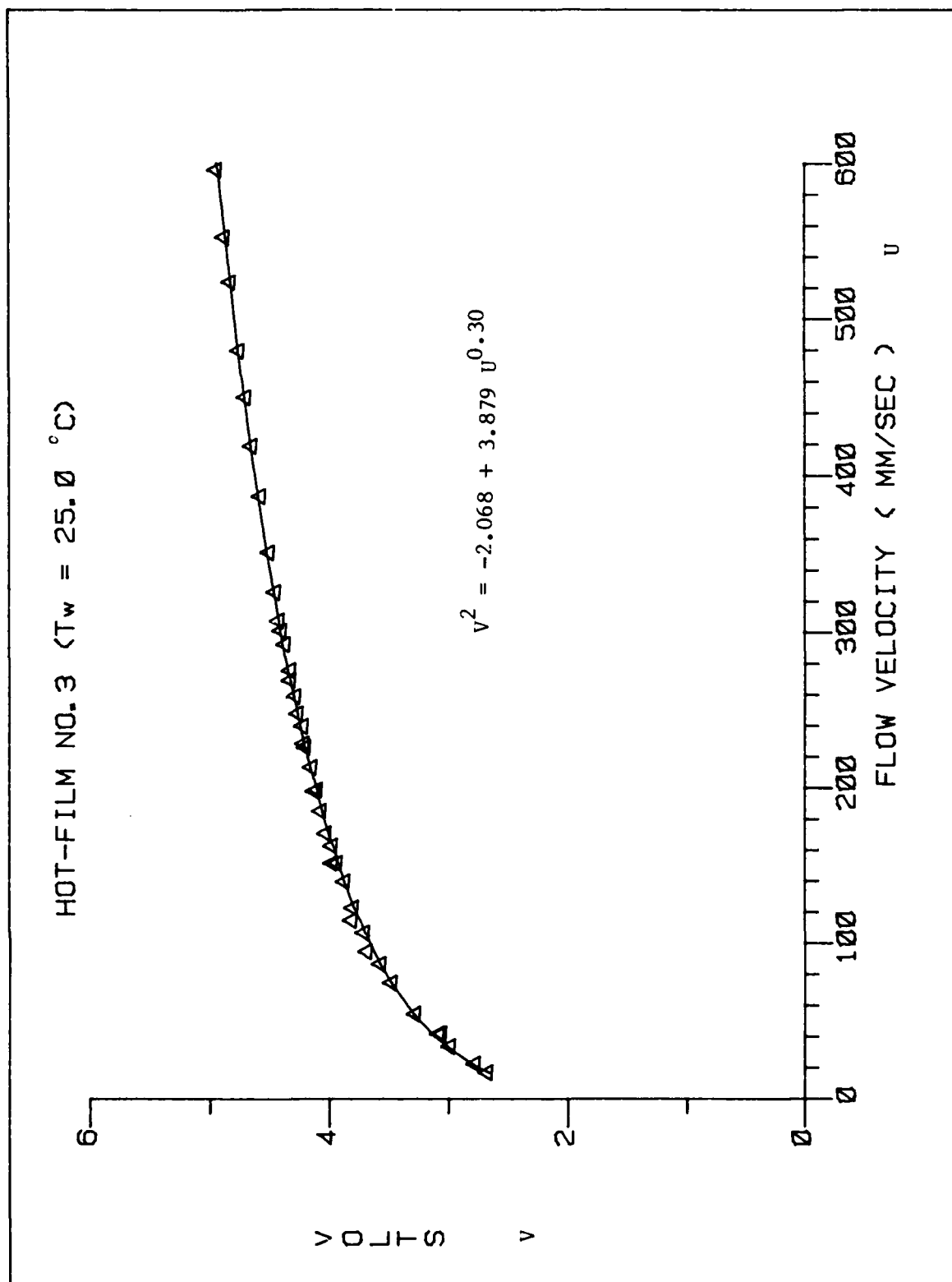


Figure A-2 (Continued)

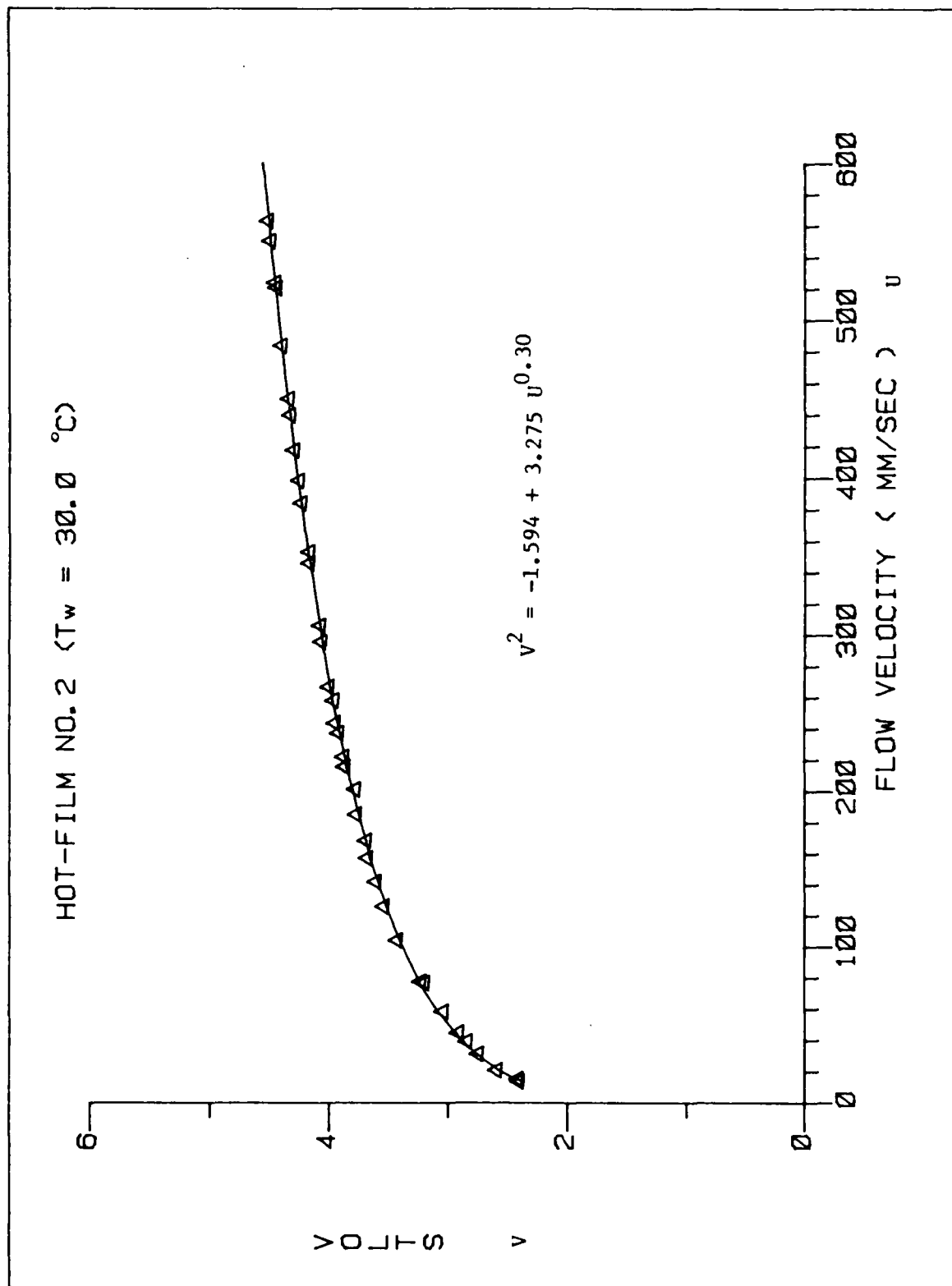


Figure A-2 (Continued)

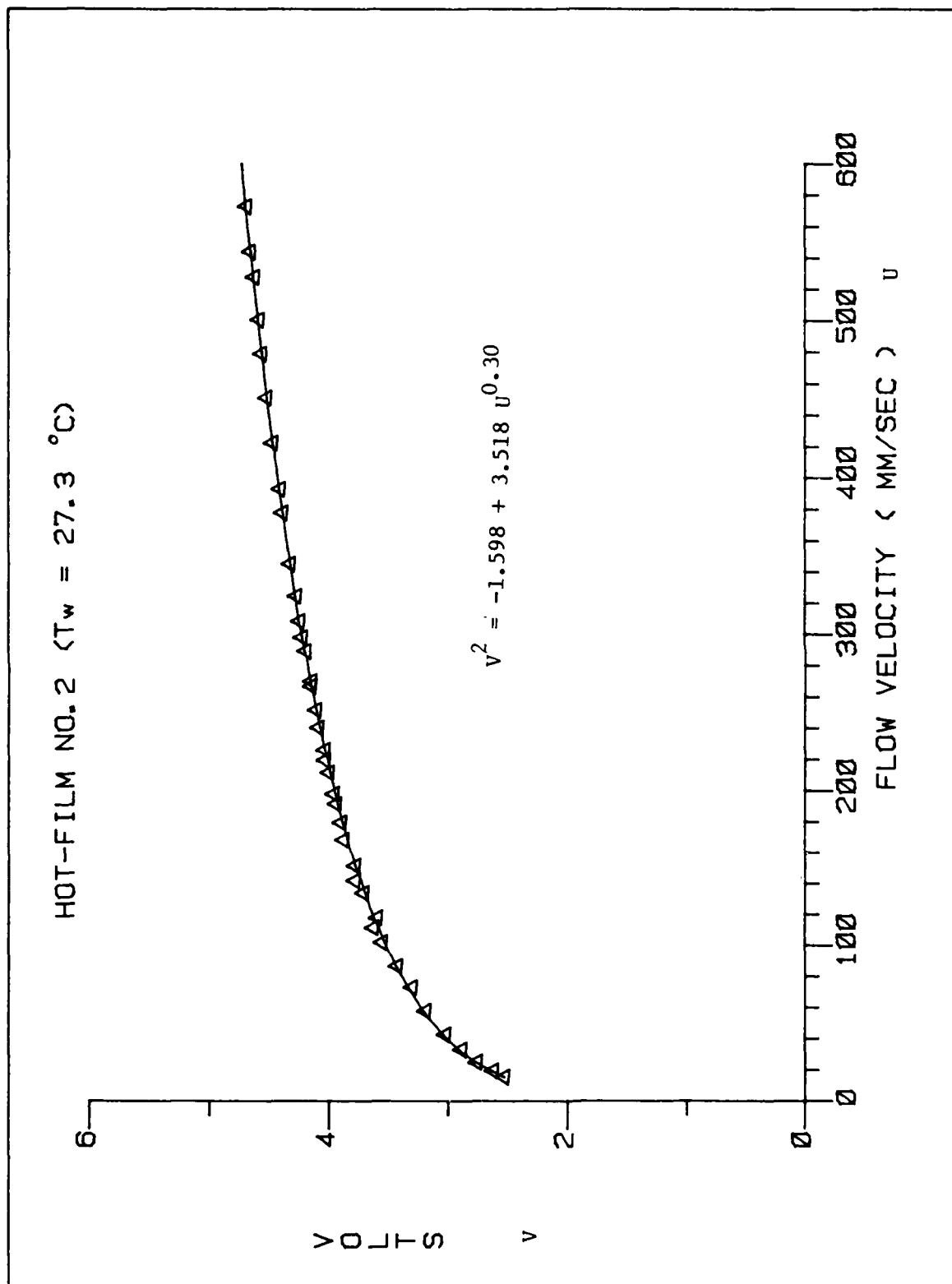


Figure A-2 (Continued)

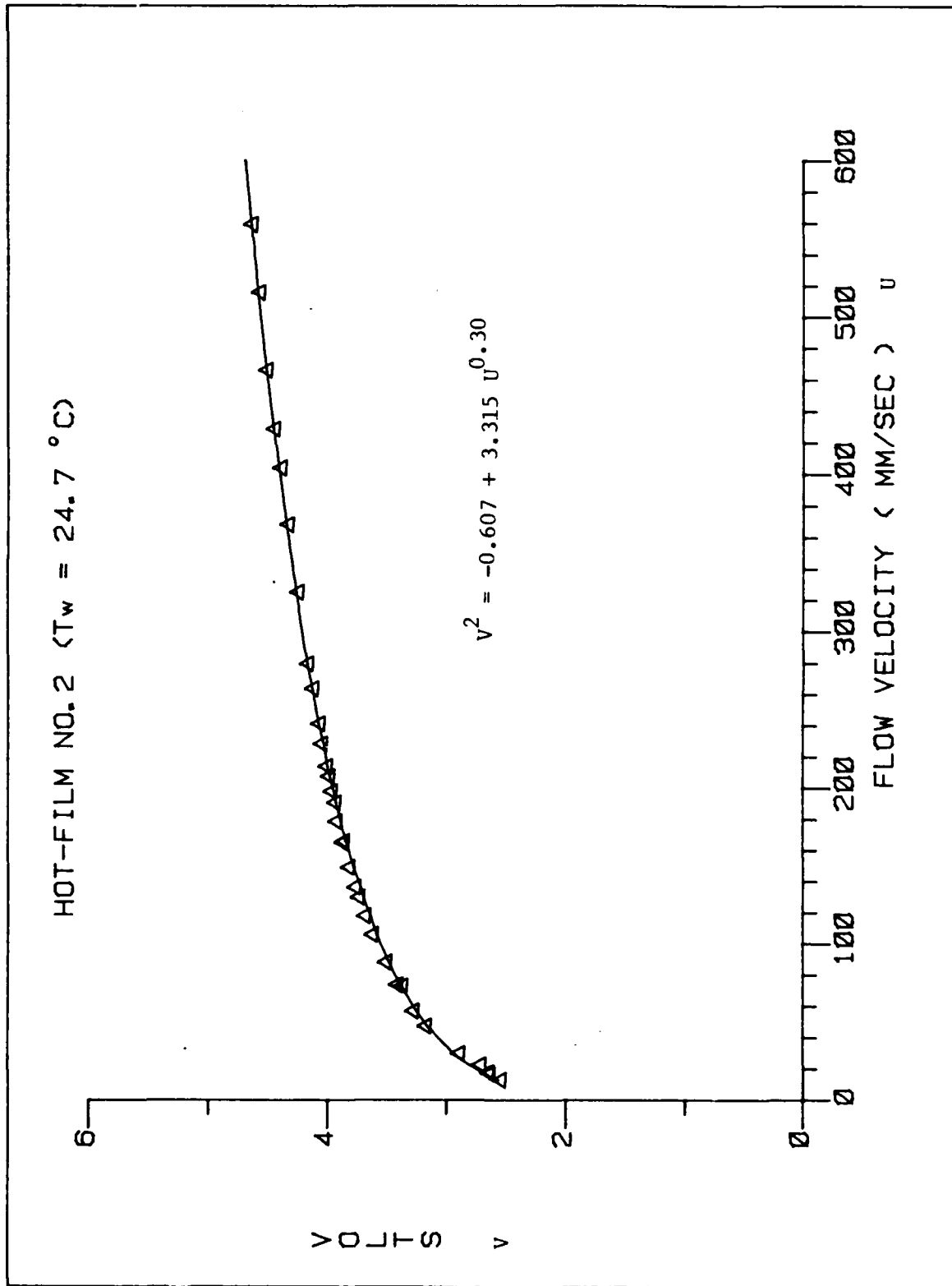


Figure A-2 (Continued)

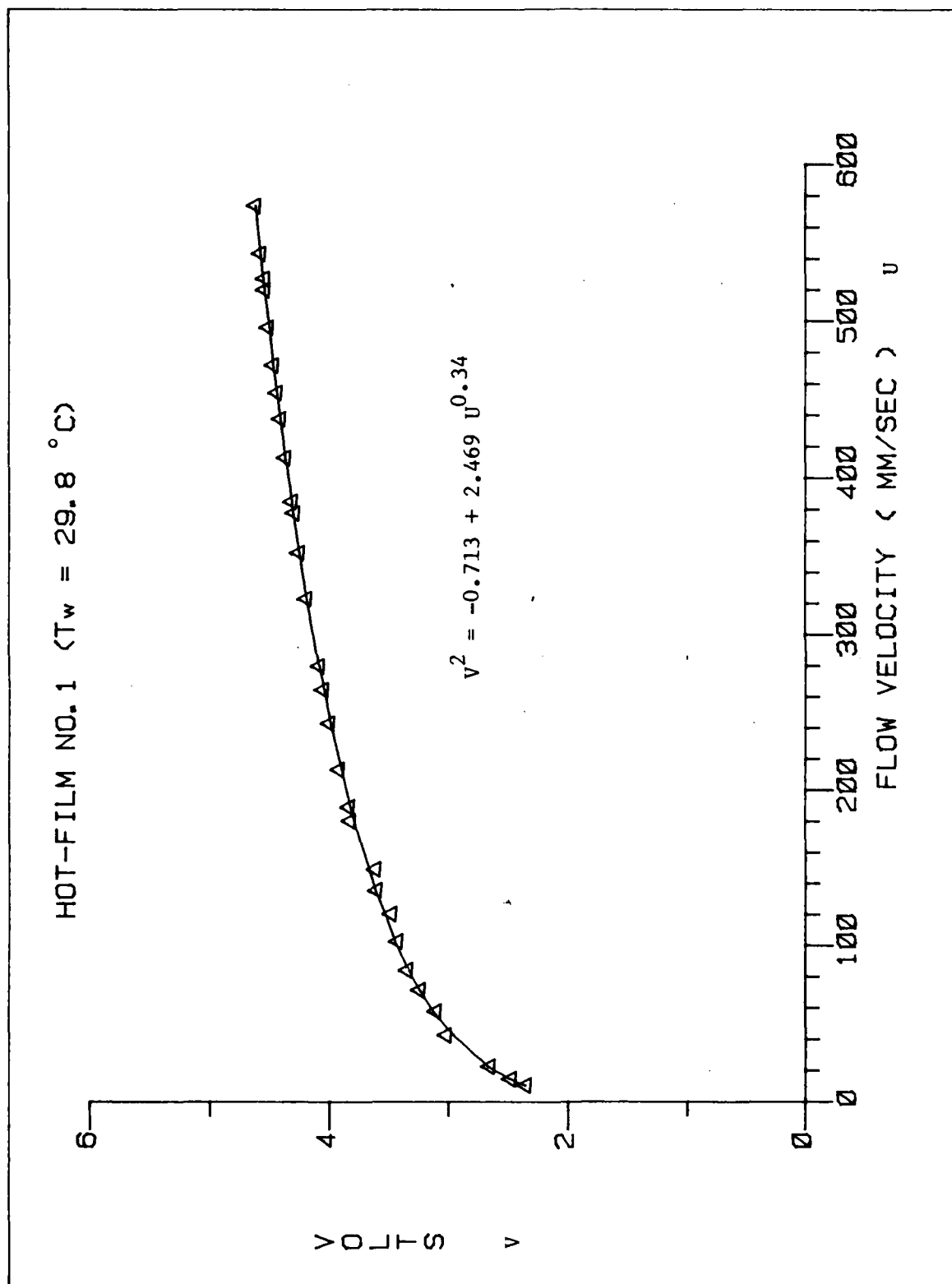


Figure A-2 (Continued)

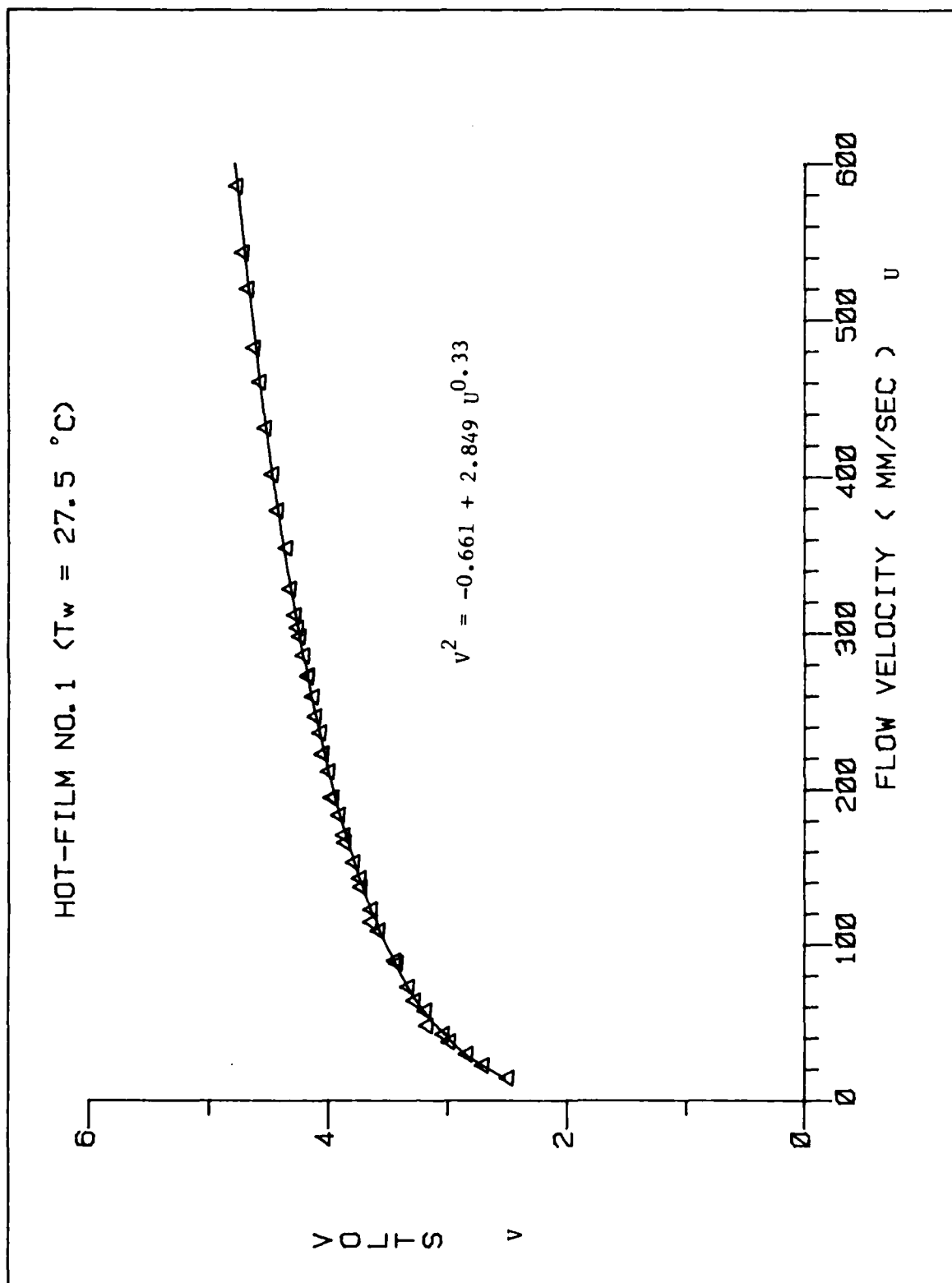


Figure A-2 (Continued)

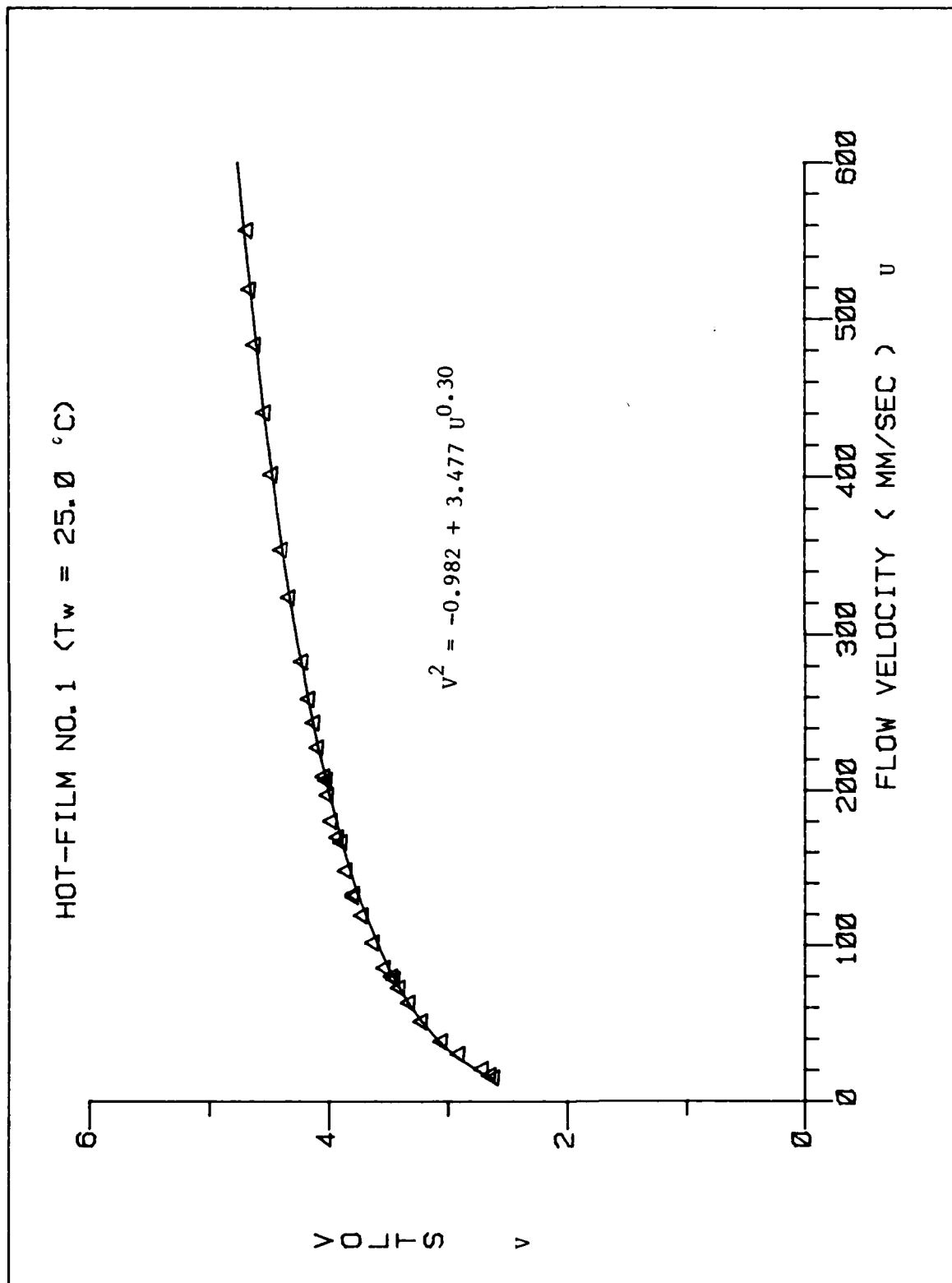


Figure A-2 Hot-film probe components calibration curves.

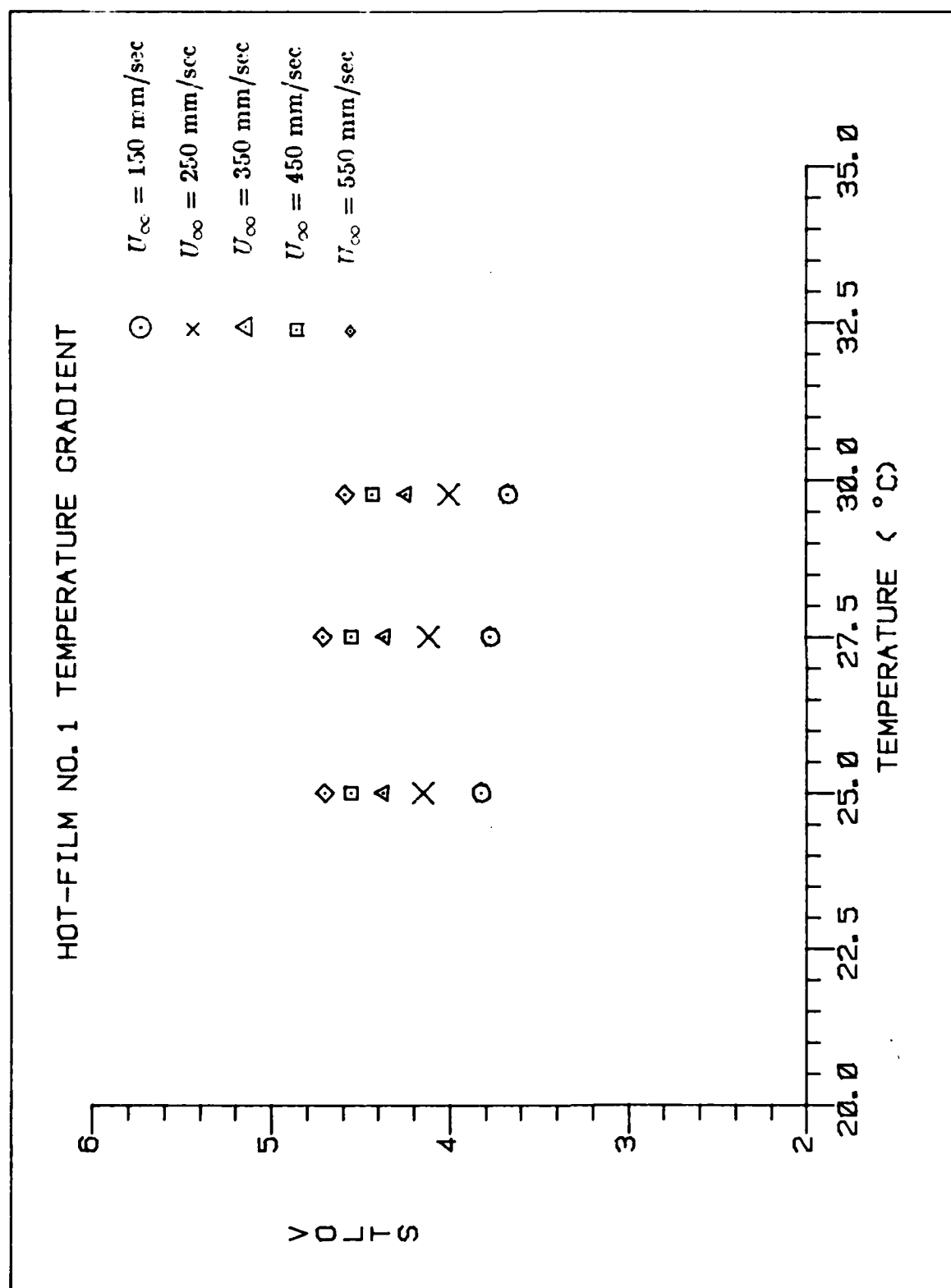


Figure A-3 Temperature gradient calibration results.

# HOT-FILM NO. 2 TEMPERATURE GRADIENT

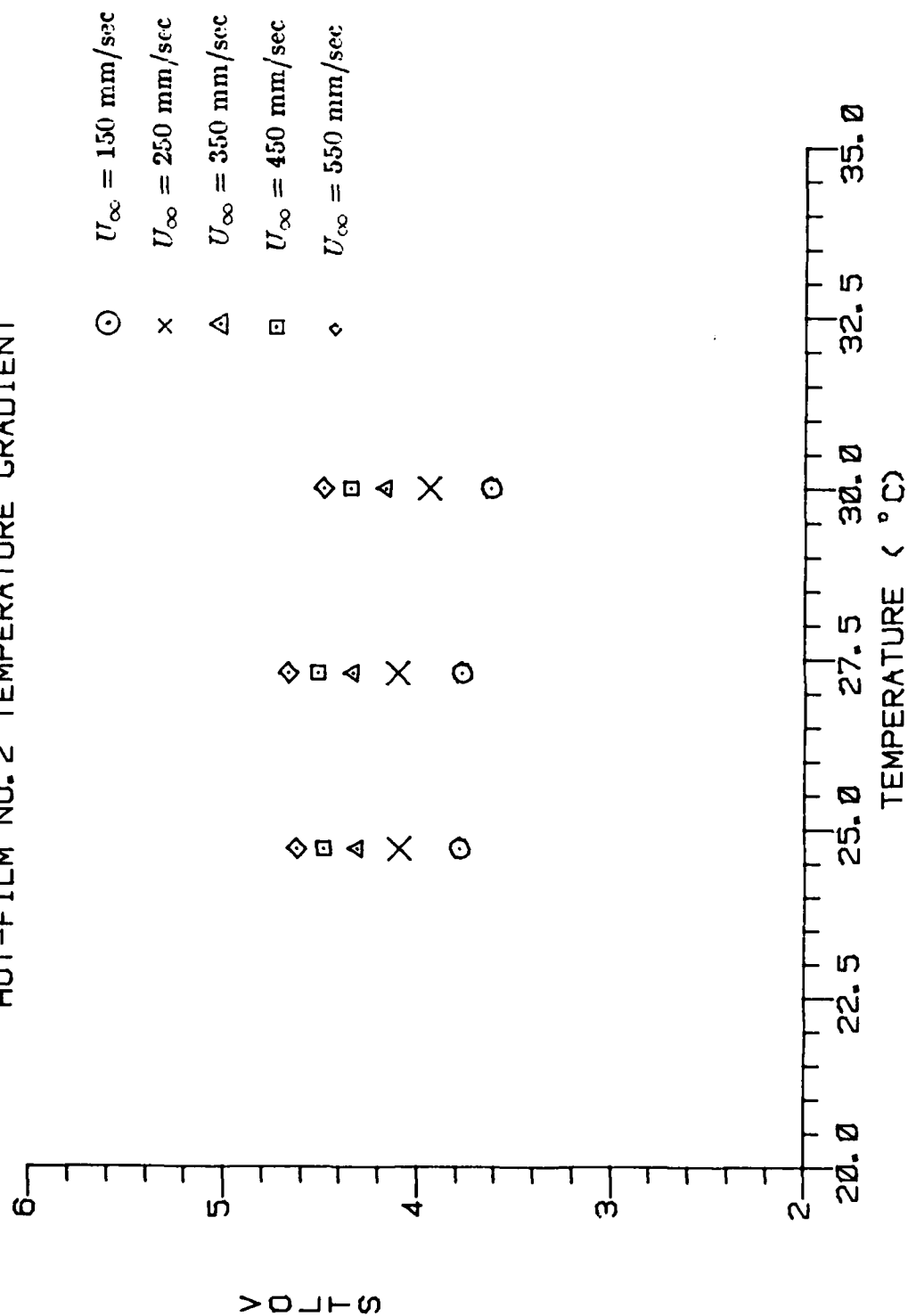


Figure A-3 (Continued)

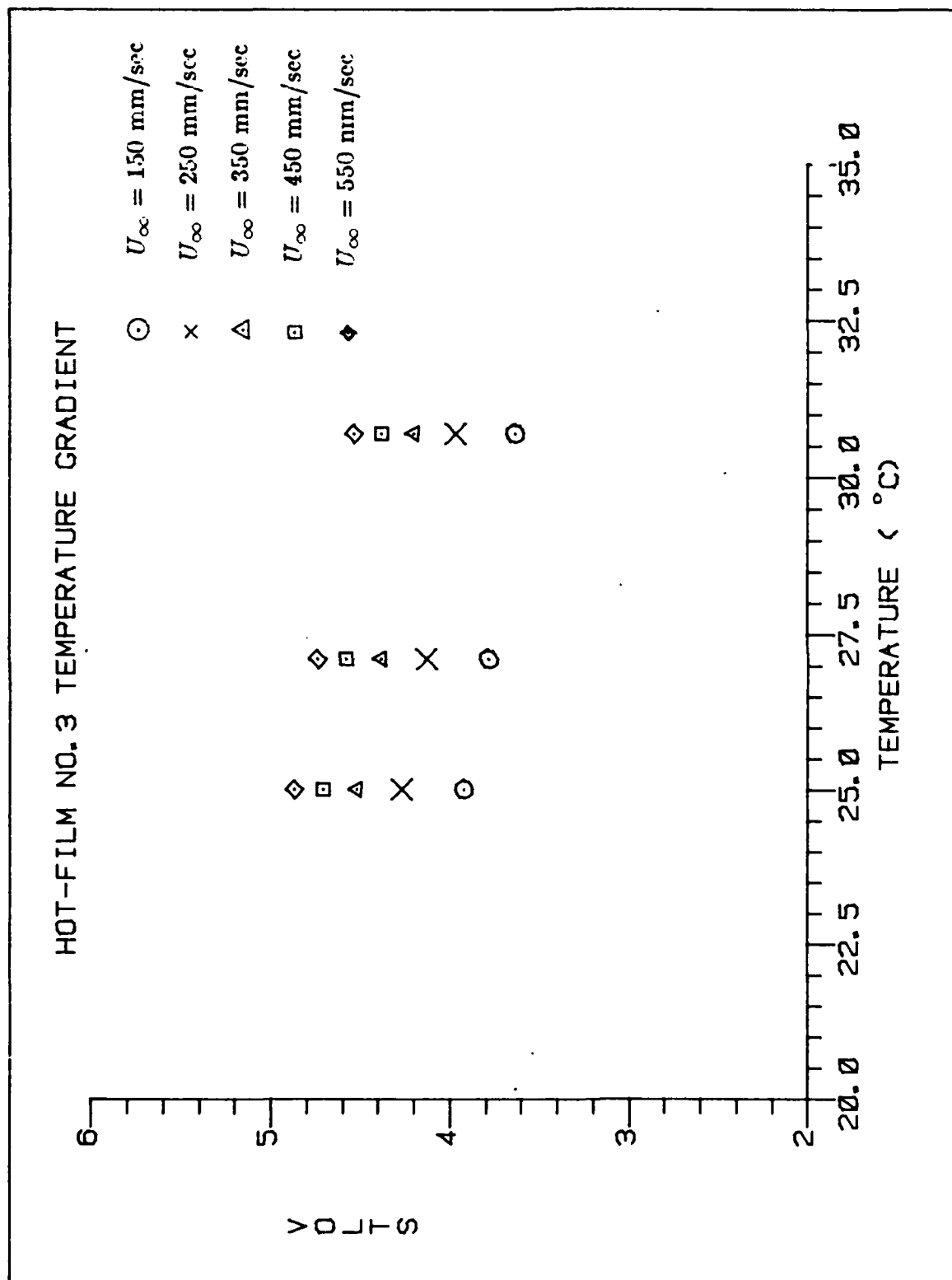


Figure A-3 (Continued)

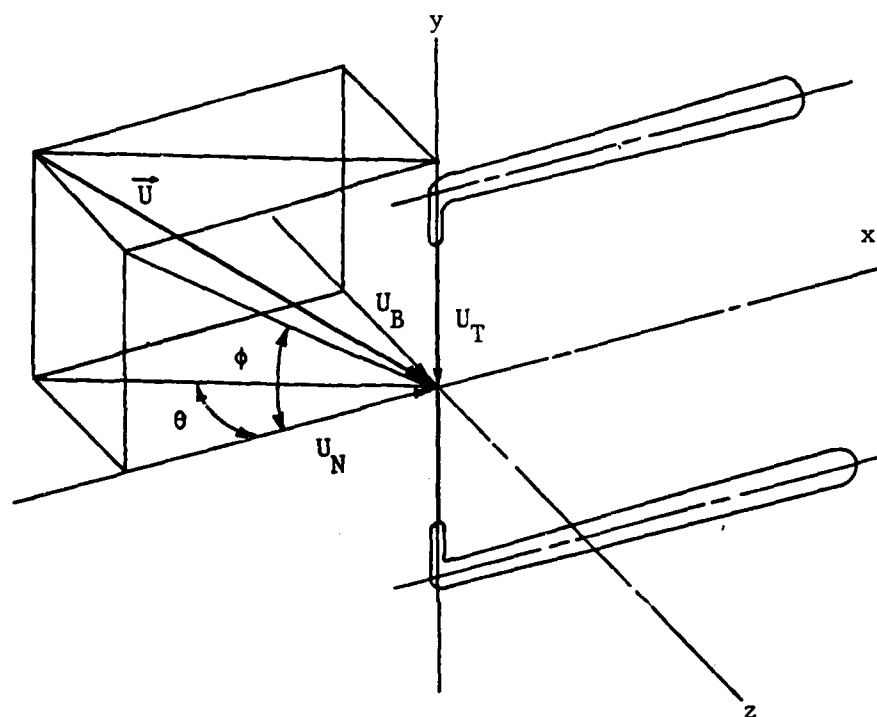


Figure A-4 The coordinates defined on each component of hot-film probe.

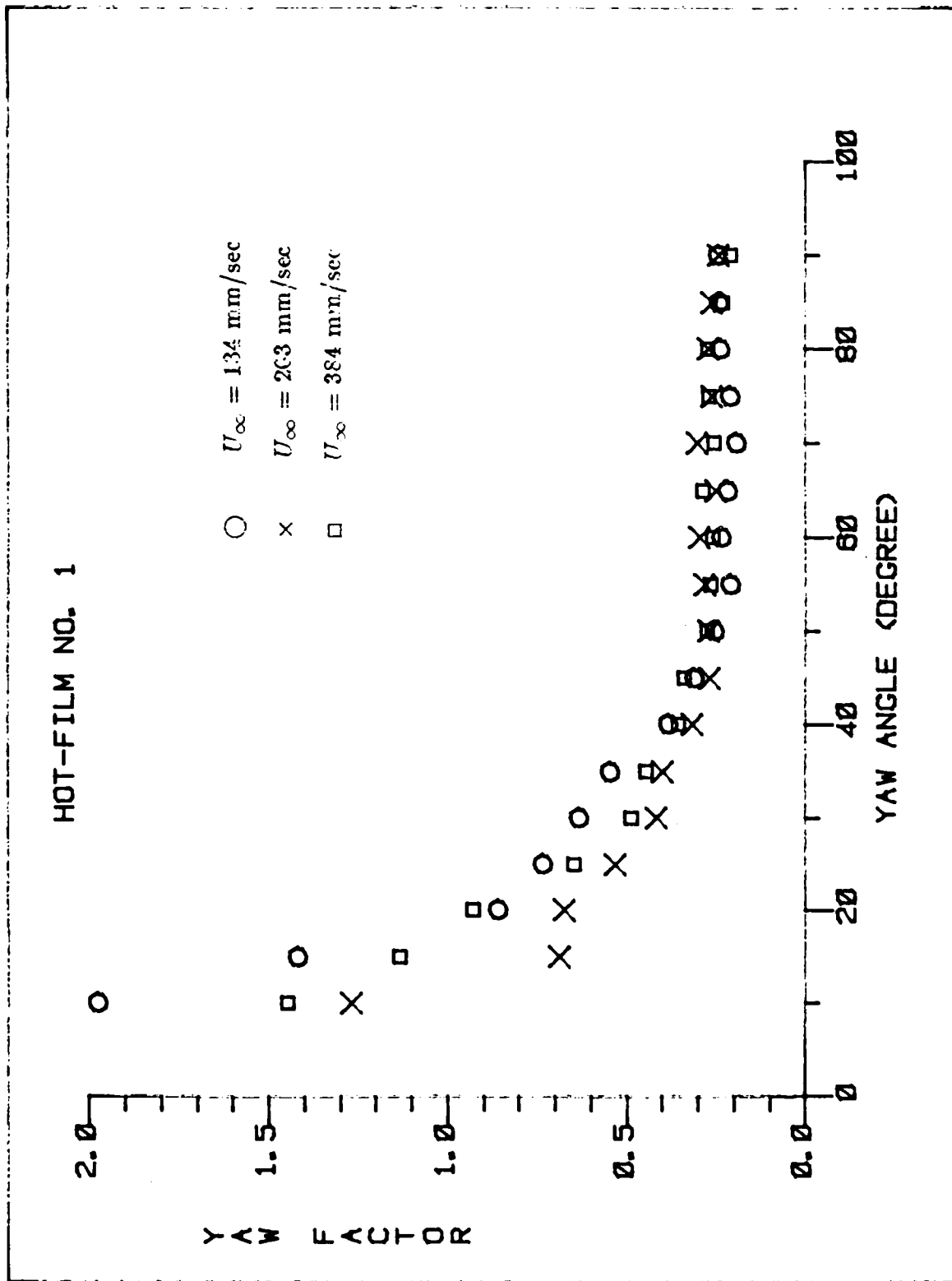


Figure A-5 The calibrated component yaw factors of hot-film probe.

# HOT-FILM NO. 2

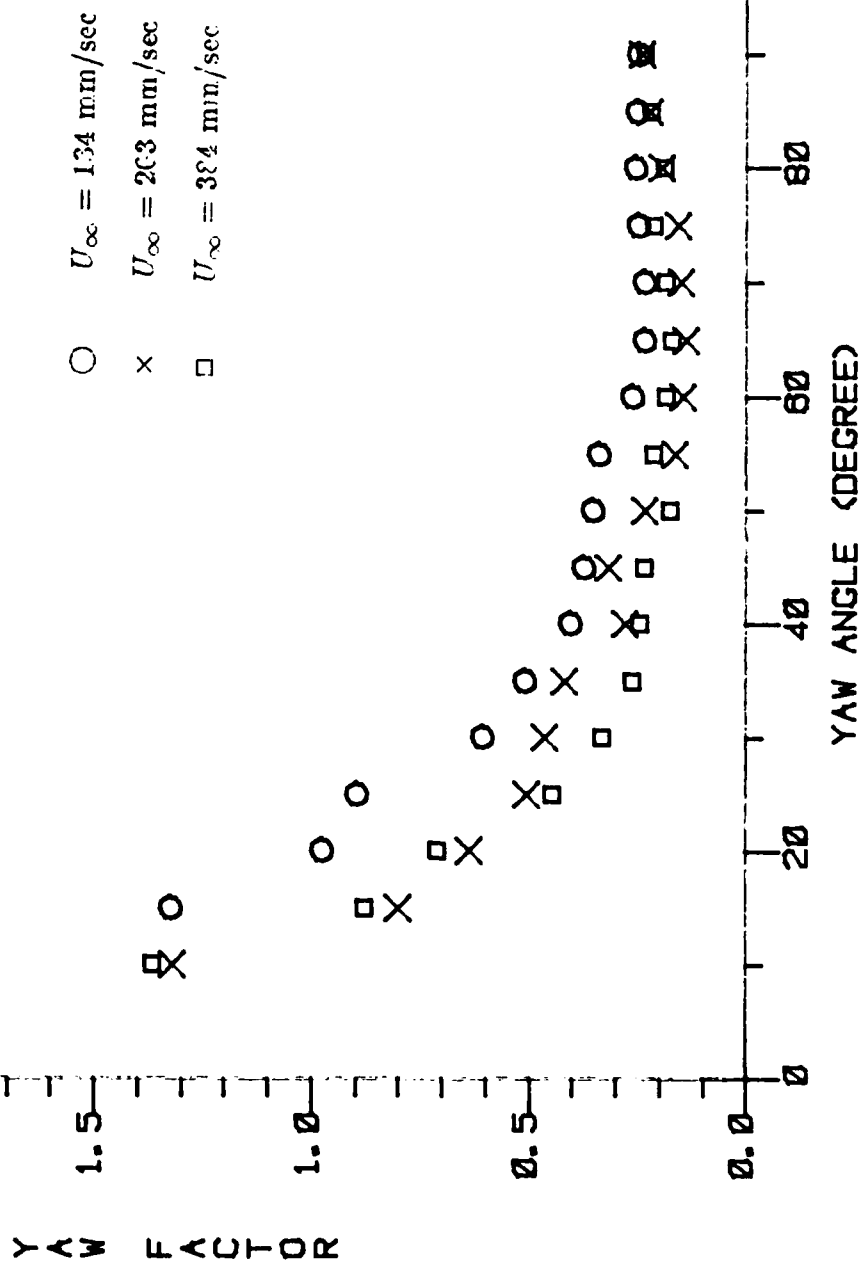


Figure A-5 (Continued)

# HOT-FILM NO. 3

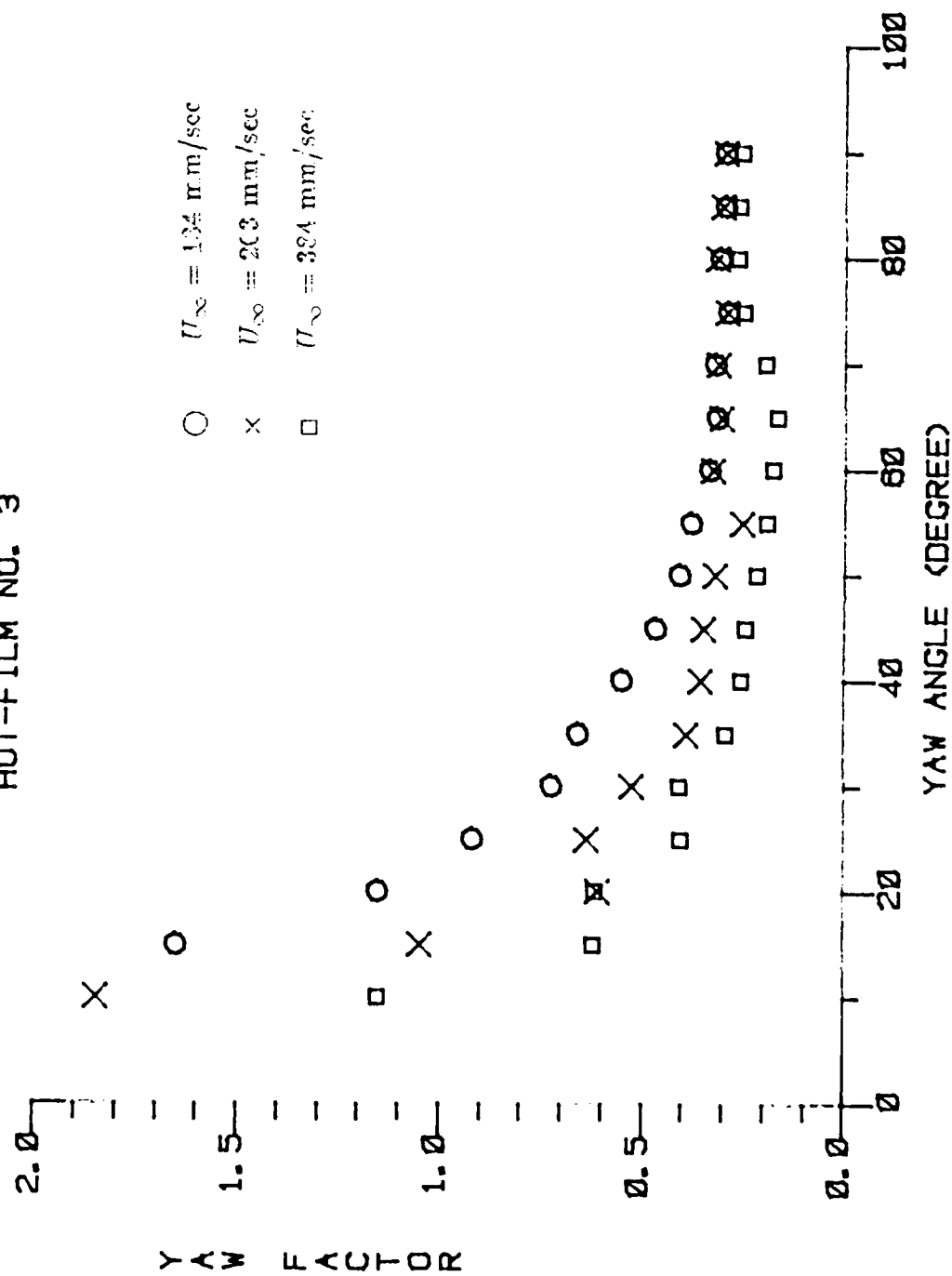


Figure A-5 (Continued)

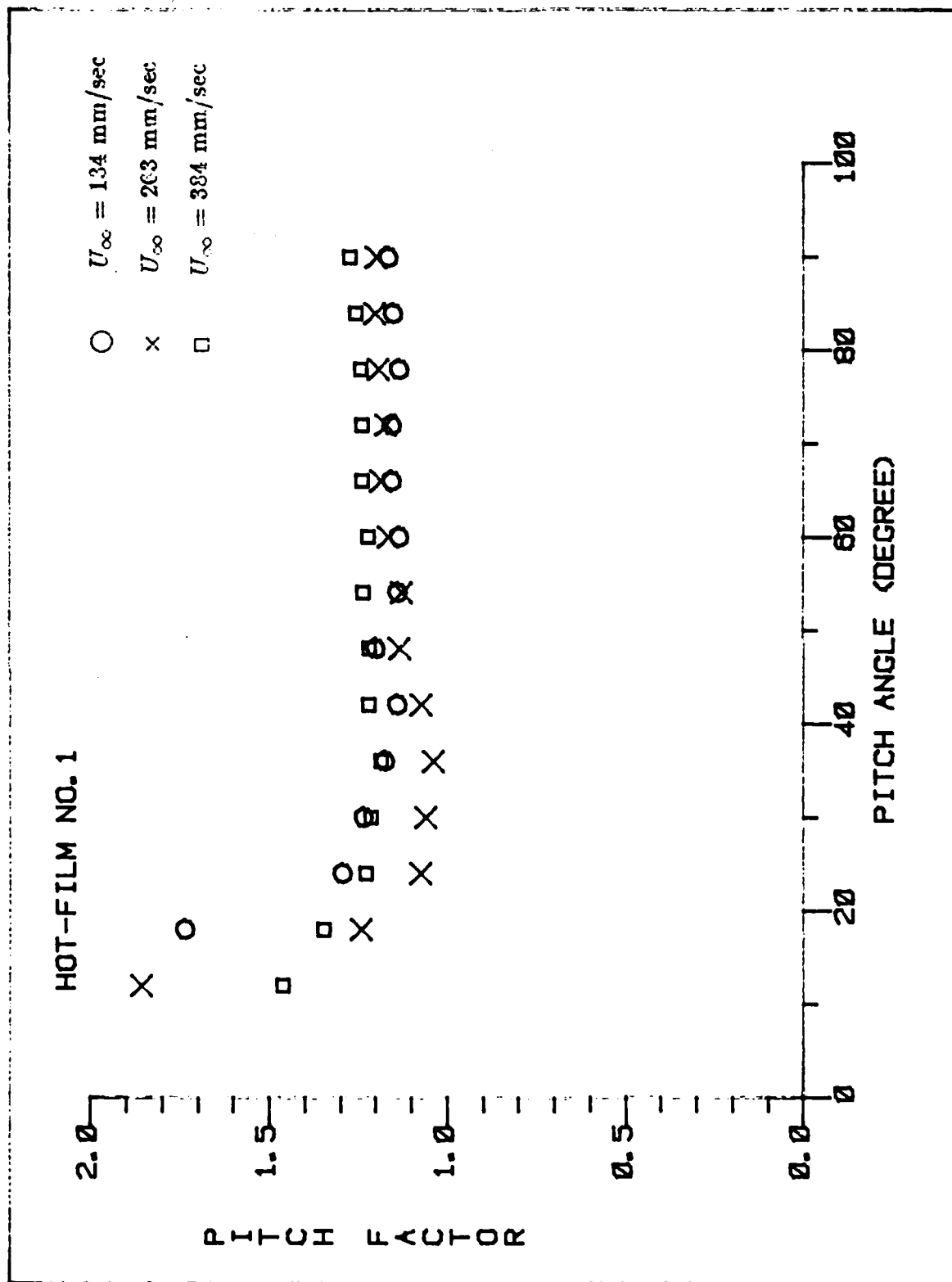


Figure A-6 The calibrated component pitch factors of hot-film probe.

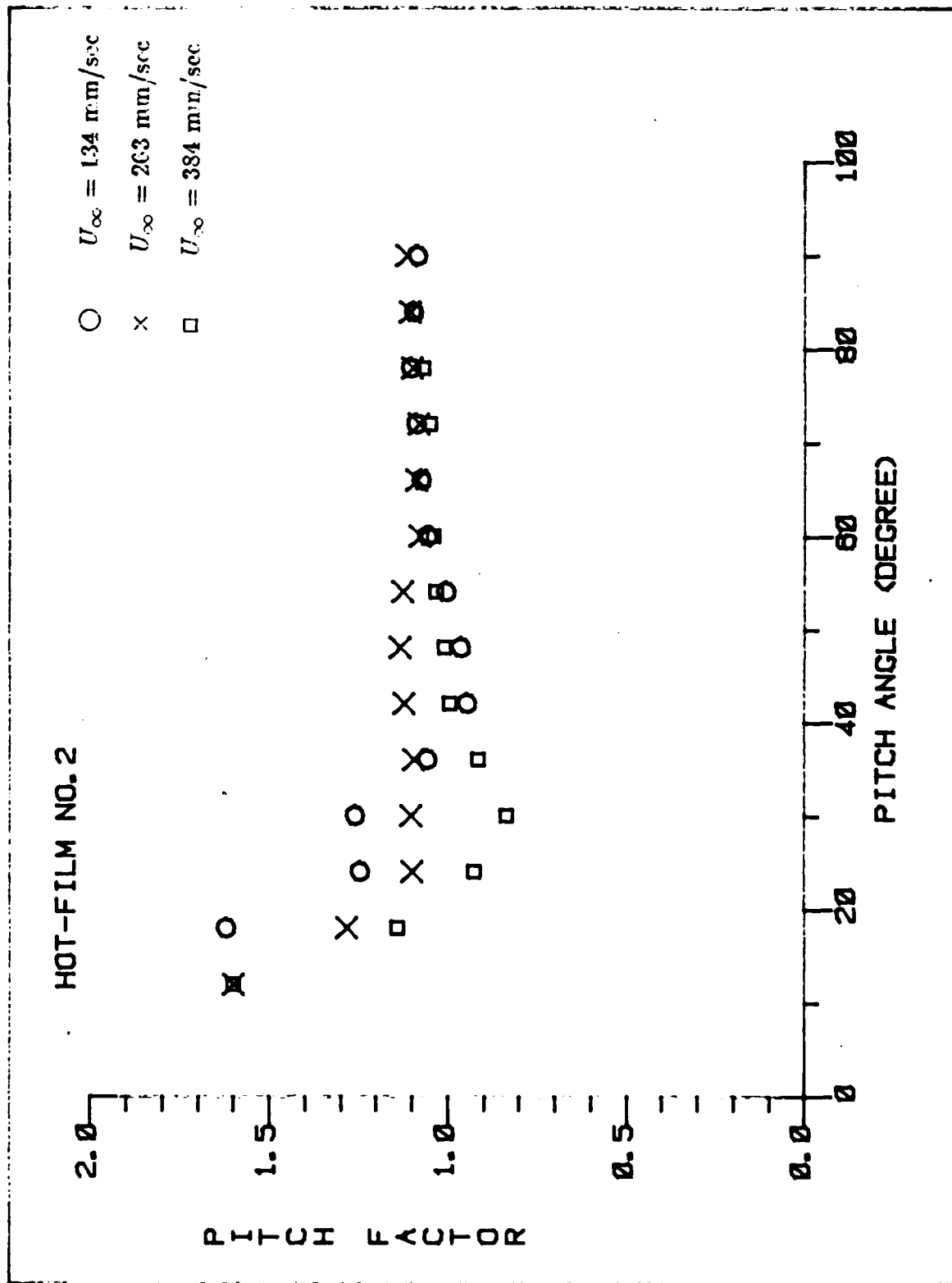


Figure A-6 (Continued)

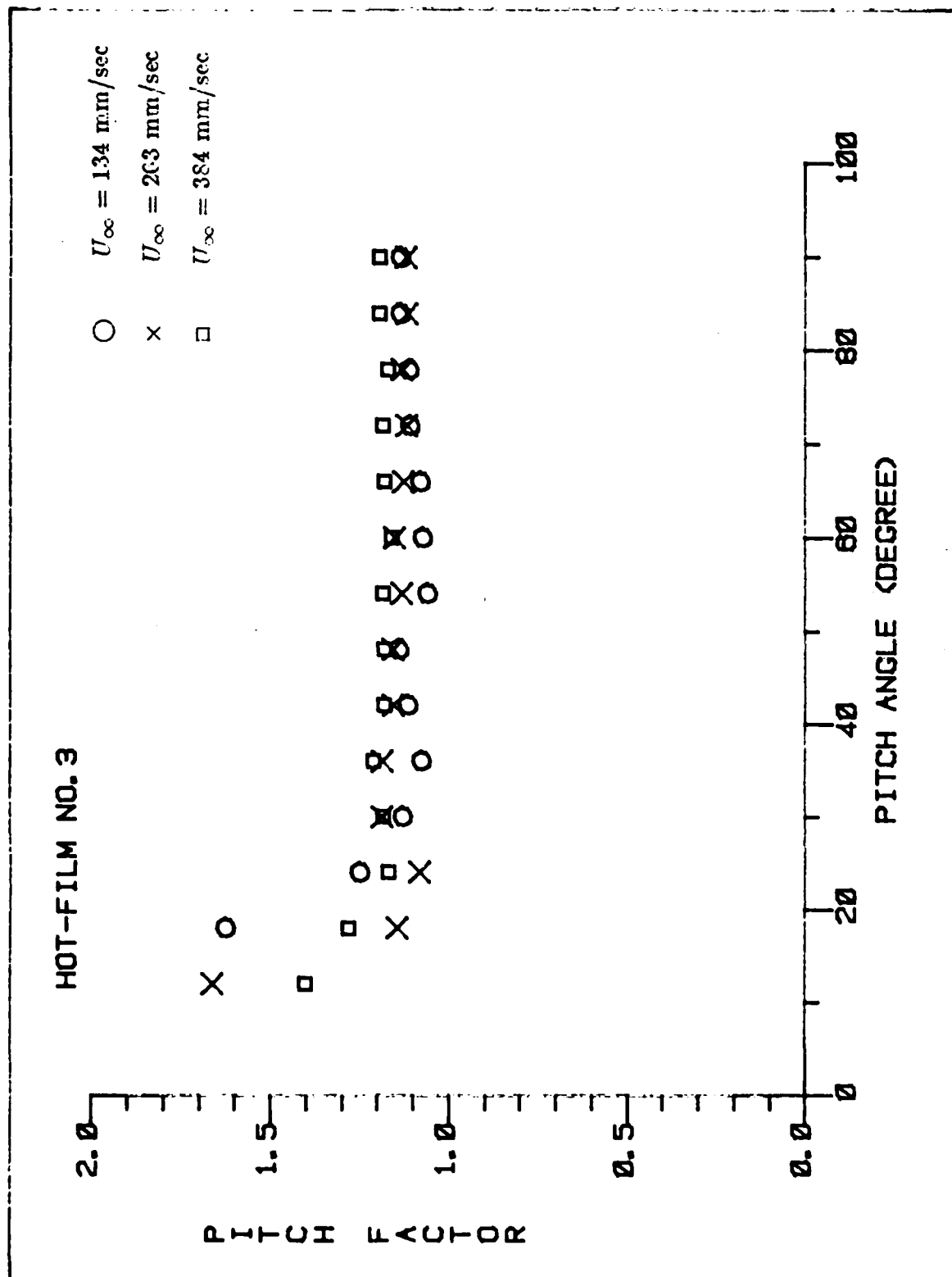


Figure A-6 (Continued)

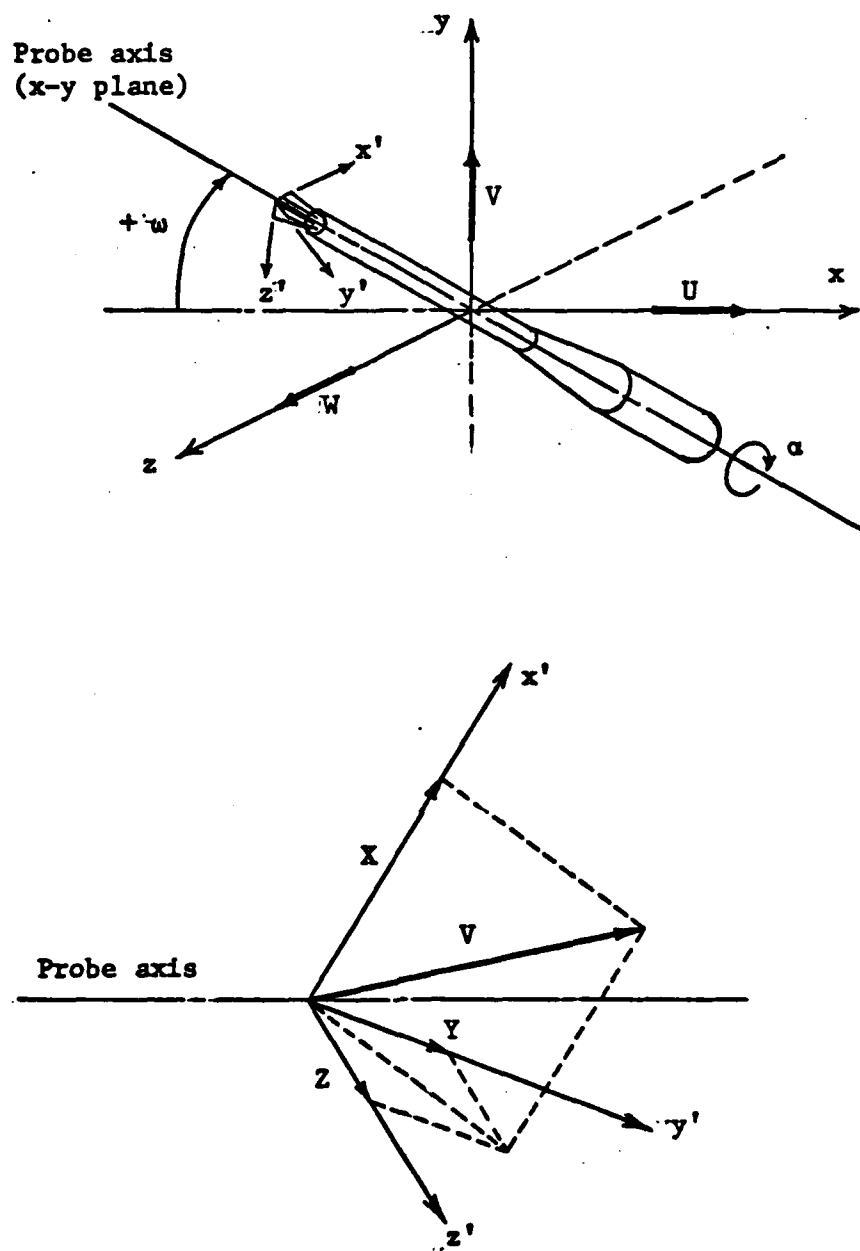


Figure A-7. Sketch of hot-film probe and coordinates systems on hot-film components.

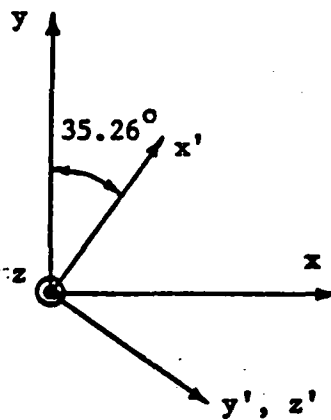
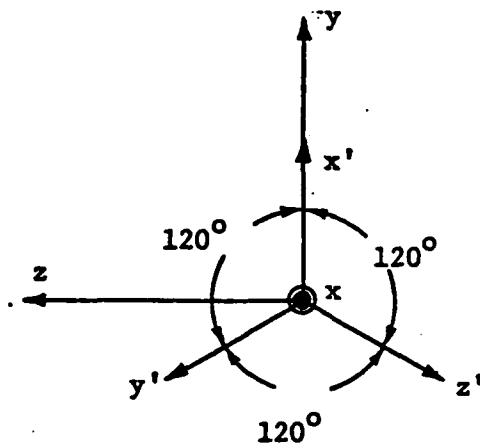
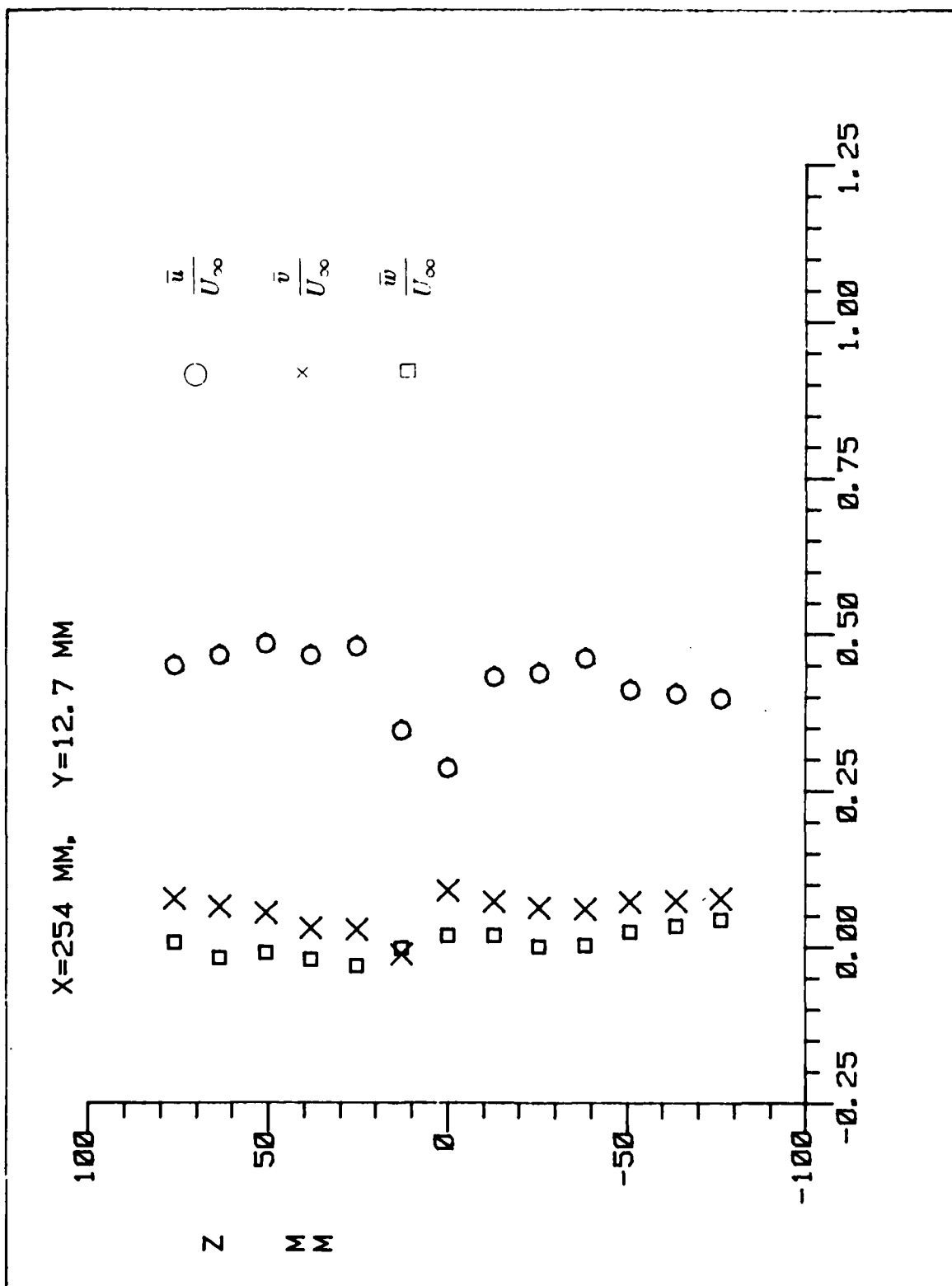
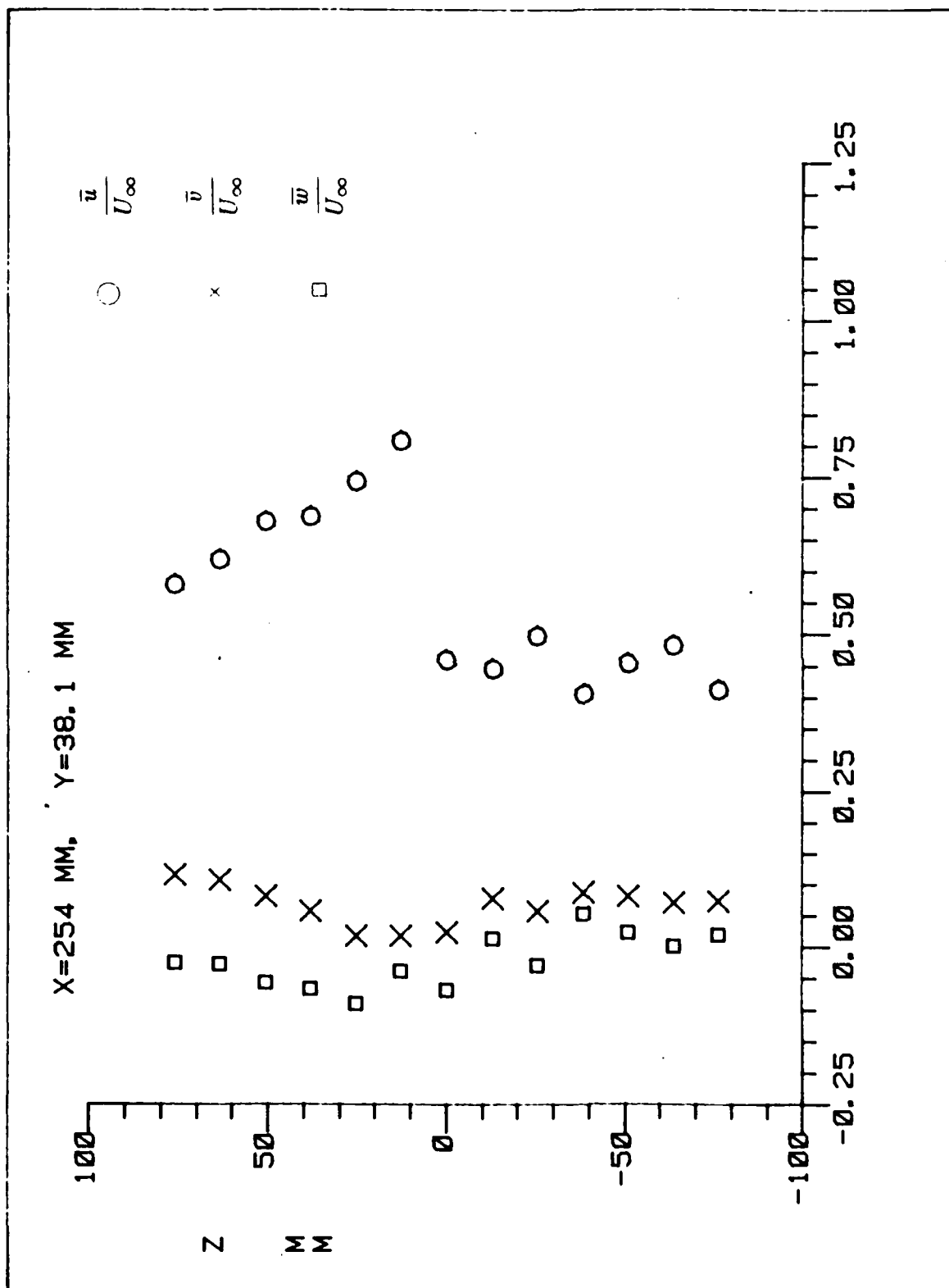


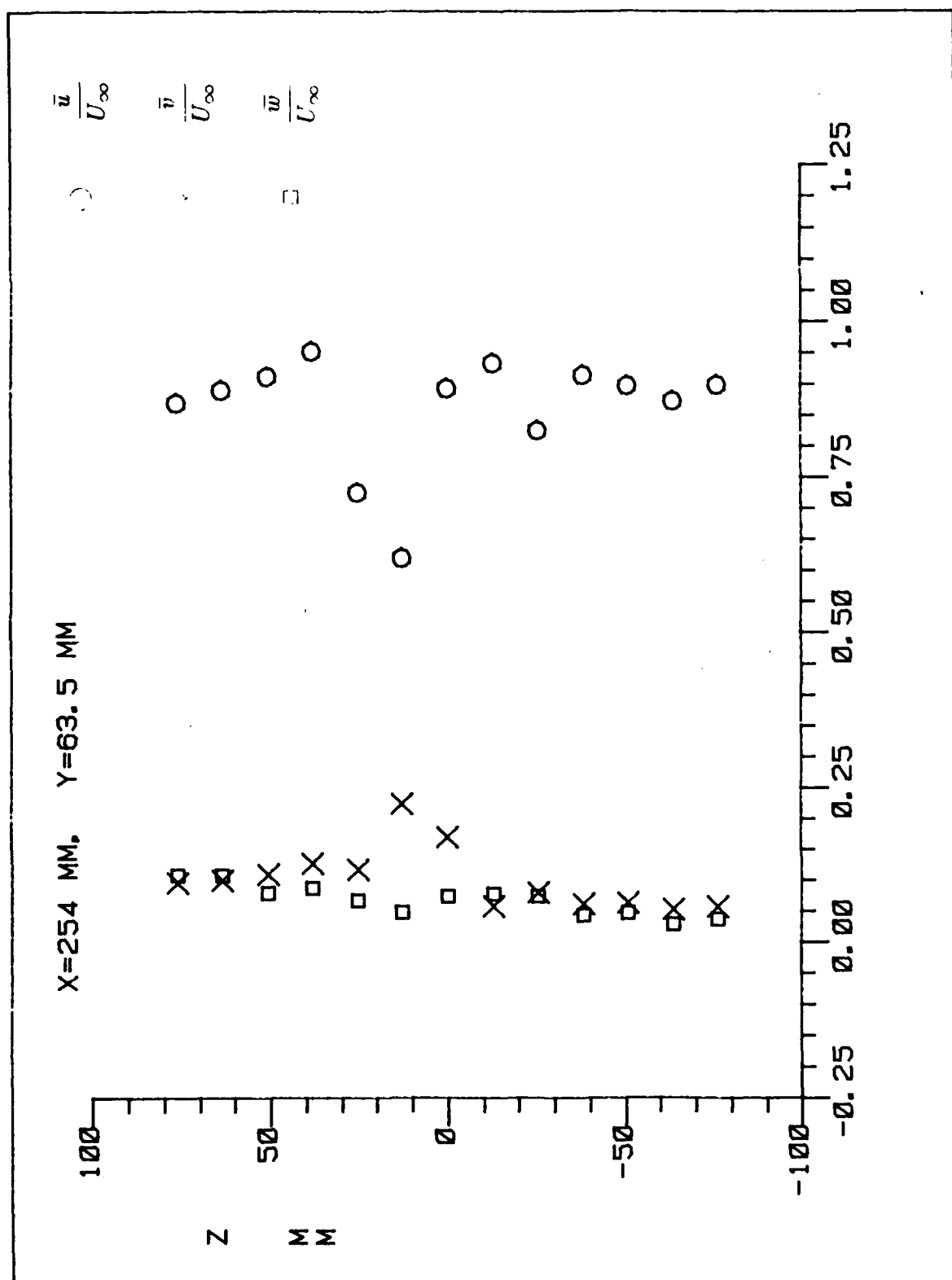
Figure A-8. The directional relationship between coordinates  $(x, y, z)$  and coordinates  $(x', y', z')$ .

## **Appendix B**

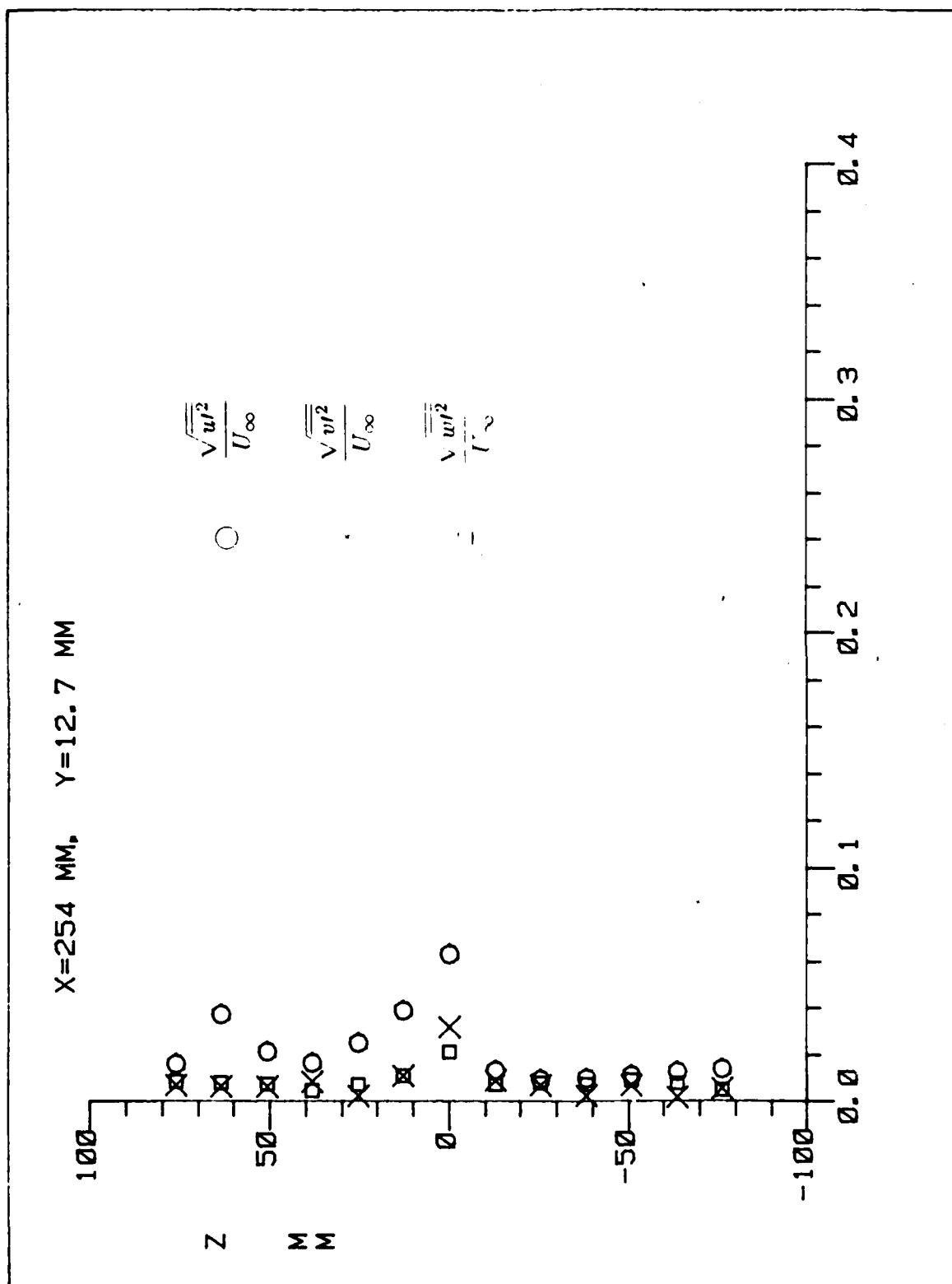
Selected results of the hot film measurements  
in the down stream of the tear-drop jet model.  
(For coordinates see the main text and Appendix A.)

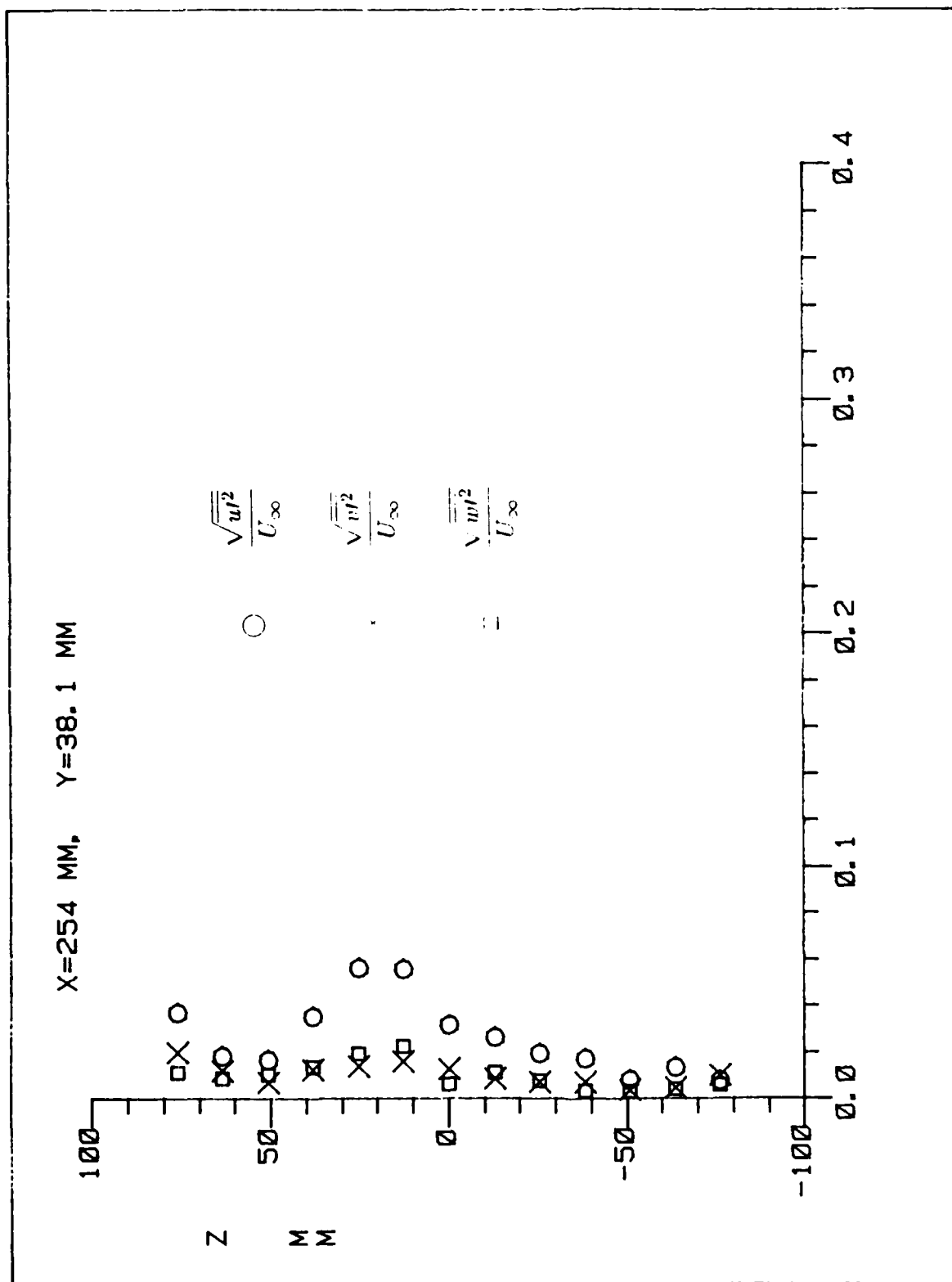


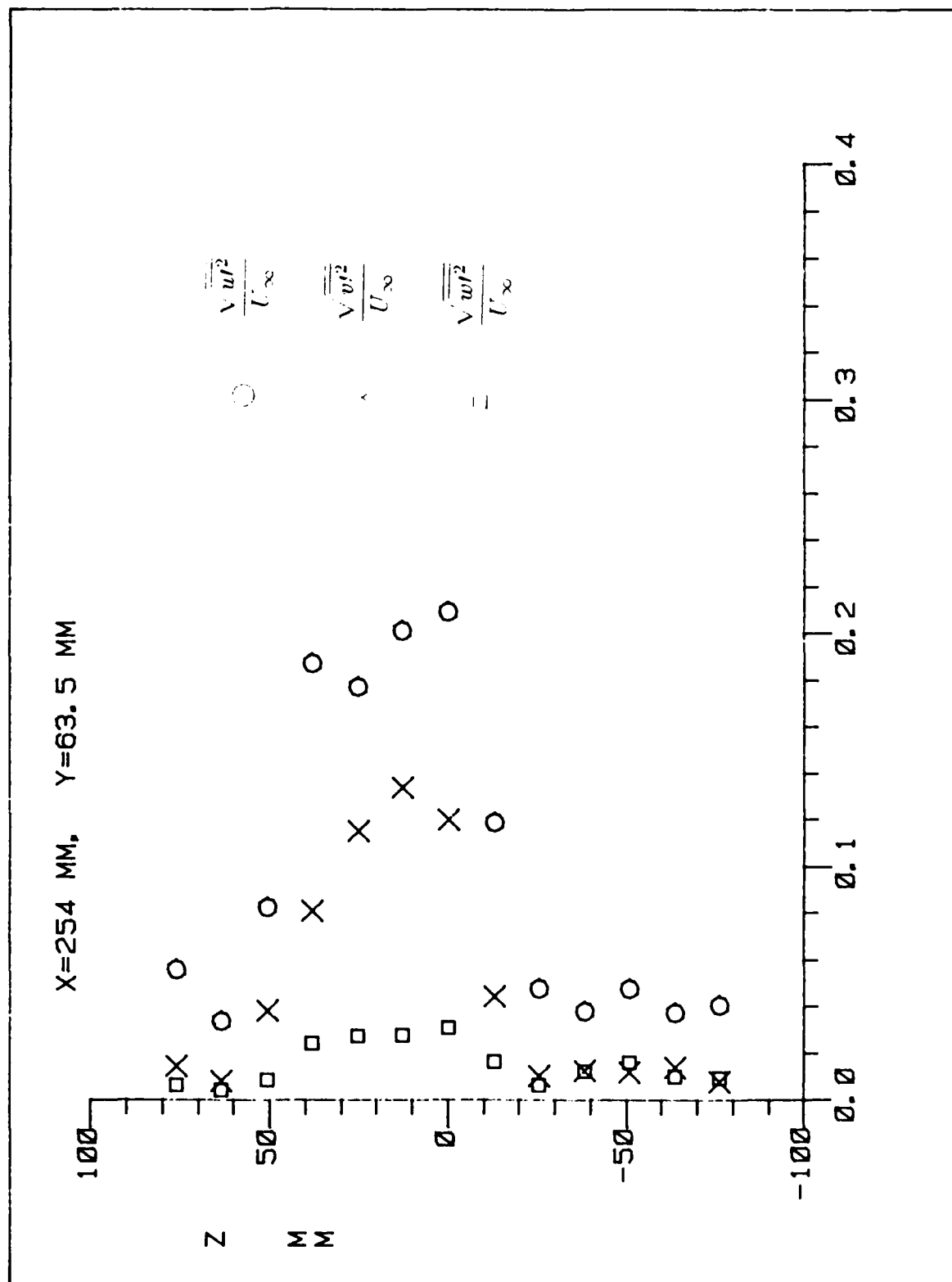


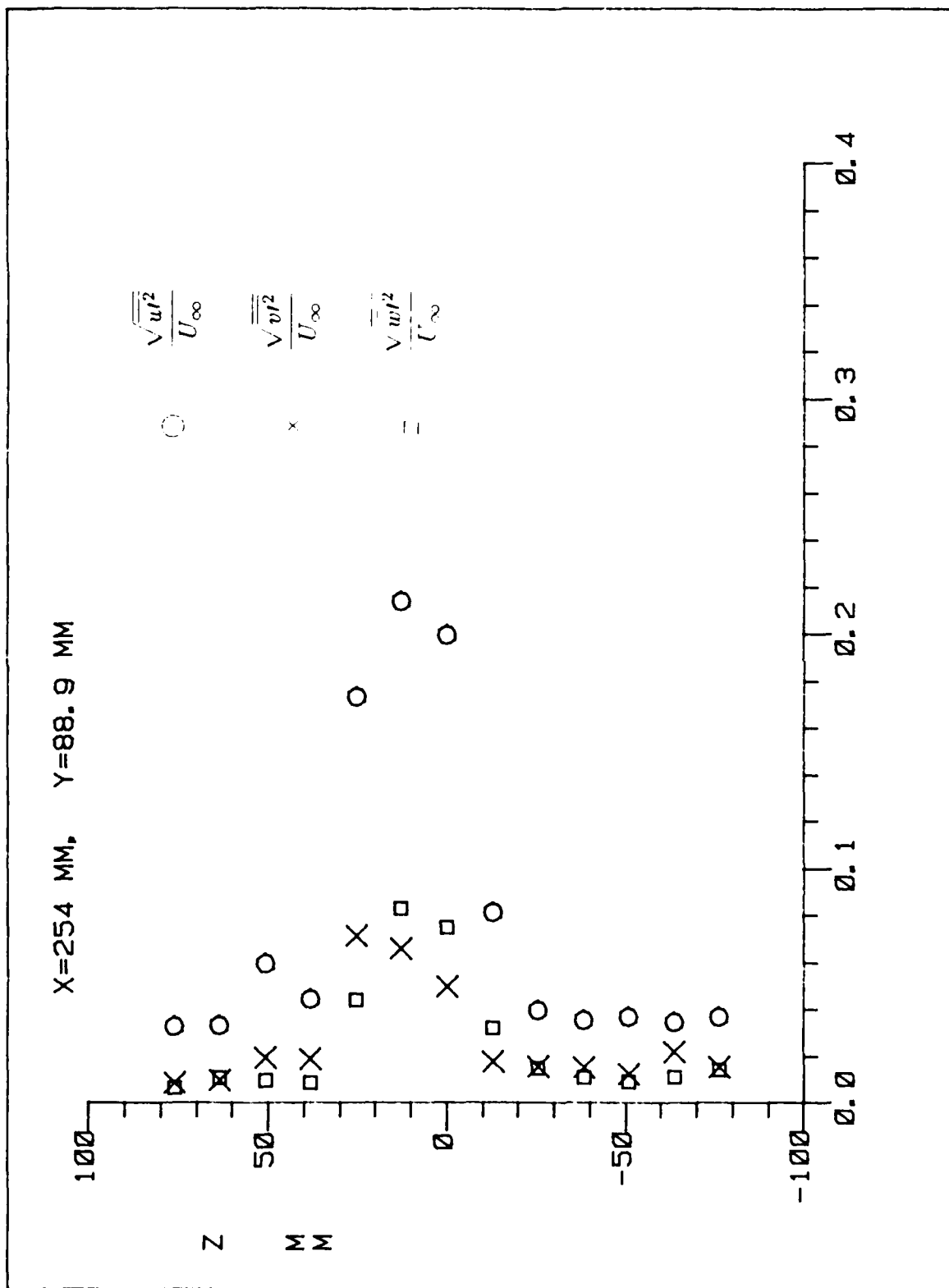




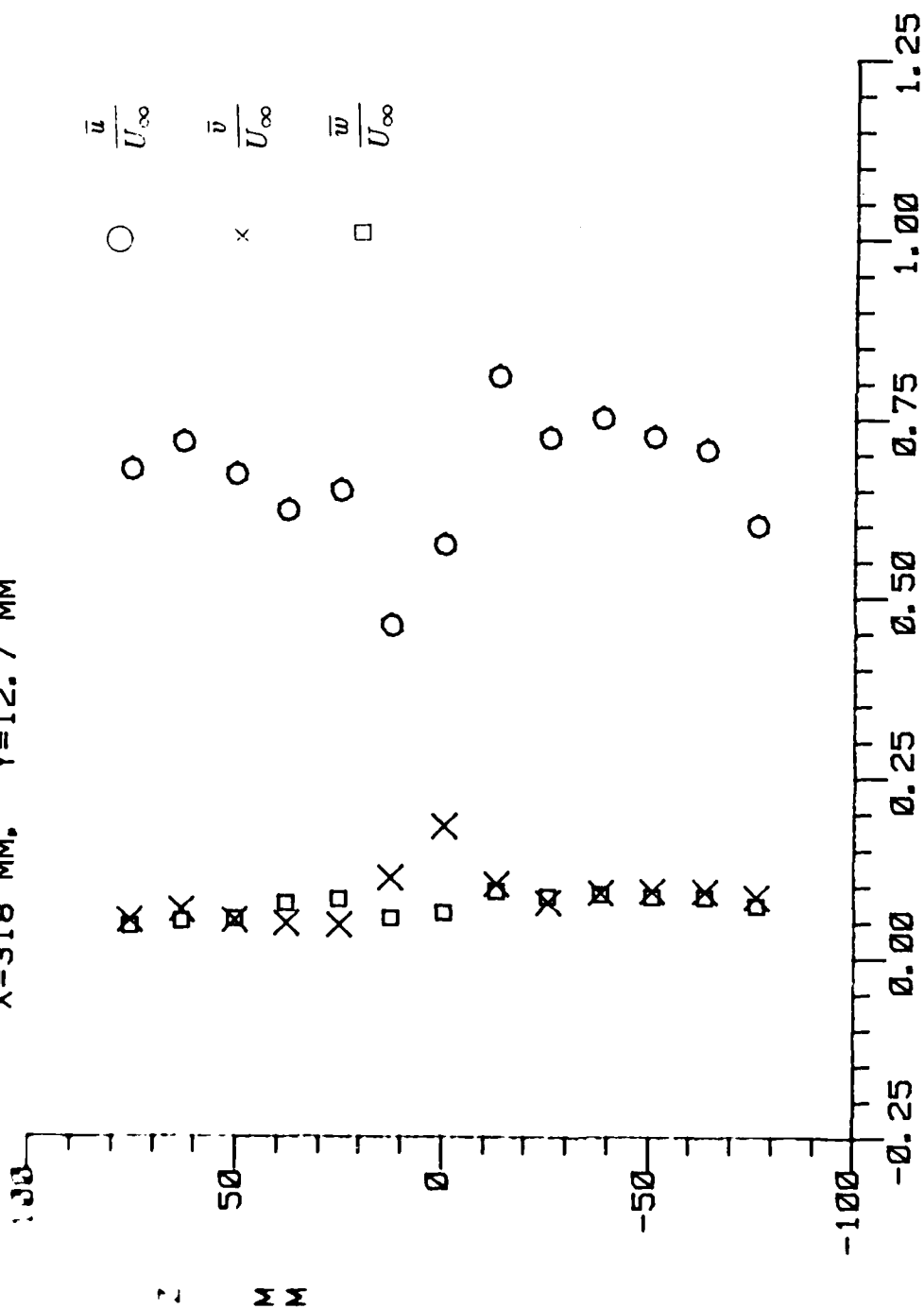


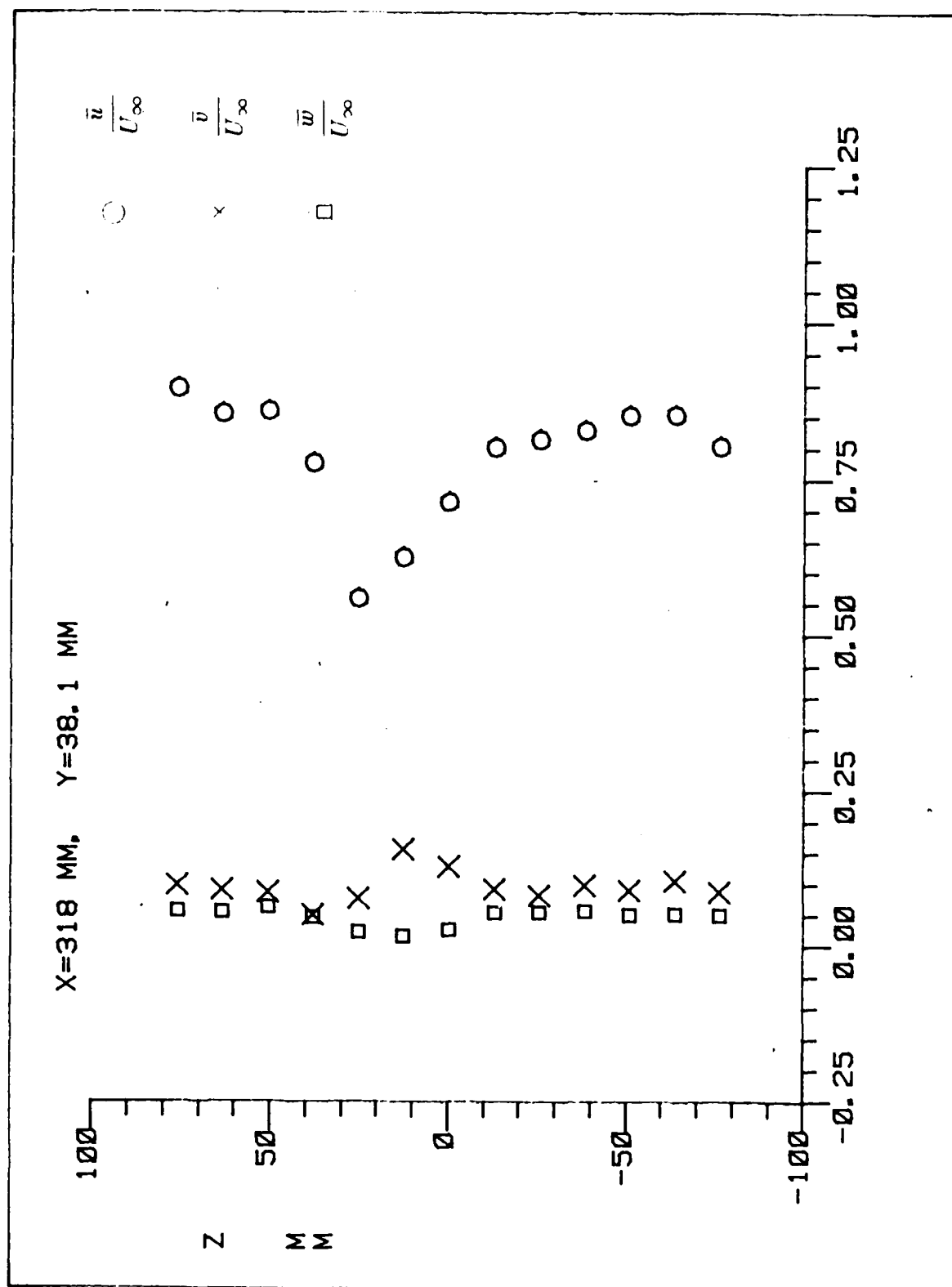




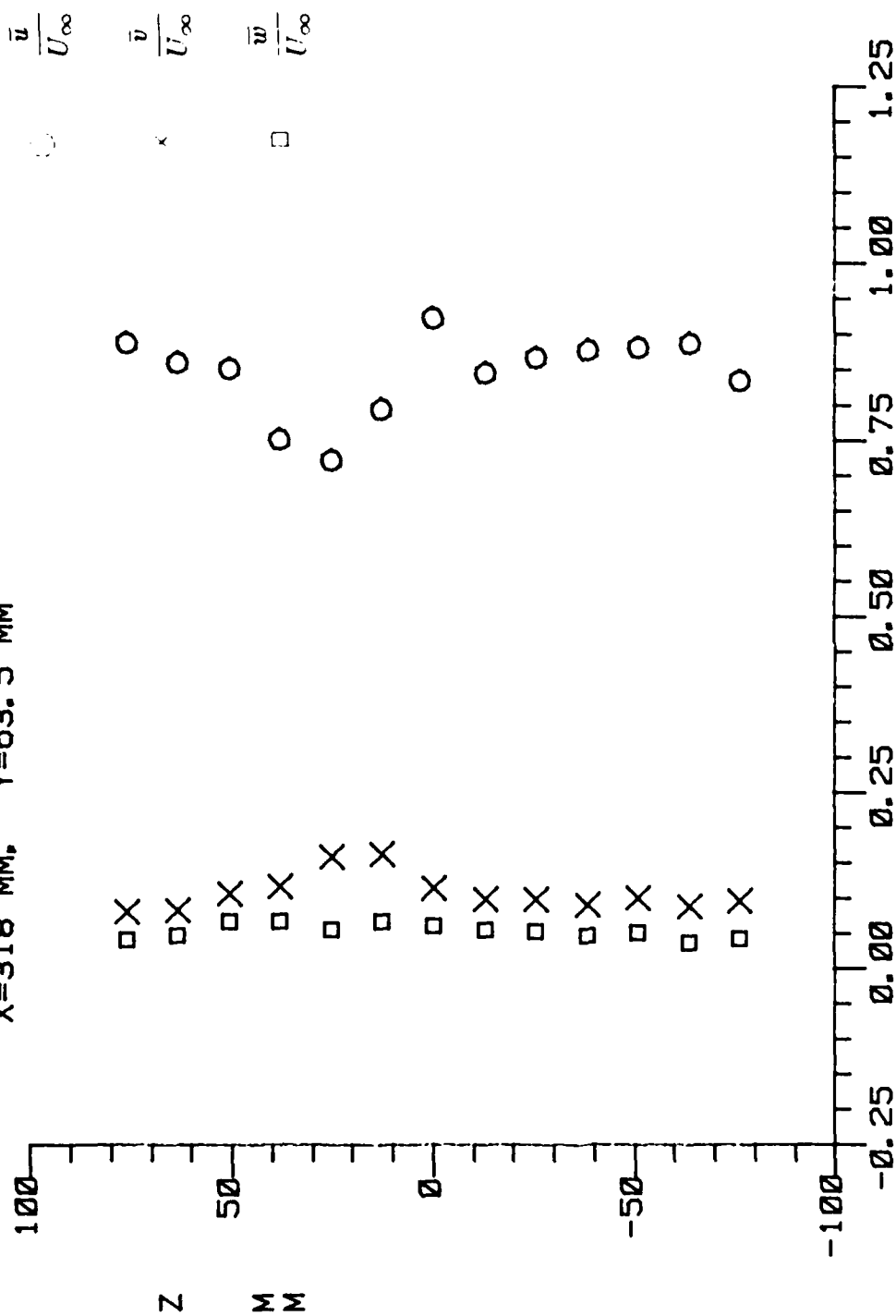


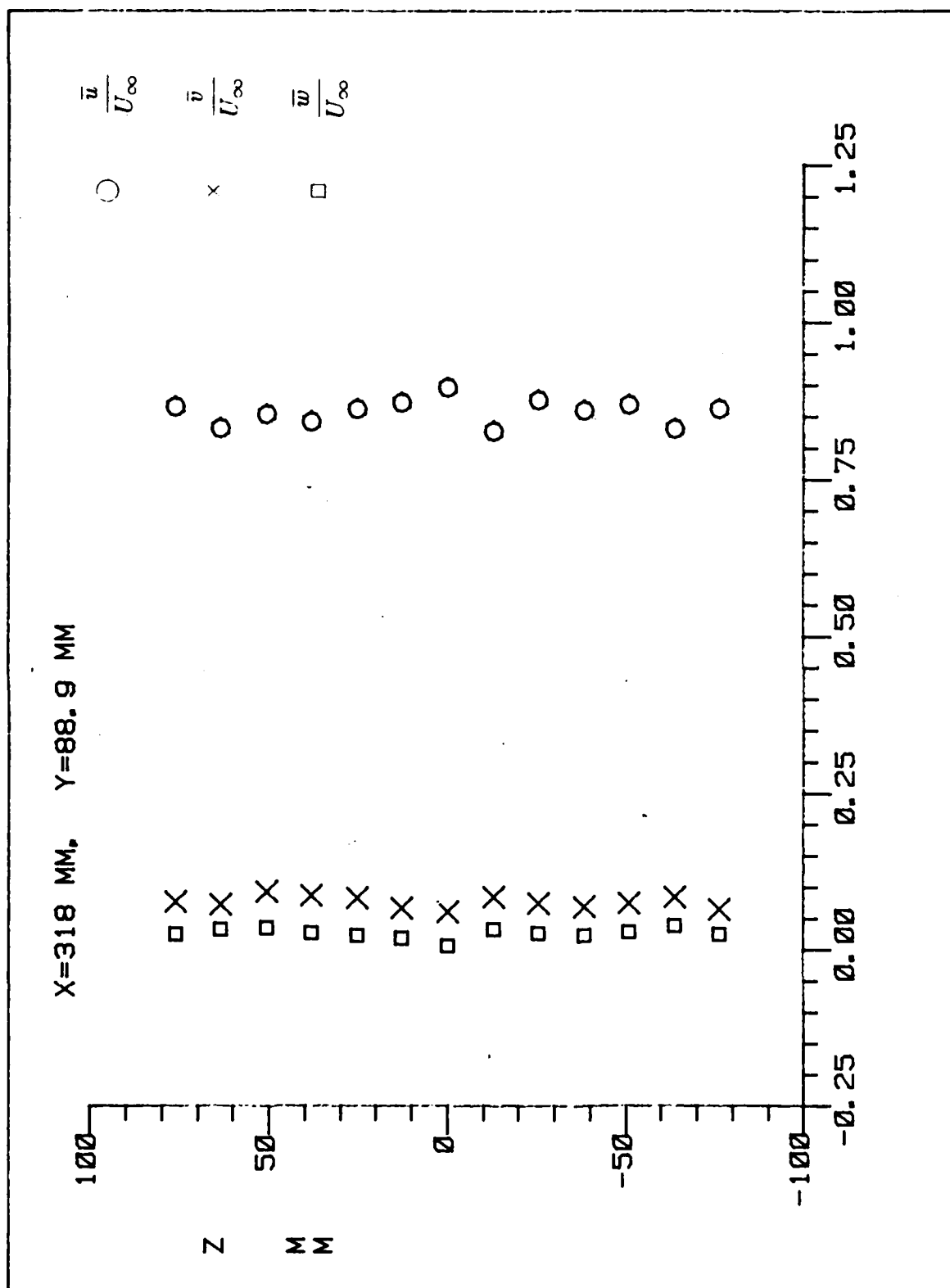
X=318 MM. Y=12.7 MM

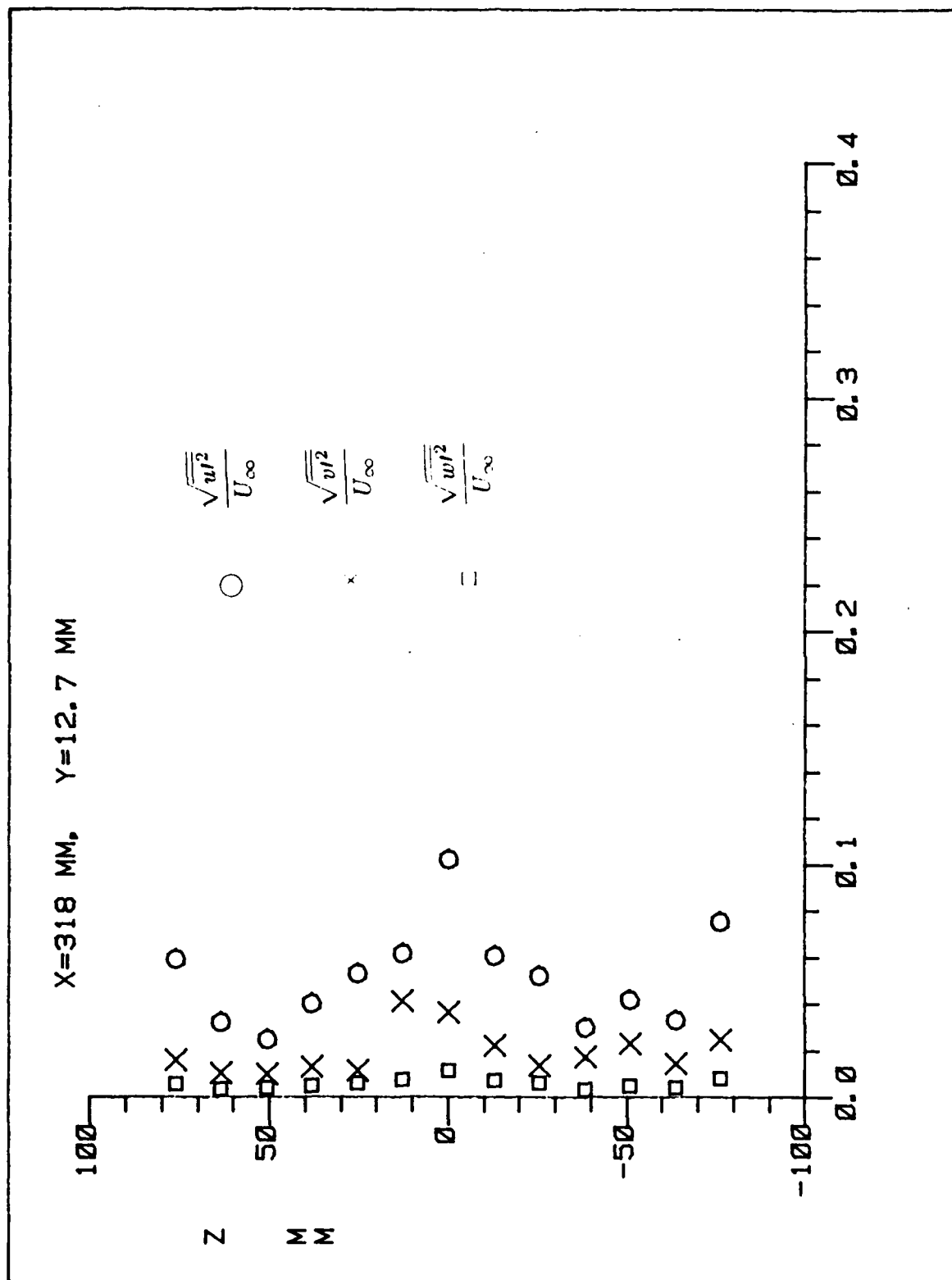




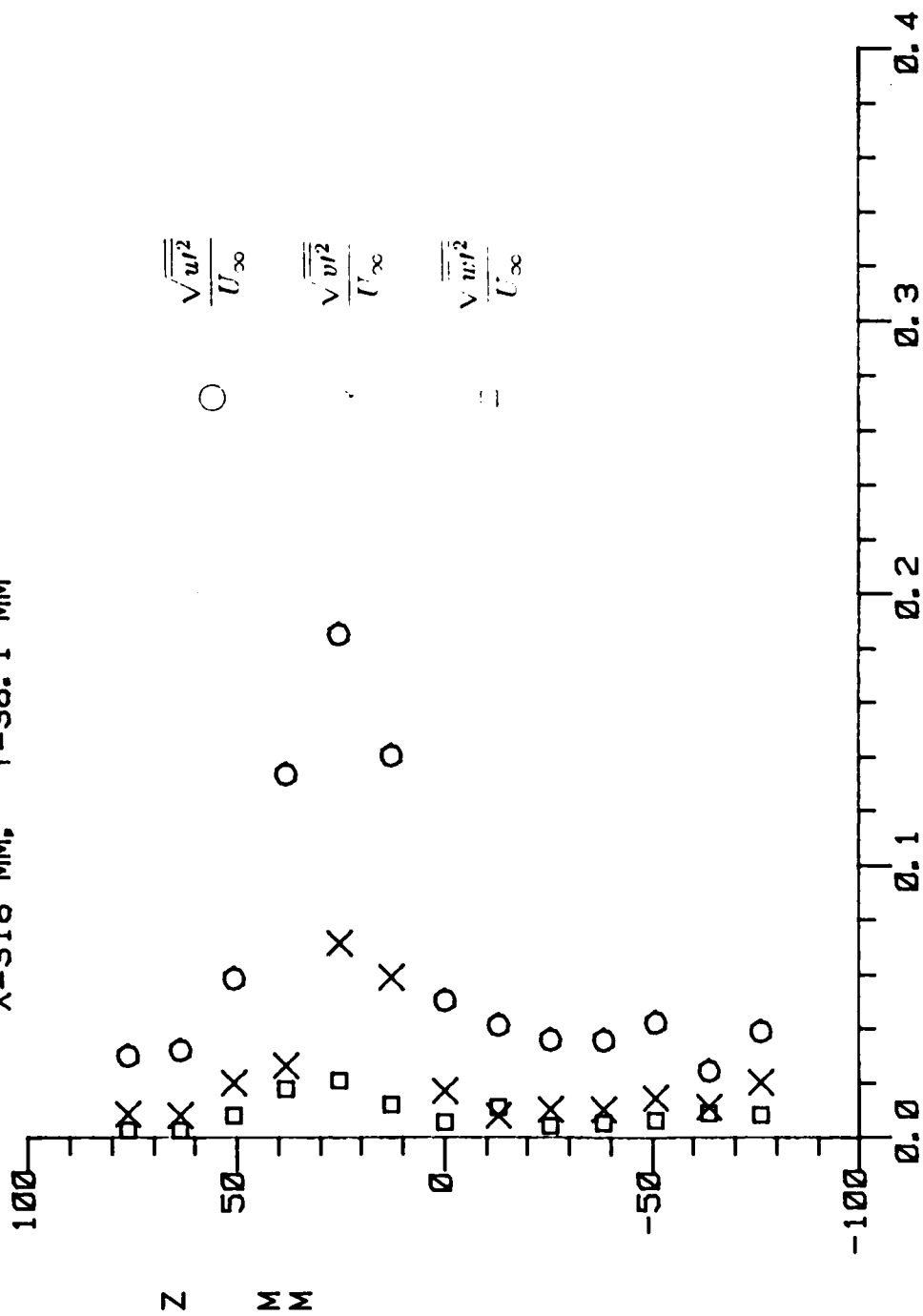
X=318 MM, Y=63.5 MM

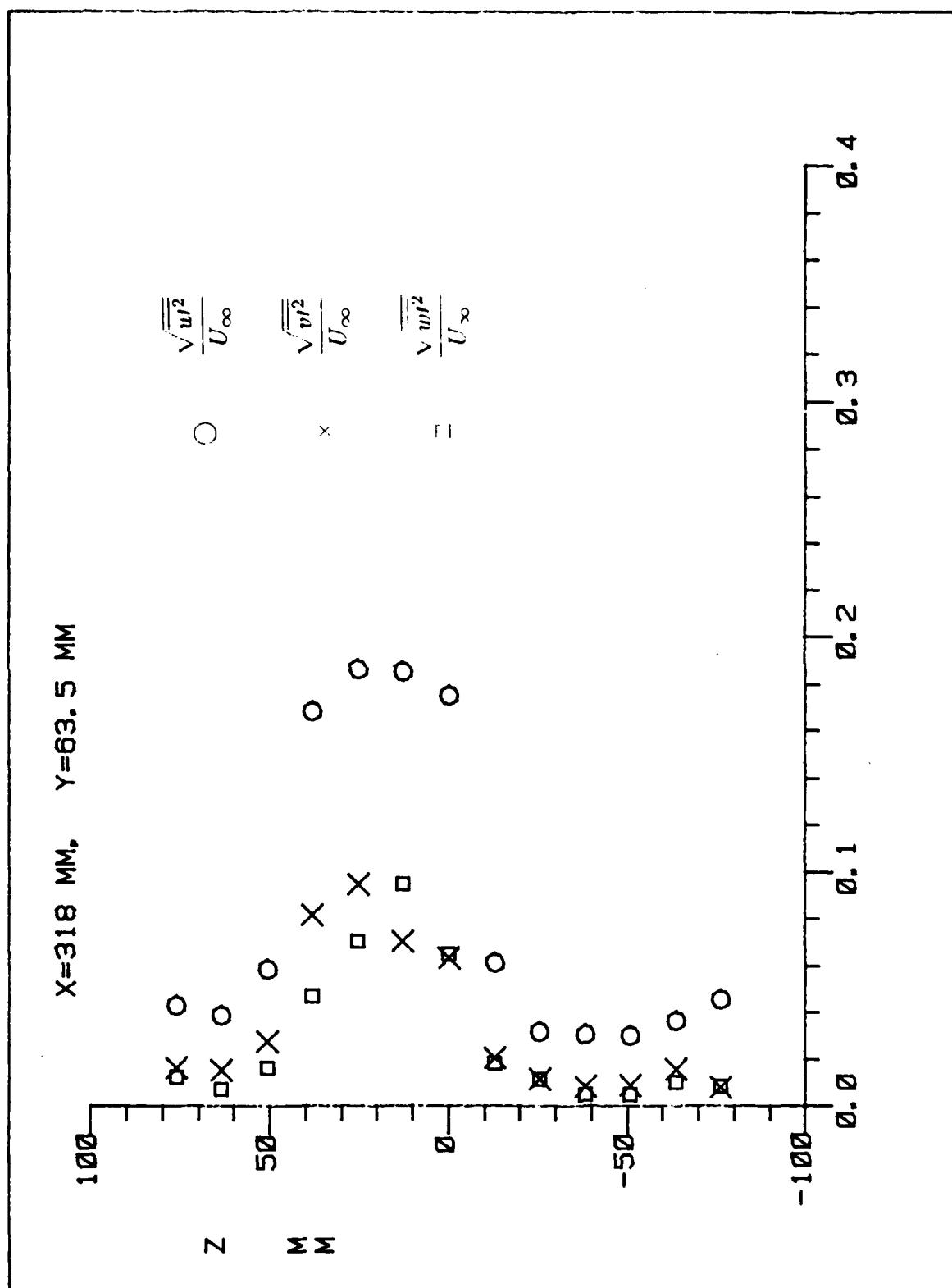


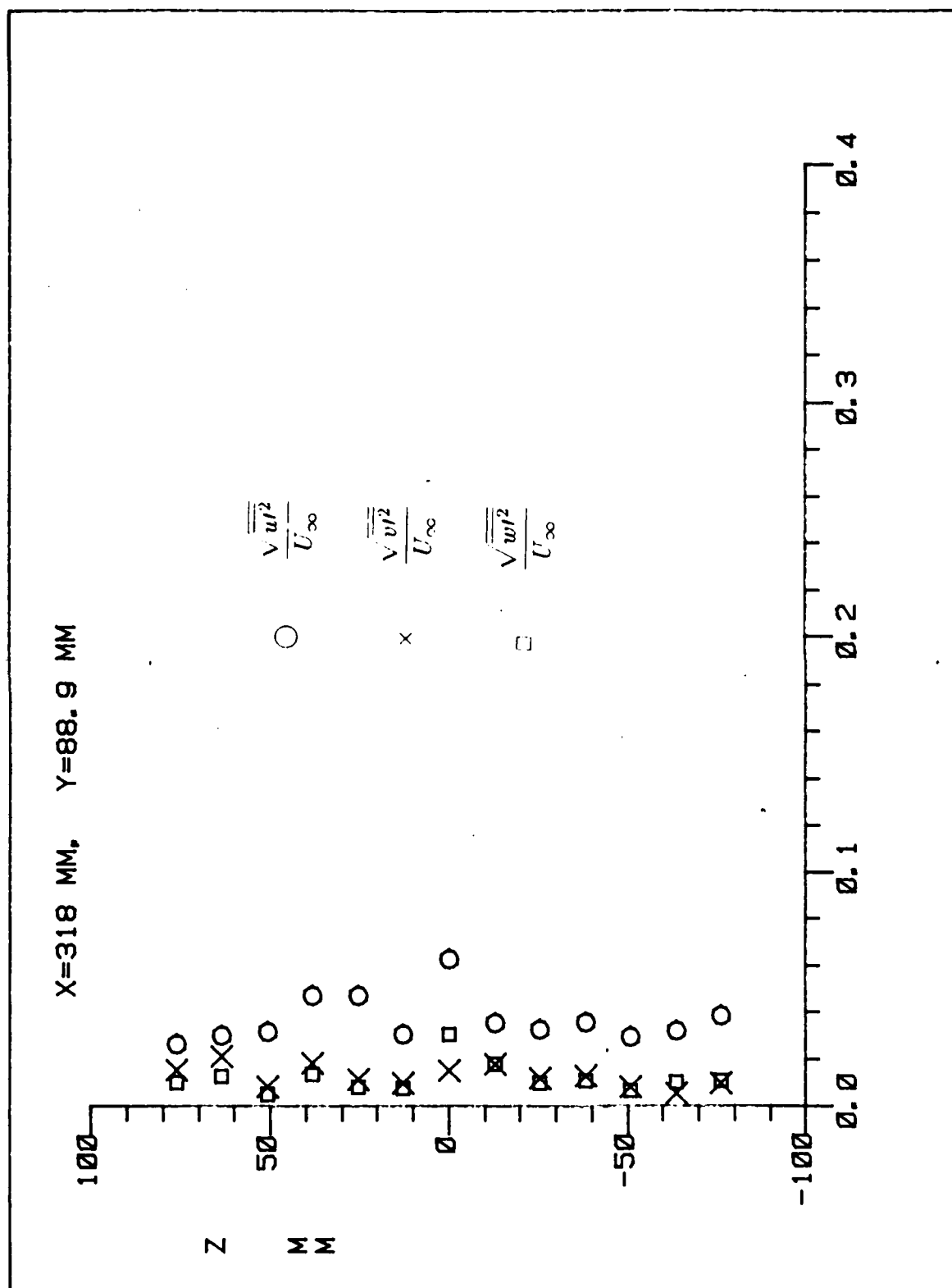


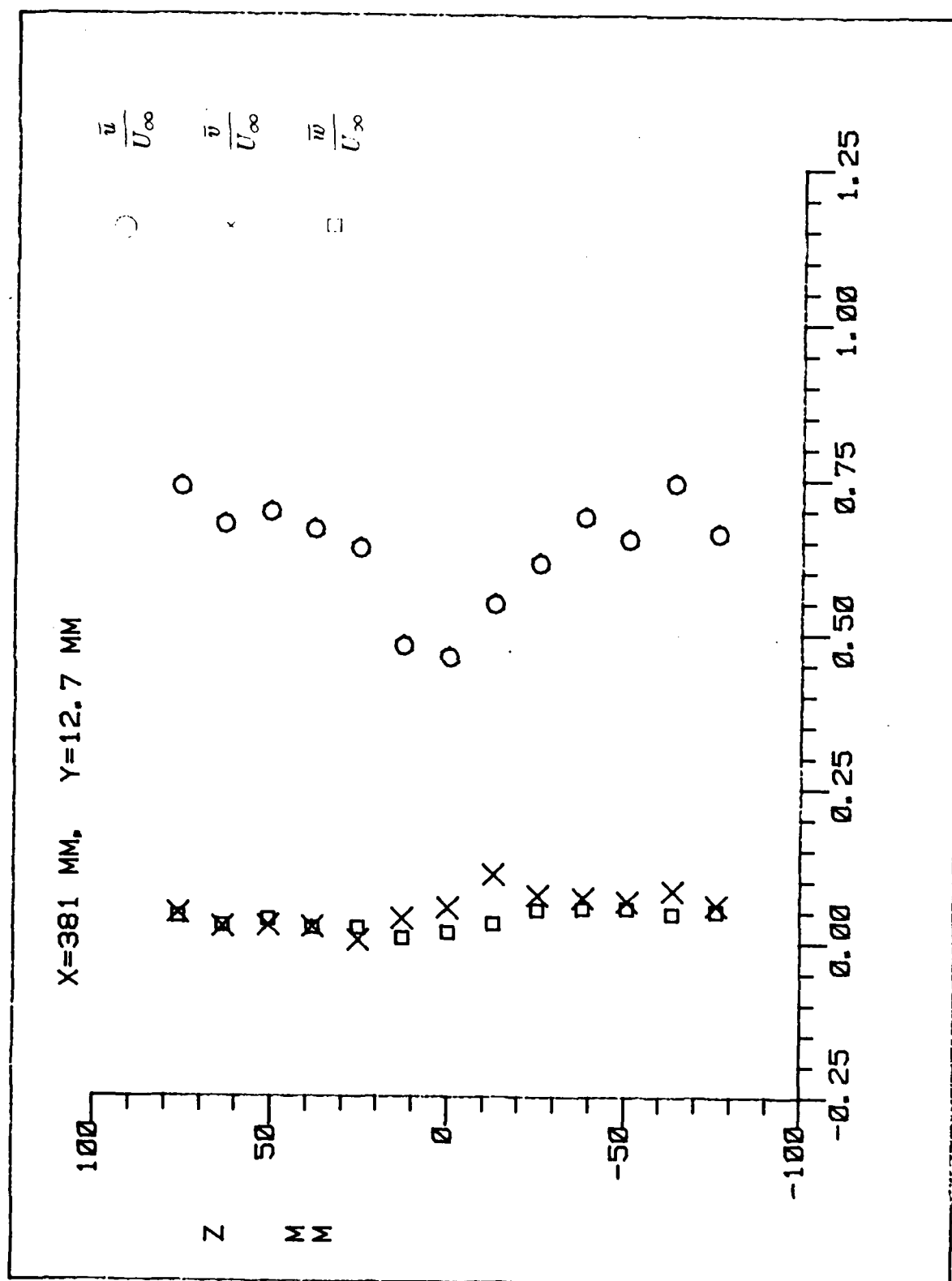


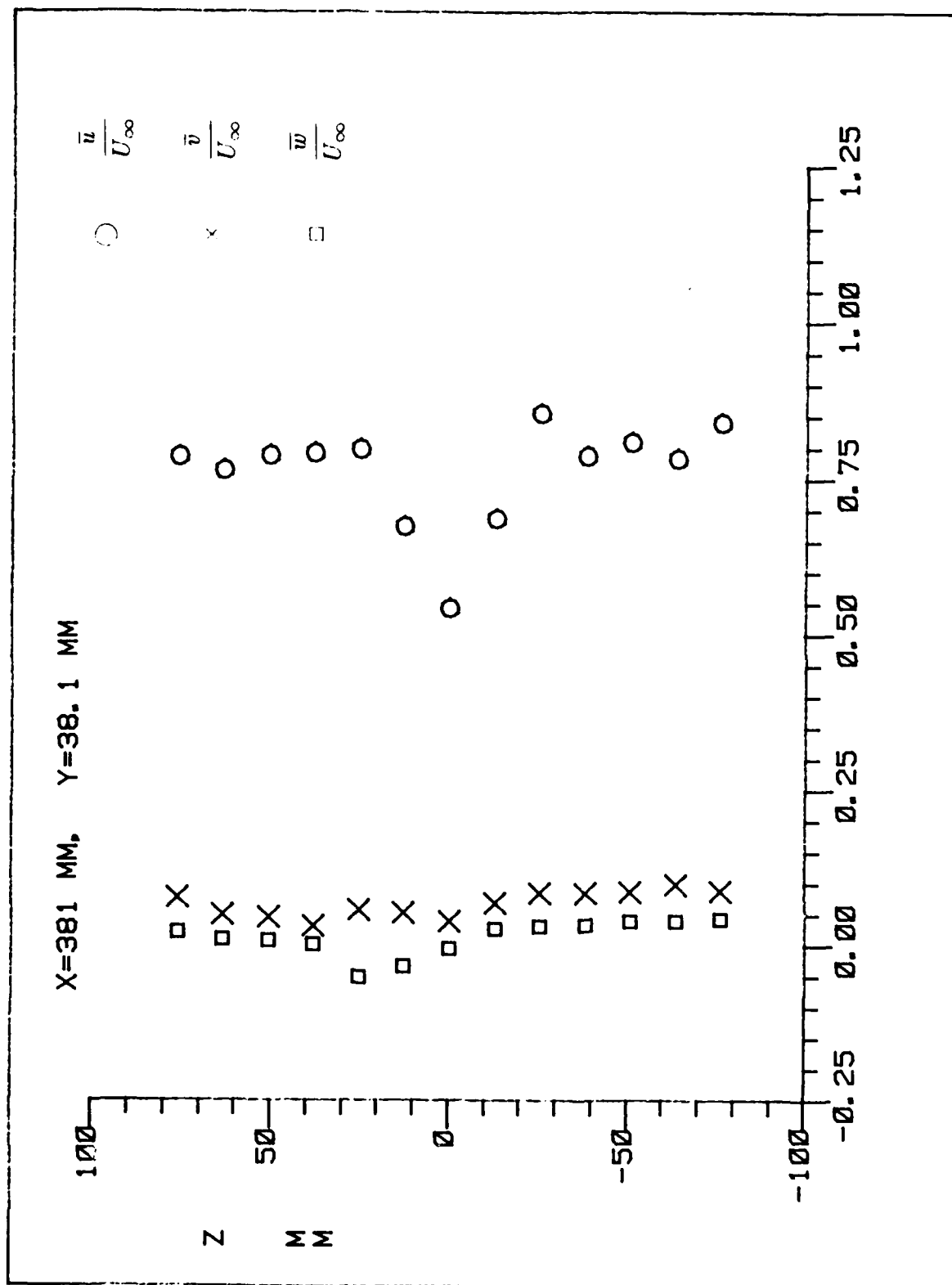
X=318 MM, Y=38.1 MM



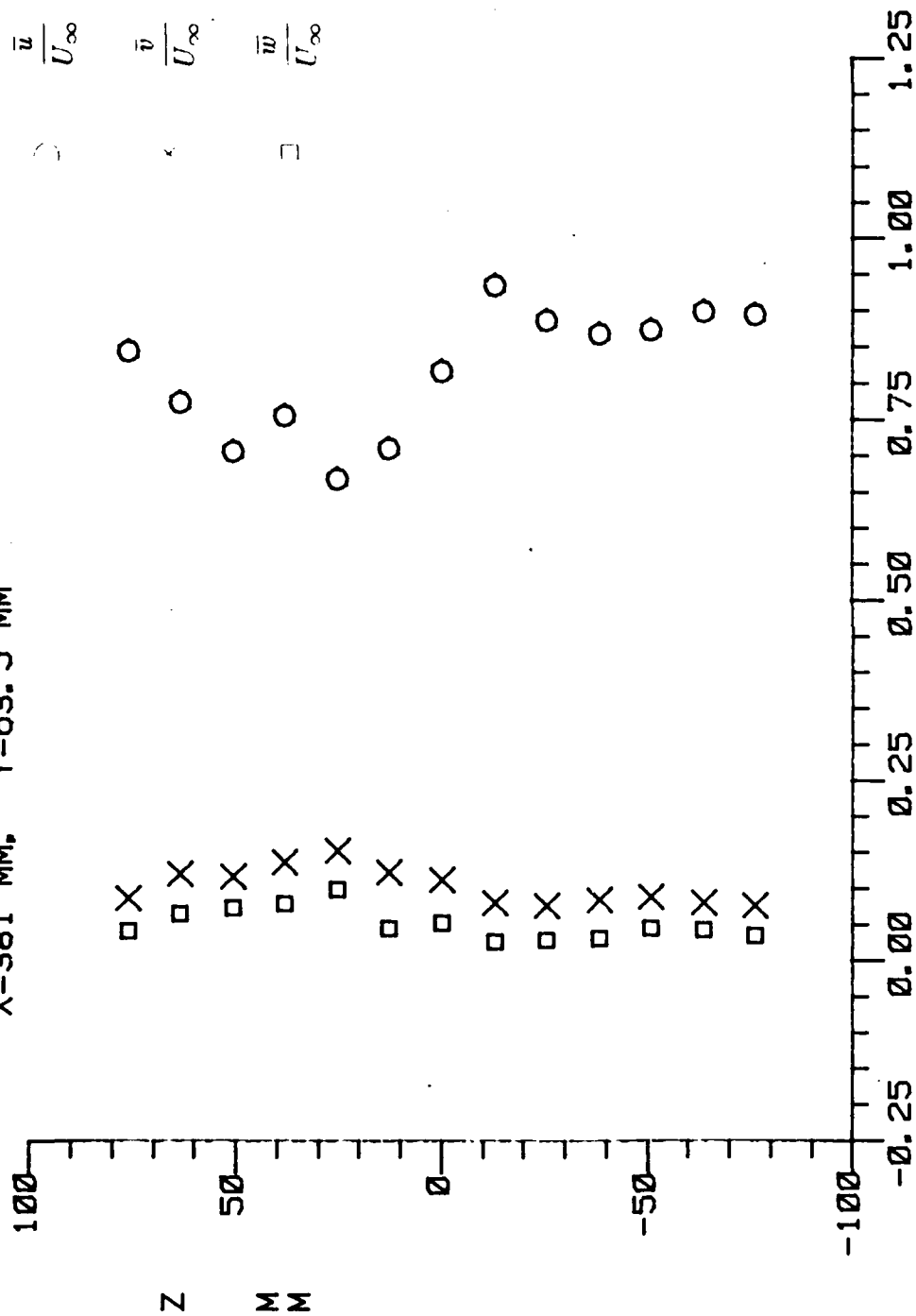






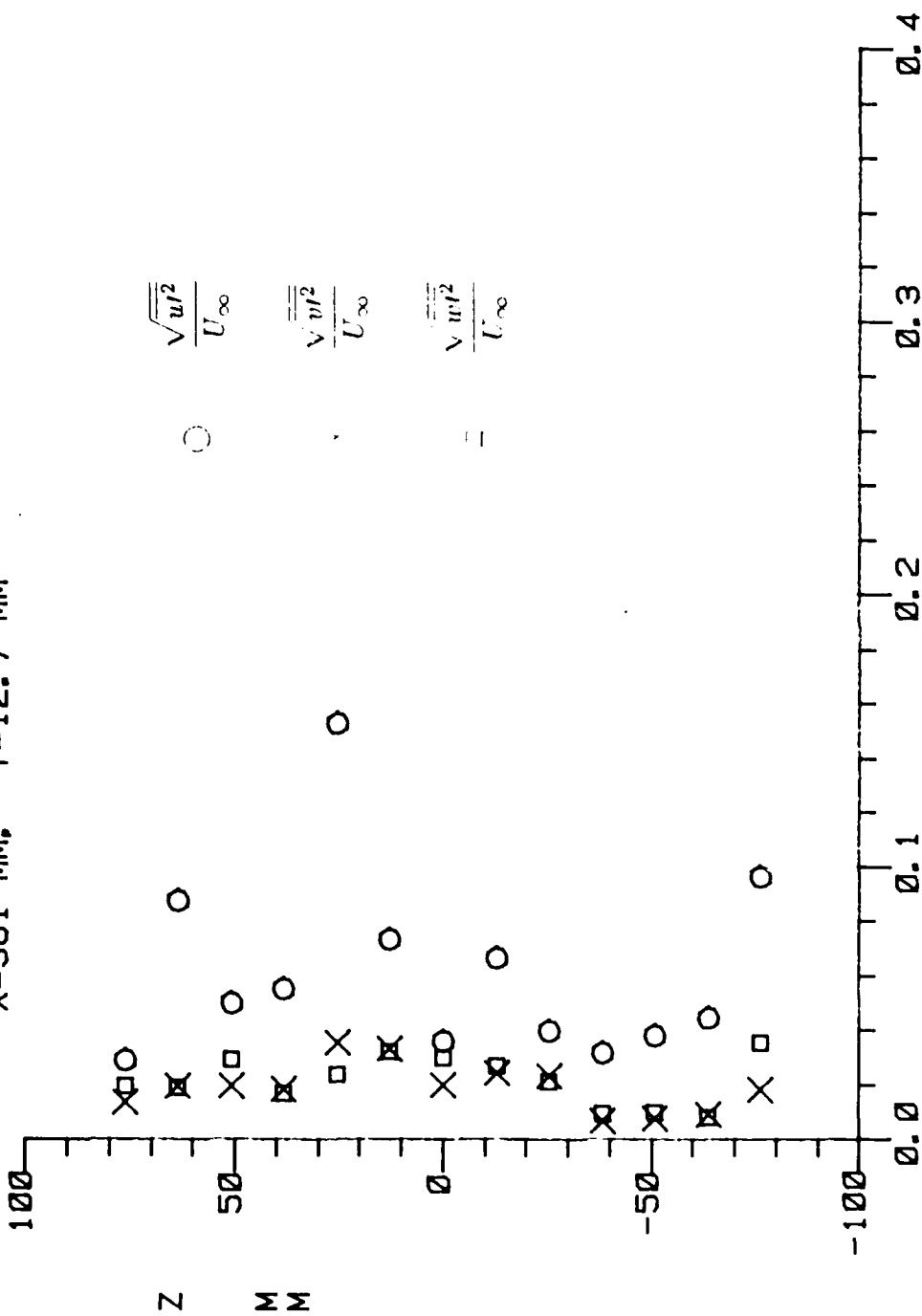


X=381 MM, Y=63.5 MM

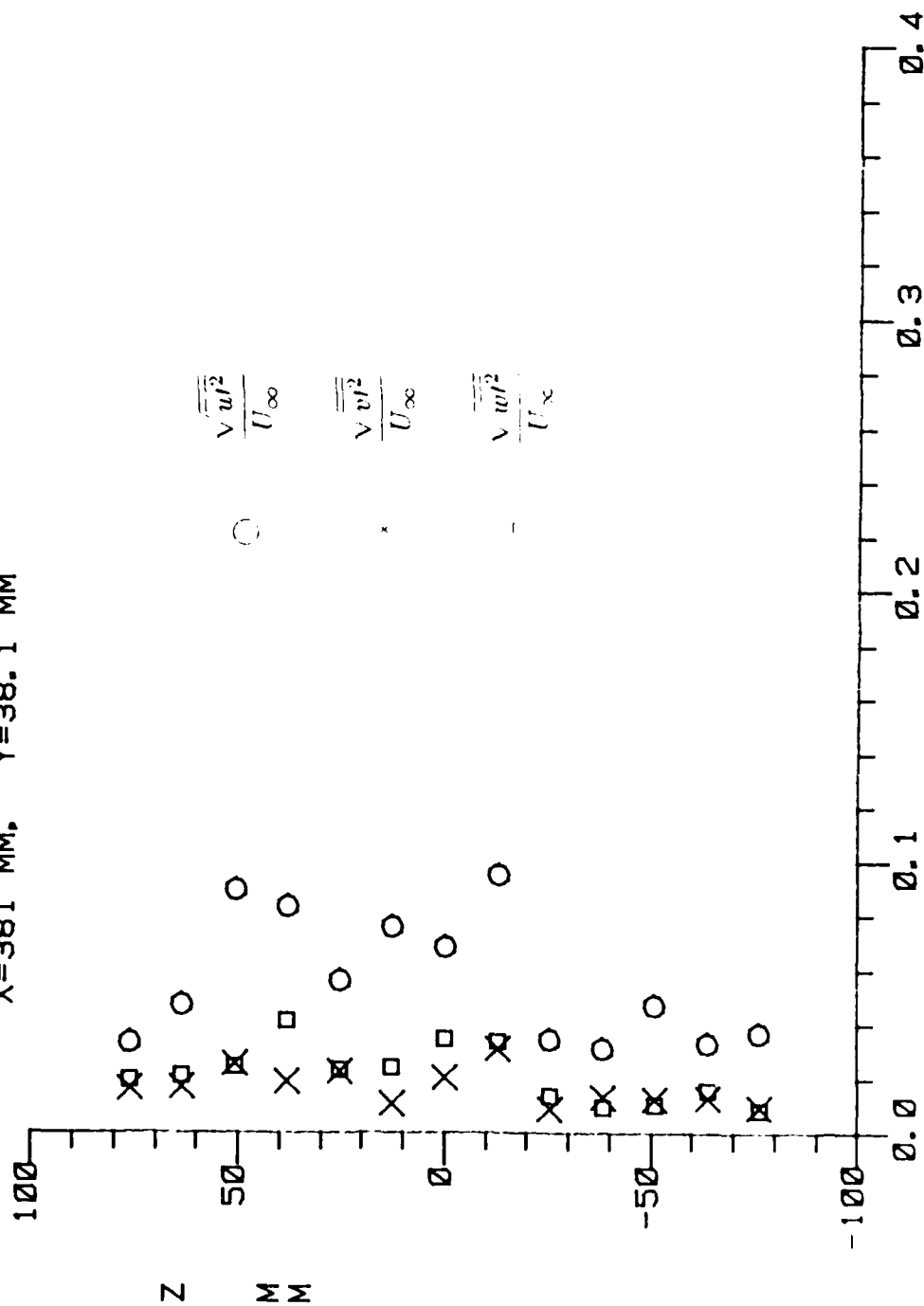




X=381 MM, Y=12.7 MM



X=381 MM, Y=38.1 MM



AO-A179 783

INVESTIGATION OF NON-SYMMETRIC JETS IN CROSS FLOW  
(DISCRETE WING TIP JET.. (U) TENNESSEE UNIV SPACE INST  
TULLAHOMA J M MU ET AL. DEC 86 UTSI-86-13

2/2

UNCLASSIFIED

AFOSR-TR-87-0543 AFOSR-84-0114

F/G 20/4

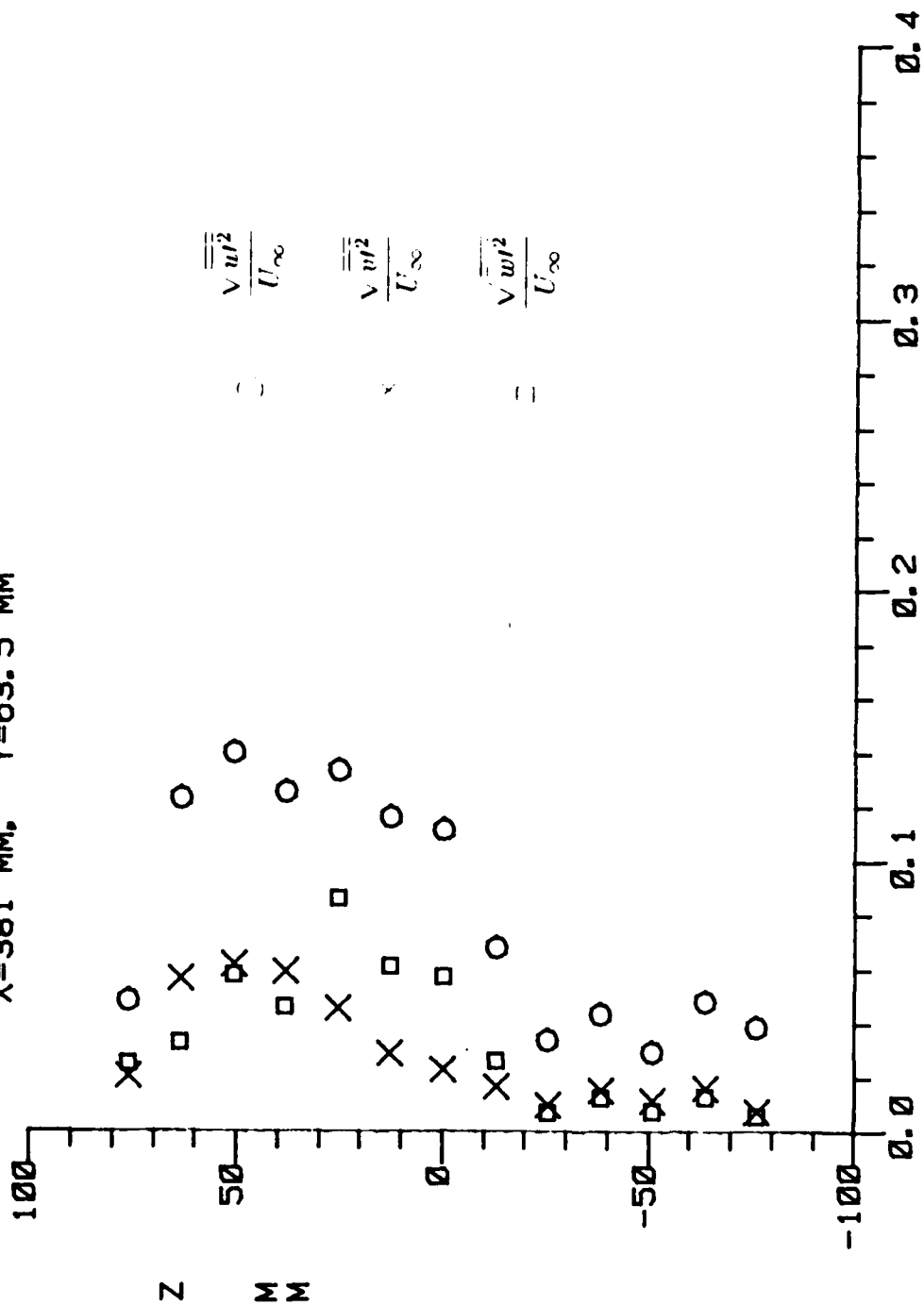
NL



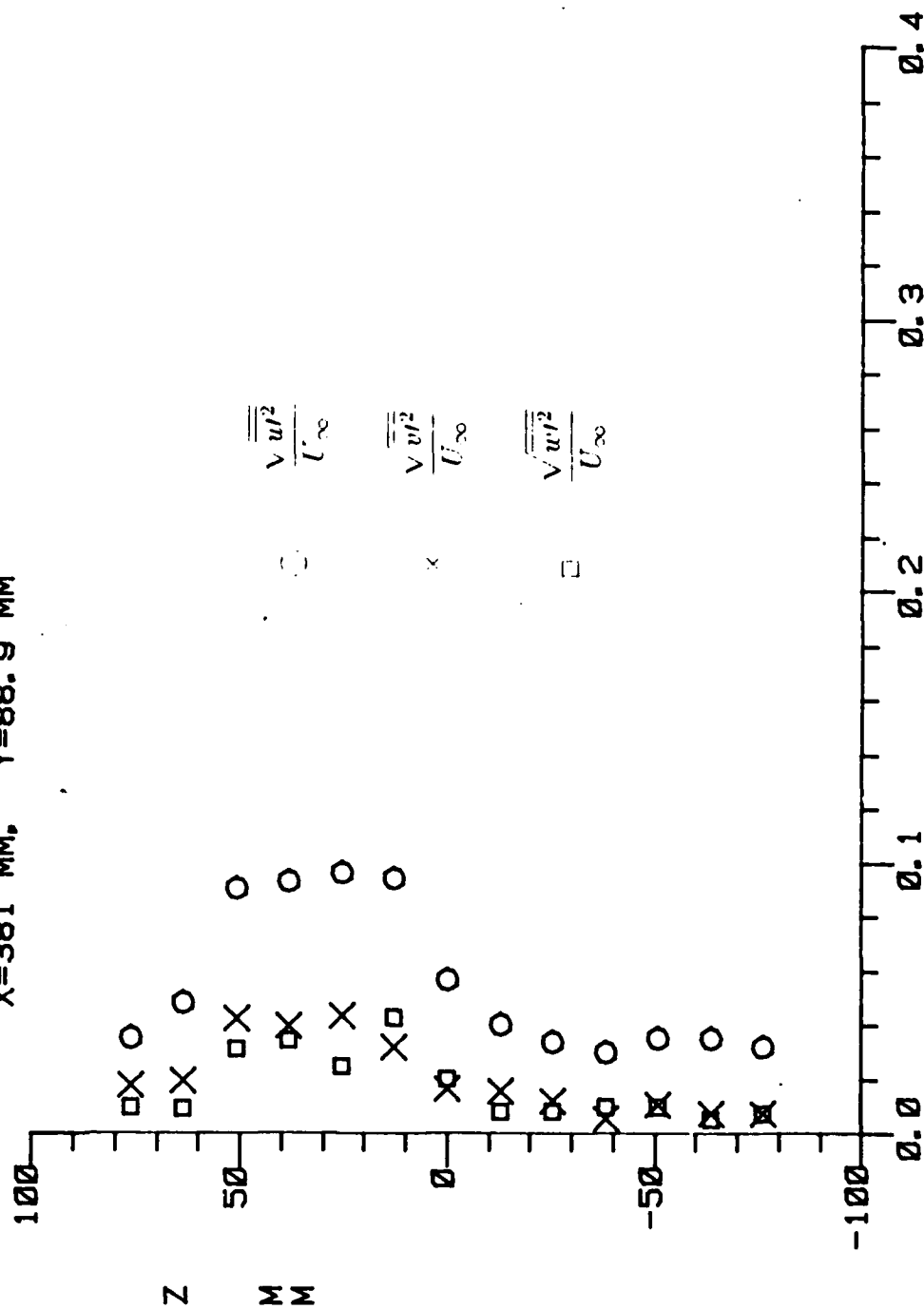


MI

X=381 MM, Y=63.5 MM



X=381 MM, Y=88.9 MM



END

5-87

DTIC